

VISVESVARAYA TECHNOLOGICAL UNIVERSITY

Jnana Sangama, Belgaum – 590014



A Project Report on

“Non-Invasive Intracranial Monitoring for Detection of Epilepsy Using EEG Signals”

A Dissertation work submitted in partial fulfilment of the requirements for the award of the degree

**Bachelor of Engineering
In
Electrical and Electronics Engineering**

Submitted by

Mr Nandhakumar S	1AY22EE029
Mr Nsenga Ngoie	1AY22EE031
Mr Pavan Krishna K R	1AY22EE032
Mr Shreyas S	1AY22EE039

Under the guidance of
Prof. Lakshmikanth Reddy
Asst. Professor



**Department of
Electrical and Electronics Engineering**

Acharya Institute of Technology

(An Institute Affiliated to Visvesvaraya Technological University, Belgaum, Recognized by AICTE,)

Acharya Dr. Sarvepalli Radhakrishnan Road, Soldevanahalli, Bangalore-560107

2025 - 2026

ACHARYA INSTITUTE OF TECHNOLOGY

SOLDEVANAHALLI, BENGALURU -560107



DEPARTMENT OF ELECTRICAL AND ELECTRONICS ENGINEERING

2025-2026

CERTIFICATE

This is to certify that the major project work entitled "**“Non-Invasive Intracranial Monitoring for Detection of Epilepsy Using EEG Signals”**" is carried out by Mr Nandhakumar S 1AY22EE029, Mr Pavan Krishna K R 1AY22EE032, Mr Nsenga Ngoie 1AY22EE031, Mr. Shreyas S 1AY22EE039, bonafide students of **ACHARYA INSTITUTE OF TECHNOLOGY** in partial fulfilment for the assessment of 7th semester Major Project in Electrical and Electronics Engineering of **Visvesvaraya Technological University, Belagavi**. It is certified that all corrections/suggestions indicated for the assessment have been incorporated in the report deposited in the departmental library. The Major Project Report has been approved as it satisfies the academic requirement during the academic year **2025-2026**.

Signature of Guide
Prof. Lakshmikanth Reddy,
Asst. Professor, Gr-1
Department of EEE
AIT, Bengaluru

Signature of H.O.D.
Dr Lakshmikanth S,
Asso Prof. and HOD
Department of EEE
AIT, Bengaluru

Signature of Principal
Prof. C.K. Marigowda
Principal
AIT, Bengaluru

External Viva

Name of Examiner

Signature with Date

1. _____

2. _____

ACKNOWLEDGEMENT

The satisfaction and euphoria that accompany the successful completion of a task would be incomplete without mentioning the people who made it possible. Without their constant guidance and encouragement success would not have been possible.

I am grateful to the Acharya Institute of Technology management for its ideas and inspiration, and for providing us with excellent infrastructure, laboratories, facilities, and an inspiring staff that have made this Major Project successful.

I want to express my sincere gratitude to the Internal Guide **Prof. Lakshmikanth Reddy** Assistant Professor, Dept. of EEE AIT for his invaluable guidance and support.

I want to express my sincere gratitude to the Major Project Coordinator **Prof. Sudharshan S**, Assistant Professor, Dept. of EEE, AIT for his valuable guidance and support.

I heartily thank and express my sincere gratitude to **Dr Lakshmikanth S**, HOD, Dept. of EEE, AIT for his valuable support and a constant source of enthusiastic inspiration to steer us forward.

I would like to express my sincere gratitude to **Dr C.K. Mari Gowda**, Principal of AIT, for all the facilities he has extended throughout our work.

Finally, I would like to express my sincere gratitude to my parents, all teaching and non-teaching faculty members, and friends for their moral support, encouragement, and help throughout the completion of the Major Project.

NANDHAKUMAR S **1AY22EE029**

NSENGA NGOIE **1AY22EE031**

PAVAN KRISHNA K R **1AY22EE032**

SHREYAS S **1AY22EE039**

DECLARATION

We, Mr Nandhakumar S (1AY22EE029), Mr Nsenga Ngoie (1AY22EE031), Mr Pavan Krishna K R (1AY22EE032) and Mr Shreyas S (1AY22EE039), students of VII Semester B.E in the Department of Electrical and Electronics Engineering, AIT, Bengaluru, hereby declare that the project entitled "Non-Invasive Intracranial Monitoring for Detection of Epilepsy Using EEG Signals" has been carried out under the supervision of Prof. Lakshmikanth Reddy, Assistant Professor, Dept. of EEE, AIT. This project is submitted in partial fulfilment of the requirements for the award of the degree of Bachelor of Engineering in Electrical and Electronics Engineering of Visvesvaraya Technological University, Belagavi, during the academic year 2025-2026.

This project has been conducted with dedication, adherence to academic guidelines, and alignment with the ethical standards set by our institution. We extend our gratitude to Prof. Lakshmikanth Reddy for his valuable guidance, encouragement, and insightful feedback throughout this project. Additionally, we express our appreciation to the Department of Electrical and Electronics Engineering at Acharya Institute of Technology for providing the necessary resources and support to make this project successful.

We acknowledge the collaborative effort and teamwork that has driven this project forward, enabling us to explore innovative solutions and expand our knowledge in the field of Electronics, Digital signal processing and embedded systems.

Nandhakumar S 1AY22EE029

Nsenga Ngoie 1AY22EE031

Pavan Krishna K R 1AY22EE032

Shreyas S 1AY22EE039

PLACE: Bengaluru

DATE:

Abstract

Epilepsy is a chronic neurological disorder characterised by sudden, recurrent seizures caused by abnormal brain activity. This project presents a non-invasive EEG-based intracranial monitoring system designed to detect early seizure patterns using advanced DSP algorithms and machine-learning-driven feature extraction. The system integrates real-time data acquisition, noise filtering, spectral analysis, and classifier-based decision support to improve diagnostic accuracy and latency. A dual-microcontroller architecture optimises performance for STM32 for DSP computation and ESP8266 for visualisation, providing a low-cost, portable, and accessible solution suited for clinical and remote monitoring applications.

Keywords: **Epilepsy, EEG, Seizure Detection, Digital Signal Processing, Feature Extraction, Machine Learning, Biomedical Monitoring, Low-Cost Healthcare.**

Contents

Chapter 1: Introduction	1
1.1 Background and Motivation	2
1.2 Problem Statement	3
1.3 Need for a Portable, Non-Invasive Monitoring System	4
1.4 Scope of the Project	4
1.5 Objectives	4
Chapter 2: Literature Review	7
2.1 Medical and Clinical Techniques	7
2.2 Signal Processing and AI-Based Techniques	11
2.2.1 Classical DSP + Feature-Based Machine Learning Approaches	11
2.2.2 Deep Learning Approaches	13
2.2.3 Wavelet and Time–Frequency Analysis	13
2.2.4 Nonlinear and Fractal-Based Approaches	14
2.3 Deployment Challenges and Embedded Implementations	15
2.4 Identified Research Gaps	20
Chapter 3: Methodology and System Design	25
3.1 Methodology	25
3.1.1 EEG Acquisition Method	25
3.1.2 Dataset Used for Model Training	26
3.1.3 Signal Preprocessing and Noise Handling	27
3.1.4 Segmentation	28
3.1.5 Feature Extraction Overview	30
3.1.6 Classification Models	30
3.1.7 Embedded Deployment Strategy	31
3.1.8 Wireless Transmission and Alerting	32

3.2	Hardware Implementation	33
3.2.1	EEG Electrodes and Sensor Interface	34
3.2.2	BioAmp EXG Pill – Analog Front-End (AFE)	35
3.2.3	STM32F446RE Microcontroller Unit	37
3.2.4	ESP-12E (ESP8266) Wireless Module	40
3.2.5	Local Alerting Mechanism	41
3.2.6	Power Supply and Regulation	42
3.2.7	Wiring Diagram and PCB Layout	43
3.3	Software Implementation	45
3.3.1	Firmware Execution Model	46
3.3.2	ADC Sampling and Preprocessing	47
3.3.3	Digital Signal Processing (DSP) Pipeline	48
3.3.4	Windowing and Segmentation	50
3.3.5	Feature Extraction (24 Features)	51
3.4	Machine Learning Model Development	62
3.4.1	CNN–LSTM Architecture	62
3.4.2	Random Forest Classifier	64
3.4.3	Embedded Seizure Detection Logic	64
3.4.4	Wireless JSON Transmission (ESP-12E)	66
3.4.5	ESP-12E Web Dashboard Firmware	66
Chapter 4: Advantages, Limitations and Applications		74
4.1	Advantages	74
4.1.1	Non-Invasive, Safe, and Comfortable for Long-Term Use	74
4.1.2	Real-Time Seizure Detection With Low Latency	74
4.1.3	High Diagnostic Reliability Through DSP + ML Fusion	75
4.1.4	Low Power Consumption and Embedded Efficiency	76
4.1.5	Wireless Connectivity and Remote Health Monitoring	76

4.1.6	Cost-Effective Compared to Clinical EEG Systems	76
4.1.7	Enhanced Patient Safety Through Immediate Alerts	77
4.1.8	Suitable for Home, Community, and Clinical Use	77
4.2	Limitations	78
4.2.1	Analog Front-End (AFE) and Electrode Limitations	78
4.2.2	Hardware Constraints of STM32 Microcontroller	79
4.2.3	Limitations of Non-Invasive Scalp EEG	79
4.2.4	DSP and Feature Extraction Limitations	80
4.2.5	Machine Learning Limitations	81
4.2.6	Wireless Communication Constraints	83
4.2.7	Dataset and Model Generalizability Limitations	83
4.2.8	Clinical Validation Limitations	83
4.3	Applications	84
4.3.1	Clinical Epilepsy Monitoring	84
4.3.2	Home-Based Long-Term Epilepsy Management	84
4.3.3	Wearable IoT Health Devices	85
4.3.4	Seizure Alerting Systems to Reduce SUDEP Risk	85
4.3.5	Remote Patient Monitoring and Telemedicine	85
4.3.6	Mobile and Rural Healthcare Deployment	86
4.3.7	Academic, Engineering, and Research Applications	86
4.3.8	Data Acquisition for AI-Based Epilepsy Research	87
4.3.9	Educational Tool for DSP, Embedded Systems, and Neuroscience	87
4.3.10	Assistive Technology for Vulnerable Populations	87
Chapter 5: Results and Discussion		90
5.1	Results	90
5.1.1	Evaluation of DSP Filtering Pipeline	90
5.1.2	Feature Extraction Behaviour Across Classes	92

5.2	Machine Learning Performance (RF vs. CNN–LSTM)	94
5.3	PCA Clustering (2D and 3D)	99
5.4	Embedded Real-Time Performance on STM32	101
5.5	Discussion	101
5.5.1	Effectiveness of the DSP Pipeline	102
5.5.2	Discriminative Power of Extracted Features	102
5.5.3	Machine Learning Performance and Model Comparison	103
5.5.4	Embedded Feasibility and Real-Time Constraints	103
5.5.5	Implications for Real-World Seizure Monitoring	104
5.5.6	Overall Interpretation	104
Chapter 6: Conclusion and Future Scope		106
6.1	Conclusion	106
6.2	Future Scope	107
APPENDIX		109
REFERENCES		110

List of Figures

1.1	Global epilepsy distribution and prevalence statistics [51].	1
1.2	Typical EEG seizure waveforms (spike, sharp wave, spike-and-wave) [52].	1
1.3	Comparison between traditional clinical EEG systems and wearable embedded EEG devices [25].	2
1.4	Key challenges in existing EEG monitoring systems.	3
2.1	Representative clinical EEG seizure patterns illustrating spikes, sharp waves, spike-and-wave complexes, and rhythmic ictal activity, adapted from classical EEG literature [55].	8
2.2	Traditional feature-based EEG seizure detection pipeline consisting of preprocessing, handcrafted feature extraction, feature selection, and classical ML classification, adapted from Acharya et al. [3].	12
2.3	Hybrid wavelet-based EEG seizure detection pipeline illustrating DWT subband decomposition, feature extraction, and classification, adapted from Hassan and Bhuiyan [17].	14
3.1	Complete system workflow from acquisition to alerting.	25
3.2	EEG acquisition using electrodes and BioAmp EXG Pill. [58]	26
3.3	Distribution of Sensor-Inactive, Normal, and Seizure classes.	27
3.4	High-level DSP pipeline for EEG preprocessing.	28
3.5	Sliding window segmentation for EEG classification.	29
3.6	Circuit diagram of the system.	33
3.7	Electrode placement diagram (following 10–20 reduced montage)[58].	34
3.8	BioAmp EXG Pill module photograph.[58]	35
3.9	BioAmp EXG Pill pinout diagram.[58]	35
3.10	STM32F446RE Development Board [63]	37
3.11	STM32F446RE pinout diagram.[61]	38
3.12	ESP-12E (ESP8266) module photograph.[62]	40
3.13	ESP-12E pinout diagram.[62]	40

3.14	Buzzer and LED alerting subsystem diagram.	42
3.15	Full wiring diagram for STM32, EXG Pill, ESP-12E, and sensors.	44
3.16	PCB design layout for the complete system.	44
3.17	Firmware architecture block diagram illustrating data flow and processing stages.	45
3.18	ADC + DMA double-buffer diagram.	48
3.19	50 Hz notch filter response plot.	48
3.20	FIR band-pass magnitude response (0.5–45 Hz).	49
3.21	Subband filter responses.	50
3.22	Window segmentation.	50
3.23	CNN–LSTM architecture diagram.	62
3.24	Random Forest architecture.[60]	64
3.25	ESP-12E EEG Dashboard in Light Mode showing real-time seizure graph, dominant frequency, spectrogram, waveform, feature grid, and logs.	71
3.26	ESP-12E EEG Dashboard in Dark Mode with enhanced contrast for low-light monitoring.	71
4.1	BioAmp EXG Pill and electrode placement for EEG acquisition [58].	79
4.2	Variation of nonlinear EEG features (Higuchi FD, Petrosian FD, Shannon Entropy) under increasing noise levels.	81
5.1	EEG signal before and after FIR band-pass filtering (0.5–45 Hz).	91
5.2	Effect of 50 Hz notch filter on the EEG power spectrum.	91
5.3	RMS and Variance distribution for Inactive, Normal, and Seizure EEG segments.	92
5.4	Band-power distribution (Delta, Theta, Alpha, Beta) across Inactive, Normal, and Seizure EEG classes.	93
5.5	Nonlinear feature variation across EEG states, showing Shannon Entropy, Spectral Entropy, Higuchi Fractal Dimension, and Petrosian Fractal Dimension.	94
5.6	Confusion Matrix – Random Forest Model.	95
5.7	Confusion Matrix – CNN–LSTM Model.	96
5.8	ROC Curve for Random Forest (Seizure vs. Non-Seizure).	97
5.9	ROC Curve for CNN–LSTM (Seizure vs. Non-Seizure).	98

5.10 2D PCA visualization showing class-wise clustering in reduced feature space. . . 99

5.11 3D PCA visualization showing improved separation between EEG classes. . . . 100

List of Tables

2.1	Comparison Between Clinical EEG Systems and Wearable EEG Devices	10
2.2	Embedded system constraints affecting real-time EEG seizure detection models.	17
2.3	Identified research gaps motivating the development of a portable EEG-based seizure detection system.	22
3.1	Operating parameters and analog front-end specifications of the BioAmp EXG Pill [58].	36
3.2	Key specifications of the STM32F446RE microcontroller [63].	39
3.3	Key specifications of the ESP-12E (NodeMCU ESP8266) Wi-Fi module [62]. .	41
3.4	Power supply characteristics of the prototype EEG system.	43
3.5	Time-domain features extracted for seizure detection.	61
3.6	Frequency-domain features extracted for seizure detection.	61
3.7	Advanced DSP and nonlinear features extracted for seizure detection.	62
3.8	MFCC-like features extracted from log-mel energies.	62
4.1	Electrical attenuation of EEG signals through tissue layers.	78
4.2	Key hardware constraints of the STM32F446RE microcontroller [63].	80
4.3	Principal Component Analysis (PCA) Results on EEG Feature Dataset	82
5.1	Performance comparison of RF and CNN–LSTM.	98

List of Algorithms

2.1	End-to-End Processing Pipeline for Non-Invasive EEG-Based Epilepsy Detection	19
3.1	Firmware Execution Pipeline for Real-Time Seizure Detection	47
3.2	RMS Computation for EEG Buffer	51
3.3	Variance Computation for EEG Buffer	51
3.4	Computation of Hjorth Parameters (Activity, Mobility, Complexity)	52
3.5	Bandpower Computation for EEG Signal	52
3.6	Shannon Entropy Computation for EEG Signal	53
3.7	Spectral Centroid Computation for EEG Signal	53
3.8	Spectral Flatness Computation for EEG Signal	54
3.9	Kurtosis and Skewness Computation for EEG Signal	55
3.10	Zero-Crossing Rate Computation for EEG Signal	55
3.11	Peak-to-Peak Amplitude and Crest Factor Computation	56
3.12	Higuchi Fractal Dimension (HFD) Computation	57
3.13	Petrosian Fractal Dimension (PFD) Computation	58
3.14	MFCC-like Feature Computation for EEG Signal	59
3.15	Burg Autoregressive (AR) Residual Computation	60
3.16	Model Training Pipeline	63
3.17	PCA Feature Reduction Workflow	63
3.18	Hybrid Seizure Detection Logic	65

CHAPTER 1

Chapter 1

Introduction

Epilepsy is a chronic neurological disorder characterised by recurrent, unprovoked seizures caused by abnormal, excessive electrical activity in the brain. According to the World Health Organization (WHO), nearly 50 million individuals worldwide are living with epilepsy, making it one of the most widespread neurological conditions [49]. The disorder is associated with significant social, psychological, and economic challenges, especially in low-resource regions where diagnostic and monitoring facilities are limited.

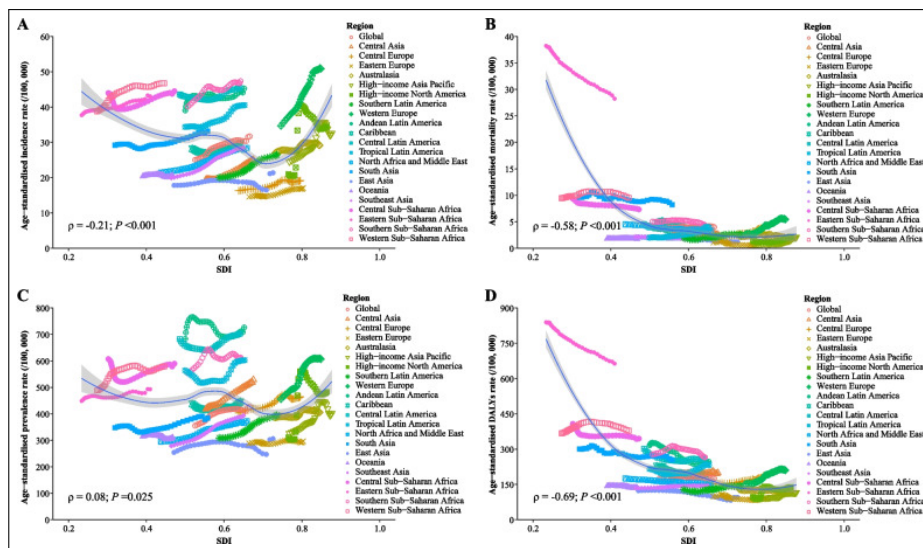


Figure 1.1: Global epilepsy distribution and prevalence statistics [51].

Seizures can vary widely, from focal seizures involving specific brain regions to generalised seizures that affect both hemispheres. These events generate distinct electrophysiological signatures observable through Electroencephalography (EEG), which remains the gold-standard non-invasive tool for identifying epileptiform activity [27]. Clinicians visually inspect EEG waveforms for hallmark patterns such as spikes, sharp waves, and spike-and-wave complexes.

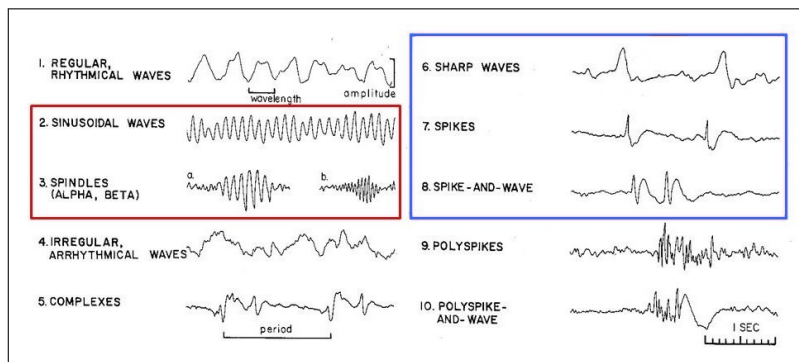


Figure 1.2: Typical EEG seizure waveforms (spike, sharp wave, spike-and-wave) [52].

Despite its diagnostic value, traditional EEG systems pose several limitations:

- They require clinical-grade amplifiers, shielded rooms, and controlled environments.
- Long-term EEG monitoring is costly and impractical outside hospitals.
- The equipment is bulky and restricts patient mobility.
- Continuous supervision by trained technicians is necessary.

These challenges hinder effective monitoring, particularly since many seizures occur unexpectedly outside clinical environments [36]. Portable, real-time EEG systems can bridge this gap by enabling continuous monitoring in homes, schools, workplaces, and rural health settings.

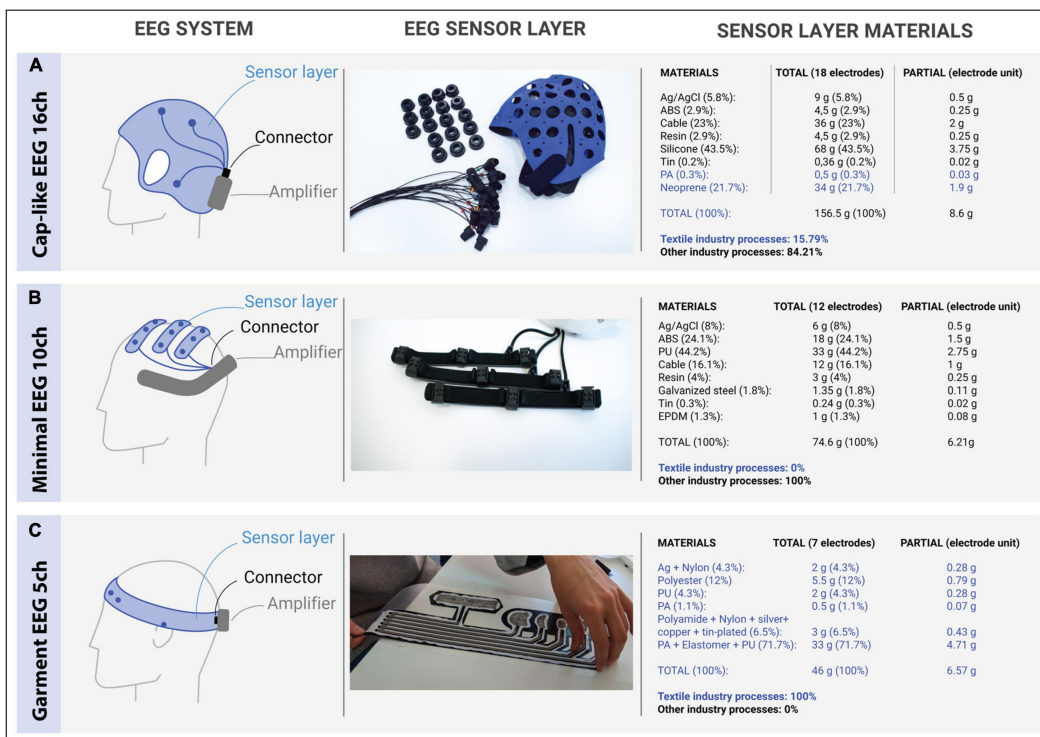


Figure 1.3: Comparison between traditional clinical EEG systems and wearable embedded EEG devices [25].

1.1 Background and Motivation

Epilepsy poses risks not only due to the seizures themselves but also due to complications such as injuries, falls, and Sudden Unexpected Death in Epilepsy (SUDEP). Continuous long-term monitoring significantly improves diagnostic yield; however, conventional EEG cannot provide practical round-the-clock observation [14]. The unpredictability of seizures amplifies the need for systems capable of real-time detection in everyday environments. Recent advancements have made this possible. Research in biosignal acquisition has produced compact, low-noise analogue front ends (AFEs) capable of capturing microvolt-level EEG signals reliably outside

laboratory conditions [9]. Concurrently, embedded processors like the STM32 enable real-time digital signal processing (DSP), and machine learning (ML) models provide automated seizure classification [2, 38]. Furthermore, IoT-enabled health systems allow wireless transmission of EEG-derived alerts to caregivers, dramatically improving patient safety [11]. These technological developments collectively motivate the design of a portable EEG monitoring system capable of real-time seizure detection.

1.2 Problem Statement

Although several EEG-based seizure detection systems exist, most face the following limitations:

- High cost and lack of portability.
- Noise sensitivity and reduced signal quality outside clinical settings.
- Absence of automated DSP and ML-based detection.
- Limited availability in rural healthcare infrastructure.
- Inability to perform real-time monitoring with low power consumption.

Thus, there is a clear need for a compact, affordable, embedded EEG system capable of continuous non-invasive monitoring and real-time seizure classification [43].

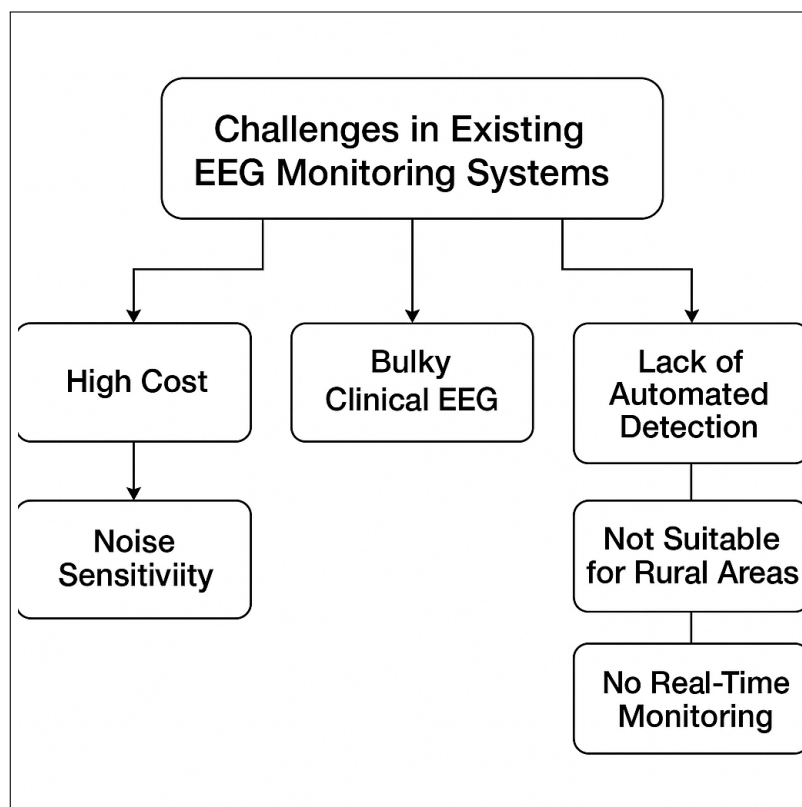


Figure 1.4: Key challenges in existing EEG monitoring systems.

1.3 Need for a Portable, Non-Invasive Monitoring System

Non-invasive EEG offers a safe and scalable method for long-term monitoring compared to intracranial EEG (iEEG), which requires surgical implantation and carries additional medical risks [13]. Recent advancements in embedded biosignal processing show that even single-channel or reduced-lead EEG can be effectively used for seizure detection when paired with ML and DSP pipelines [39].

The need for such a system is driven by:

- increased accessibility in rural and low-income regions,
- elimination of dependence on continuous hospital-based monitoring,
- real-time alerting for caregivers,
- lower operational and maintenance costs,
- improved diagnostic yield from long-term monitoring.

1.4 Scope of the Project

The project focuses on developing a complete end-to-end embedded seizure detection system incorporating:

- non-invasive EEG acquisition using the BioAmp EXG Pill,
- real-time DSP filtering, segmentation, and feature extraction,
- CNN–LSTM and Random Forest classification (both evaluated),
- on-device inference using optimised feature-based models,
- wireless transmission via ESP-12E,
- buzzer-based local alerts.

This scope ensures a functional, low-cost system suitable for both home use and clinical preliminary screening.

1.5 Objectives

The main objectives of this work are:

1. To design a portable, non-invasive single-channel EEG acquisition system for continuous monitoring.
2. To implement real-time digital signal processing for noise suppression and signal en-

hancement.

3. To extract clinically relevant EEG features and evaluate machine learning models for seizure classification.
4. To deploy a computationally efficient seizure detection model on an STM32 microcontroller.
5. To enable real-time alerting through wireless communication using the ESP-12E module.

CHAPTER 2

Chapter 2

Literature Review

Epileptic seizure detection has been widely studied across clinical neurology, biomedical engineering, digital signal processing (DSP), and artificial intelligence (AI). Over the past two decades, research has shifted from manual EEG interpretation to automated ML and deep learning models, and more recently toward embedded, real-time, low-power seizure detection systems. This chapter reviews the state of the art, divided into three major domains:

1. Medical and clinical techniques for epilepsy diagnosis,
2. AI and DSP-based automated seizure detection approaches,
3. Deployment challenges, embedded implementations, and research gaps.

The structure and depth of coverage follow the style commonly used in EEG research papers and reflect the methodological framework adopted in this project.

2.1 Medical and Clinical Techniques

Electroencephalography (EEG) has served as the principal diagnostic modality for epilepsy for more than eight decades, owing to its ability to non-invasively record cortical electrical activity with high temporal resolution. Since the foundational work of Hans Berger, EEG has been extensively used to detect abnormal neuronal firing patterns associated with epileptic seizures. In modern clinical practice, EEG interpretation relies predominantly on expert neurologists visually examining EEG waveforms to identify characteristic epileptiform discharges, including spikes, sharp waves, spike-and-wave complexes, polyspikes, and high-frequency oscillations [27].

Niedermeyer and da Silva provided one of the most comprehensive clinical frameworks for EEG interpretation in epilepsy, detailing the morphological characteristics, amplitude ranges, frequency content, and temporal evolution of epileptiform waveforms across focal and generalized seizure types [27]. Their work established EEG as the gold standard for non-invasive epilepsy diagnosis and continues to serve as a primary reference in both clinical neurology and biomedical engineering research. Building upon this foundation, Noachtar et al. standardized EEG terminology and diagnostic criteria through international consensus, emphasizing the importance of waveform morphology, rhythmicity, spatial distribution, and background abnormalities in distinguishing epileptic activity from benign variants and artefacts [28]. This standardization

has been instrumental in enabling reproducibility across clinical studies and in facilitating the development of automated seizure detection algorithms.

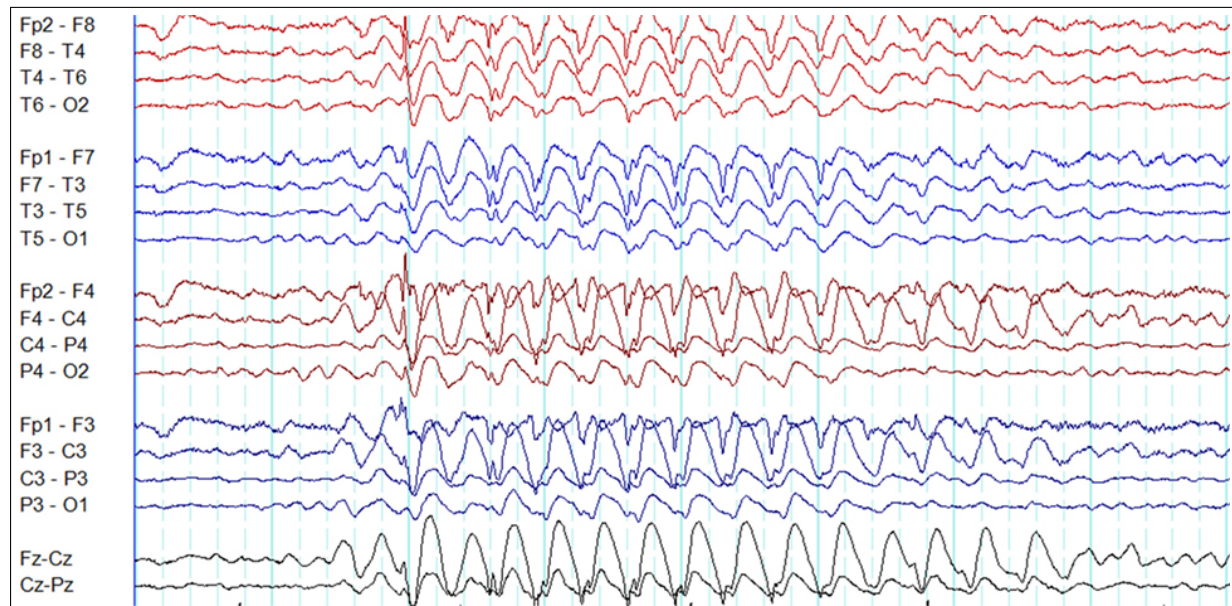


Figure 2.1: Representative clinical EEG seizure patterns illustrating spikes, sharp waves, spike-and-wave complexes, and rhythmic ictal activity, adapted from classical EEG literature [55].

Despite its diagnostic value, routine clinical EEG exhibits several inherent limitations that restrict its effectiveness for long-term seizure monitoring. One of the most significant constraints is recording duration. Standard EEG sessions typically last between 20 and 30 minutes, which is often insufficient to capture spontaneous ictal events due to the unpredictable and infrequent nature of seizures. Smith et al. reported that a single routine EEG identifies interictal epileptiform discharges in only 30–50% of epilepsy patients, underscoring the limited sensitivity of short-duration recordings [55]. Tatum et al. further demonstrated that extended or repeated EEG recordings substantially improve diagnostic yield, highlighting the need for continuous or long-term monitoring solutions [27].

In addition to temporal limitations, conventional clinical EEG systems are characterized by bulky medical-grade amplifiers, wired electrode connections, and stationary setups that significantly restrict patient mobility and comfort. Schomer and da Silva noted that such systems require controlled, shielded environments—often involving Faraday cages—to minimize electromagnetic interference, further limiting their applicability outside hospital settings [36]. Continuous EEG monitoring typically necessitates hospital admission, trained EEG technicians, and neurologist supervision, resulting in high operational costs and limited accessibility. These challenges are particularly acute in rural and low-resource regions, where specialized neurological infrastruc-

ture is scarce.

Long-term video-EEG monitoring, although considered the clinical gold standard for seizure classification and presurgical evaluation, is prohibitively expensive and impractical for widespread deployment. Schomer et al. reported that the cost and logistical complexity of prolonged hospital-based monitoring significantly limit its use to specialized epilepsy centers [36]. Consequently, a substantial proportion of individuals with epilepsy remain underdiagnosed or inadequately monitored, contributing to delayed treatment and poorer clinical outcomes.

Intracranial EEG (iEEG) was introduced to overcome some of the spatial resolution limitations of scalp EEG by recording neural activity directly from the cortical surface or deep brain structures. Davis et al. demonstrated that iEEG provides superior localization of seizure onset zones compared to scalp EEG, making it an indispensable tool in the pre-surgical evaluation of patients with drug-resistant epilepsy [12]. Engel et al. further showed that accurate localization using iEEG significantly improves surgical outcomes, leading to higher rates of seizure freedom in appropriately selected patients [13]. However, iEEG requires invasive neurosurgical implantation of electrodes, introducing substantial medical risks including infection, hemorrhage, cerebral oedema, and long-term neural tissue damage. Due to these risks, ethical considerations, and high costs, iEEG is unsuitable for routine diagnosis, continuous ambulatory monitoring, or large-scale population screening.

The cumulative limitations of routine scalp EEG and invasive iEEG have motivated extensive research into alternative monitoring paradigms. In particular, wearable and non-invasive EEG systems have emerged as a promising solution for enabling long-term seizure monitoring in naturalistic environments. Casson et al. reviewed early wearable EEG devices and demonstrated that reduced-channel systems, when properly designed, can provide clinically meaningful information while significantly improving patient comfort and mobility [54]. Lopez et al. further showed that advances in low-noise analog front-end design and wireless communication have enabled portable EEG systems capable of continuous monitoring outside hospital settings [57].

Dry and semi-dry electrode technologies have also played a critical role in the evolution of wearable EEG. Liao et al. demonstrated that dry electrodes reduce preparation time and improve user comfort, albeit at the cost of increased susceptibility to motion artefacts and impedance variability [56]. These findings highlight the trade-offs inherent in wearable EEG design and underscore the need for robust signal processing techniques to compensate for reduced signal quality.

Table 2.1: Comparison Between Clinical EEG Systems and Wearable EEG Devices

Parameter	Clinical EEG Systems	Wearable EEG Devices
Number of Electrodes	19–32 electrodes following the 10–20 or 10–10 system [55]	1–8 electrodes with reduced montage [54]
Electrode Type	Wet gel electrodes (clinical standard) [27]	Dry or semi-dry electrodes [56]
Signal Quality	High-quality, low-noise medical amplifiers [57]	Moderate; susceptible to motion artefacts [56]
Amplifier	Bulky medical-grade systems [27]	Miniaturized, low-power amplifiers [54]
Environment Required	Controlled, shielded clinical environments [36]	Operates in everyday environments [54]
Portability	Low; stationary hospital equipment [27]	High; designed for continuous wear [57]
Monitoring Duration	Short-term or inpatient video-EEG [36]	Long-term continuous monitoring [57]
Technician Requirement	Requires trained EEG technician [27]	Minimal supervision [54]
Cost	Very high (5–20 lakh+) [36]	Low to moderate [57]
Wireless Capability	Rare; mostly wired systems [36]	Common (BLE, WiFi) [54]
User Comfort	Low due to gel, cables, and immobilization [27]	High due to lightweight and dry sensors [56]

Collectively, these studies demonstrate that while traditional clinical EEG and iEEG remain indispensable for diagnosis and surgical planning, their limitations severely restrict scalability, accessibility, and long-term usability. These constraints have driven a paradigm shift toward wearable, non-invasive EEG systems that prioritize continuous monitoring, patient comfort, and real-world deployment. Such systems form the foundation for automated, DSP- and ML-based seizure detection frameworks, which are reviewed in the subsequent sections.

2.2 Signal Processing and AI-Based Techniques

The evolution of automated epileptic seizure detection has progressed through multiple methodological phases, driven by advances in signal processing theory, machine learning, and computational hardware. Broadly, existing approaches can be categorized into the following classes:

1. Classical signal processing and feature-based machine learning methods,
2. Deep learning–based approaches operating on raw or transformed EEG signals,
3. End-to-end convolutional and recurrent neural network architectures,
4. Hybrid frameworks combining DSP-driven feature extraction with ML classifiers.

Each category reflects a trade-off between interpretability, computational complexity, data requirements, and suitability for real-time embedded deployment.

2.2.1 Classical DSP + Feature-Based Machine Learning Approaches

Early research in automated seizure detection focused heavily on handcrafted feature extraction from EEG signals, followed by conventional machine learning classifiers. Shoeb and Guttag were among the first to demonstrate a practical real-time seizure detection system using a support vector machine (SVM) trained on time-domain and frequency-domain features such as line length, root mean square (RMS) amplitude, spectral energy, and zero-crossing rate [38]. Their work established a baseline framework that remains influential due to its low computational complexity and suitability for embedded systems.

Subasi introduced the use of discrete wavelet transform (DWT) coefficients combined with mixture-of-experts and multilayer perceptron classifiers, demonstrating that multi-resolution analysis significantly improves seizure detection accuracy compared to purely time-domain features [41]. Subsequent studies by Subasi and colleagues showed that wavelet-based features capture transient, non-stationary characteristics of EEG signals that are strongly correlated with ictal activity [42].

Entropy-based features gained prominence due to their ability to quantify signal irregularity and complexity. Singh et al. demonstrated that Shannon entropy, spectral entropy, and Renyi entropy effectively discriminate seizure from non-seizure EEG segments, particularly in noisy conditions [40]. Acharya et al. further showed that combining entropy measures with statistical features such as variance and skewness yields high sensitivity and specificity across multiple datasets [3].

Additional classical features explored in literature include Hjorth parameters, autoregressive (AR) coefficients, band power ratios, and higher-order statistics. Temko et al. reported that combining time-domain energy features with AR modeling improves early seizure detection performance [?]. Polat and Güneş demonstrated that decision tree and k-nearest neighbor classifiers achieve competitive accuracy when trained on carefully selected feature subsets [?].

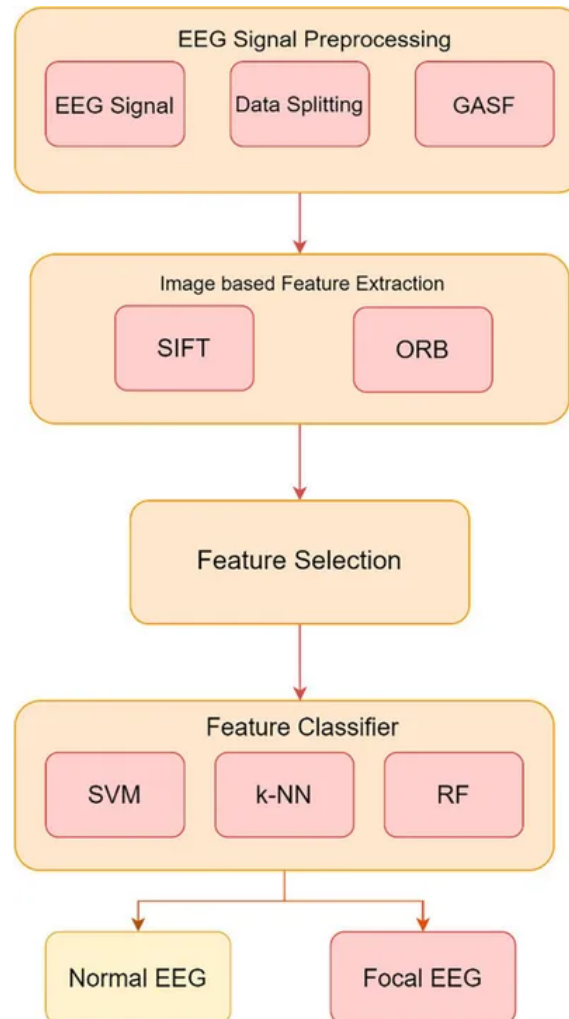


Figure 2.2: Traditional feature-based EEG seizure detection pipeline consisting of preprocessing, handcrafted feature extraction, feature selection, and classical ML classification, adapted from Acharya et al. [3].

Despite the emergence of deep learning, classical ML approaches remain highly relevant, particularly in scenarios involving limited training data, imbalanced datasets, or strict computational constraints. Roy et al. conducted a comparative study and concluded that Random Forest and SVM classifiers often outperform deep neural networks when dataset size is small or when inter-subject variability is high [33]. This observation is consistent with our experimental findings, where a Random Forest classifier achieved 93.51% accuracy, marginally outperforming a CNN–LSTM model that achieved 92.51% accuracy under identical evaluation conditions.

2.2.2 Deep Learning Approaches

The advent of deep learning marked a paradigm shift in automated seizure detection by enabling end-to-end learning directly from EEG signals, thereby reducing dependence on handcrafted features. Acharya et al. introduced one of the earliest convolutional neural network (CNN) architectures for EEG-based seizure classification, demonstrating that CNNs can automatically learn discriminative features from raw EEG data [1]. Their results showed improved generalization across subjects compared to traditional ML pipelines.

Schirrmeister et al. further advanced this approach by proposing deep and shallow CNN architectures capable of learning meaningful spatio-temporal representations from multi-channel EEG recordings [35]. Their work highlighted the ability of deep models to capture both local temporal patterns and global spatial correlations inherent in EEG data.

Other notable contributions include Lawhern et al., who proposed EEGNet, a compact CNN architecture specifically designed for EEG signal classification, emphasizing parameter efficiency and suitability for real-time applications [?]. Ullah et al. demonstrated that residual CNN architectures improve convergence and robustness in seizure detection tasks [?].

Hybrid CNN–LSTM architectures gained popularity due to their ability to model both spatial and temporal dependencies. Ahmad et al. demonstrated that CNN–LSTM models outperform stand-alone CNNs by leveraging LSTM layers to capture long-term temporal dependencies in EEG signals [4]. Truong et al. further showed that bidirectional LSTM networks enhance seizure prediction performance by incorporating past and future temporal context [45].

In this project, a CNN–LSTM architecture was evaluated to benchmark deep learning performance. The obtained accuracy of 92.51% aligns with existing literature, which consistently reports that deep learning models require large, diverse datasets and multi-channel EEG input to significantly outperform classical approaches.

2.2.3 Wavelet and Time–Frequency Analysis

Epileptic seizures are inherently non-stationary events characterized by abrupt changes in frequency content and amplitude. Time–frequency analysis techniques, particularly wavelet transforms, provide superior localization of transient EEG patterns compared to traditional Fourier-based methods. Adeli et al. demonstrated that wavelet-based energy features capture seizure-related frequency transitions more effectively than stationary spectral features [?].

Hassan and Bhuiyan proposed a hybrid framework combining discrete wavelet transform (DWT) with convolutional neural networks, showing that DWT-based subband decomposition significantly improves CNN performance by providing frequency-localized inputs [17]. Their approach achieved competitive accuracy across multiple benchmark datasets while reducing model complexity.

Other studies by Kumar et al. and Subasi et al. have shown that wavelet packet decomposition and empirical mode decomposition (EMD) further enhance seizure detection by adaptively capturing EEG oscillatory modes [?, 42].

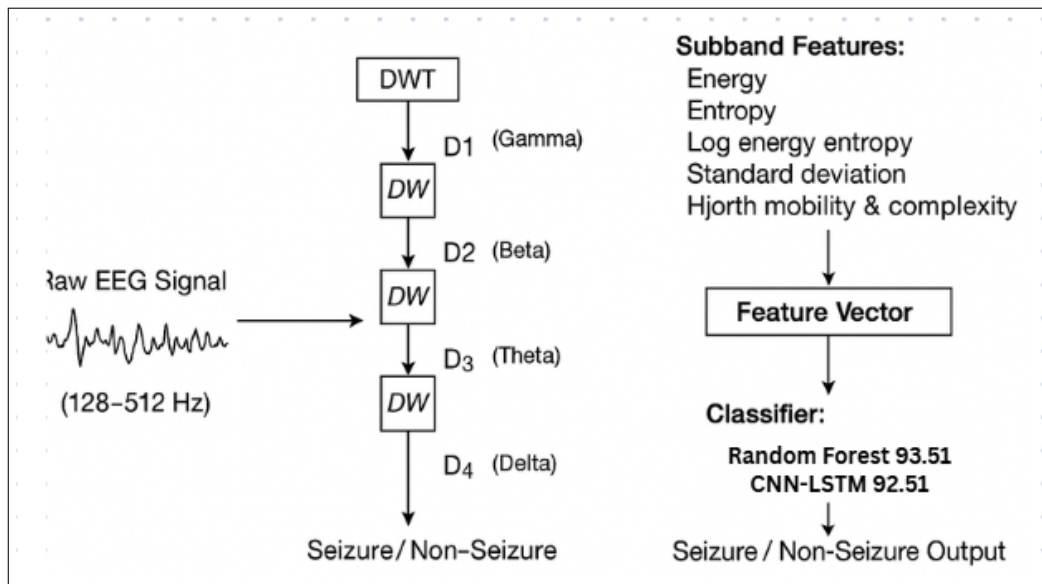


Figure 2.3: Hybrid wavelet-based EEG seizure detection pipeline illustrating DWT subband decomposition, feature extraction, and classification, adapted from Hassan and Bhuiyan [17].

2.2.4 Nonlinear and Fractal-Based Approaches

EEG signals generated during epileptic seizures exhibit complex nonlinear and chaotic dynamics that cannot be fully characterized using linear statistical measures. Nonlinear analysis techniques have therefore been widely explored to capture these dynamics. Acharya et al. demonstrated that nonlinear features such as approximate entropy and sample entropy are highly sensitive to seizure-related EEG irregularities [3].

Fractal dimension measures, including Higuchi and Petrosian fractal dimensions, have been shown to effectively quantify EEG signal complexity during seizures. Esteller et al. reported that fractal dimension features provide robust discrimination between ictal and interictal states [?]. Kannathal et al. further demonstrated that combining fractal features with entropy measures improves classification accuracy across subjects [?].

Lyapunov exponents have also been explored as indicators of chaotic neuronal dynamics. Iasemidis et al. showed that changes in the largest Lyapunov exponent precede seizure onset, suggesting potential utility for early seizure prediction [?]. However, the high computational cost of nonlinear measures often limits their applicability in real-time embedded systems.

In this project, both entropy-based and fractal features were extracted as part of the feature pool. Due to computational constraints, only 18 of the 24 extracted features were selected for training classical ML models, balancing classification performance with real-time feasibility.

2.3 Deployment Challenges and Embedded Implementations

Although numerous machine learning and deep learning models report high seizure detection accuracy under offline evaluation, only a limited subset of these approaches are suitable for real-time embedded deployment. The transition from offline experimentation to practical, on-device implementation introduces several critical constraints that significantly influence system design. These constraints include limited computational power, restricted memory availability, stringent latency requirements, energy efficiency considerations, and overall hardware cost.

Embedded microcontrollers typically operate at clock frequencies ranging from tens to a few hundreds of megahertz and lack the computational throughput required to execute large-scale deep neural networks efficiently. Vincent et al. (2020) investigated real-time seizure detection on ARM Cortex-M microcontrollers and demonstrated that deep learning models with millions of parameters are impractical on devices with less than 256 KB of SRAM and limited Flash memory [47]. Their study highlighted that memory bottlenecks, rather than raw computation alone, often become the dominant limiting factor in embedded EEG applications.

Memory constraints pose a particularly severe challenge for convolutional and recurrent neural networks. Chen (2021) reported that standard CNN and LSTM architectures frequently exceed the available memory on microcontrollers unless aggressive model compression techniques—such as quantization, pruning, or weight sharing—are applied [10]. Even with such optimizations, the deployment process often requires careful redesign of network architectures to balance accuracy against memory footprint and execution time.

Latency requirements further complicate embedded seizure detection. Real-time monitoring systems must process incoming EEG data streams continuously and generate detection decisions within strict temporal deadlines, often on the order of tens to hundreds of milliseconds. Vincent et al. emphasized that deep models with long inference pipelines can introduce unacceptable

latency spikes, particularly when combined with real-time digital signal processing (DSP) stages such as filtering, feature extraction, and windowing [47]. Excessive latency not only degrades system responsiveness but may also delay critical seizure alerts, reducing clinical usefulness.

Power consumption is another major consideration, especially for wearable and battery-powered EEG devices. Hussain et al. showed that continuous execution of DSP and ML pipelines can rapidly drain battery resources if not carefully optimized [20]. Wireless data transmission, particularly over WiFi or cellular interfaces, further exacerbates energy consumption. As a result, many embedded seizure detection systems must minimize both computational complexity and communication overhead to achieve acceptable operational lifetimes.

Hardware cost and system complexity also influence deployment feasibility. Clinical-grade EEG systems rely on high-performance processors and specialized analog front ends, making them unsuitable for low-cost or large-scale deployment. In contrast, embedded systems intended for home or rural healthcare applications must operate on inexpensive microcontrollers while maintaining adequate diagnostic performance. Murthy et al. highlighted that cost constraints often necessitate simplified feature sets and lightweight classifiers rather than deep networks [26].

Due to these challenges, several studies have advocated hybrid approaches that combine efficient DSP-based feature extraction with classical machine learning models, such as Random Forests or Support Vector Machines. Roy et al. demonstrated that such hybrid systems often achieve competitive accuracy while remaining feasible for real-time embedded execution [33]. Similarly, Shoeb et al. emphasized that feature-based models offer greater transparency, lower memory requirements, and predictable execution time—properties that are highly desirable in safety-critical medical devices [38].

Overall, existing literature indicates a clear gap between algorithmic performance reported in offline studies and practical feasibility on embedded hardware. Most published works prioritize classification accuracy without addressing memory usage, inference latency, power consumption, or system integration. These limitations underscore the need for end-to-end embedded seizure detection systems that explicitly account for hardware constraints during algorithm design. The system proposed in this work addresses these challenges by adopting a computationally efficient DSP pipeline, a lightweight feature-based classifier suitable for STM32-class microcontrollers, and a low-power wireless communication architecture for real-time alerting.

Table 2.2: Embedded system constraints affecting real-time EEG seizure detection models.

Constraint	Description
Limited Memory (RAM/Flash)	MCUs typically have 64–256 kB RAM and 256 kB–2 MB Flash, restricting model size, buffers, and multi-stage DSP pipelines [10, 47].
Low Processing Power	MCUs operate at 48–240 MHz without hardware acceleration. High-complexity CNN/LSTM models exceed feasible inference time for real-time monitoring [44].
Energy Constraints	Battery-powered systems must minimize computation, memory access, and wireless transmission to extend operation time. DSP and ML operations consume significant energy [20].
Latency Requirements	Seizure detection must run in real-time (100 ms pipeline). Large models or inefficient preprocessing cause latency spikes [47].
Lack of Floating-Point Support	Many MCUs lack hardware FPUs (floating-point units). DSP and ML must use fixed-point (Q format), quantized models, or integer arithmetic [26].
Limited Parallelism	MCUs are mostly single-core, cannot handle simultaneous DSP + ML + wireless transmission efficiently without optimized scheduling.
Thermal and Power Limits	Continuous high-frequency computation leads to heat buildup and impacts battery life, especially in wearable EEG devices [25].
Model Deployment Constraints	Models must be quantized, pruned, or converted (e.g., TensorFlow Lite Micro) to fit the MCU. Some architectures (CNN–LSTM) cannot be deployed at all [44].
No Operating System Support	Bare-metal or lightweight RTOS environments lack dynamic memory management, limiting buffering, model loading, and multi-threaded pipelines.
Noisy Input Signals	Real-time EEG feeds include movement artifacts, electrode noise, and environmental interference. Embedded filters must be efficient but low-cost [50].

Albahri et al. conducted a comprehensive review of IoT-based healthcare monitoring systems and reported that truly end-to-end frameworks integrating biosignal acquisition, digital signal processing (DSP), machine learning (ML), and wireless communication remain scarce in existing literature [5]. Their survey emphasized that most proposed seizure detection systems focus on isolated components—such as algorithmic accuracy, cloud-based analytics, or wearable hardware—without addressing full system integration and real-time operability on resource-constrained embedded platforms.

Specifically, Albahri et al. noted that many studies rely on offline processing using MATLAB or Python environments, assume continuous cloud connectivity, or neglect embedded deployment constraints such as memory usage, latency, and power consumption. As a result, there exists a significant gap between proof-of-concept algorithms and deployable seizure monitoring solutions suitable for real-world clinical and home environments. Similar observations were echoed by Hussain et al. and Chen et al., who highlighted that IoT health-monitoring systems often fail to integrate efficient on-device intelligence with low-power wireless communication [20, 11].

The system proposed in this work directly addresses this gap by implementing a fully integrated, end-to-end embedded seizure detection framework that spans signal acquisition, real-time processing, intelligent decision-making, and alert dissemination within a single portable platform. Unlike prior approaches that emphasize either algorithmic performance or hardware design in isolation, this system is architected with deployment feasibility as a primary design constraint.

The complete system integration includes:

1. **BioAmp EXG Pill** for non-invasive EEG signal acquisition with appropriate amplification and conditioning,
2. **STM32F446RE microcontroller** for real-time DSP operations, including filtering, segmentation, and feature extraction using CMSIS-DSP,
3. **CNN–LSTM and Random Forest classifiers** evaluated for seizure classification, with the Random Forest selected for embedded inference due to its computational efficiency,
4. **ESP-12E WiFi module** for low-latency wireless telemetry, visualization, and remote monitoring,
5. **Local buzzer-based alert mechanism** for immediate seizure notification independent of network connectivity.

By integrating all stages of the seizure detection pipeline on embedded hardware, the proposed system demonstrates practical feasibility for continuous, real-time monitoring outside clinical

environments. This end-to-end design ensures predictable latency, reduced reliance on cloud computation, and improved robustness in low-connectivity or resource-limited settings. Consequently, the proposed framework bridges the gap identified in existing literature and provides a scalable foundation for future wearable and IoT-enabled epilepsy monitoring solutions.

Algorithm 2.1 End-to-End Processing Pipeline for Non-Invasive EEG-Based Epilepsy Detection

Input: Raw EEG signals from scalp electrodes (512 Hz)

Output: Real-time seizure alert and dashboard visualization

Initialization:

Configure STM32 ADC and DMA (ping–pong) Initialize CMSIS-DSP buffers and filters

Establish UART link to ESP8266 Initialize ESP8266 WiFi AP and web dashboard

Stage 1: Signal Acquisition

Read EEG samples from analog front-end Fill DMA buffer and pass block to DSP stage

Stage 2: Preprocessing

Apply 0.5–45 Hz bandpass filter Apply 50/60 Hz notch filter Perform artifact suppression via adaptive thresholding Normalize signal using z-score normalization

Stage 3: Feature Extraction

Compute time-domain features (RMS, variance, Hjorth) Perform 512-point FFT Extract band powers ($\delta, \theta, \alpha, \beta, \gamma$) Compute entropy measures (spectral, permutation) Compute AR coefficients using Burg’s method Form final feature vector F

Stage 4: Seizure Classification

Load ML classifier (SVM / RF / CNN-lite) Predict label $C = \{\text{Seizure, Normal}\}$ If $C = \text{Seizure}$, set alert flag

Stage 5: Output & Communication

Package telemetry (timestamp, features, prediction) Transmit framed data to ESP8266 over UART

Stage 6: Dashboard Visualization (ESP8266)

Receive and validate frames Update circular buffer with EEG samples Render EEG waveform, bandpower bars, and prediction label If seizure detected, activate buzzer + alert LED Push updates to real-time WebSocket dashboard

Repeat until system shutdown.

2.4 Identified Research Gaps

A critical examination of existing literature on automated epileptic seizure detection reveals several unresolved challenges that limit the translational impact of many proposed methods. Although significant progress has been made in algorithmic accuracy, relatively few studies address the practical constraints associated with real-time, embedded, and wearable seizure monitoring systems. The most prominent research gaps identified from the reviewed literature are discussed below.

A dominant trend in recent seizure detection research is the reliance on deep learning models trained on multichannel EEG recordings. While multichannel EEG provides richer spatial information and often improves classification accuracy, it significantly increases system complexity, data bandwidth, and computational requirements. Most convolutional and recurrent neural network architectures reported in literature assume access to 16–32 EEG channels, making them unsuitable for low-cost, portable, or wearable devices intended for continuous monitoring. As highlighted by Roy et al., deep learning models tend to outperform classical machine learning approaches only when trained on large, high-dimensional datasets, which are rarely available in real-world embedded deployments [33]. This dependence on multichannel data limits the scalability of many existing solutions.

Another notable gap is the lack of fully integrated end-to-end seizure detection frameworks. Many studies focus exclusively on individual components, such as feature extraction techniques, classifier design, or dataset benchmarking, without addressing complete system integration. In particular, very few works combine real-time signal acquisition, digital signal processing (DSP), machine learning inference, embedded deployment, and wireless alerting within a single portable device. As noted in prior surveys, most proposed systems either assume offline processing or rely heavily on cloud-based computation, which introduces latency, connectivity dependence, and privacy concerns. Consequently, there remains a shortage of practical, self-contained seizure monitoring systems suitable for deployment in home or rural healthcare settings.

Wearable EEG systems introduce additional challenges related to signal quality and robustness. Several studies have reported that motion artefacts, electrode displacement, impedance variations, and environmental noise significantly degrade EEG signal quality during daily activities. Rema et al. demonstrated that motion-induced artefacts remain one of the primary sources of false positives in wearable seizure detection systems, necessitating advanced denoising and artefact suppression strategies [31]. However, many existing works do not adequately address

these artefacts or propose computationally efficient mitigation techniques suitable for embedded platforms.

Dataset-related limitations further constrain the generalizability of reported results. The CHB-MIT dataset, one of the most widely used benchmarks for seizure detection research, consists exclusively of pediatric EEG recordings collected in a controlled hospital environment. Truong et al. highlighted that models trained on CHB-MIT often exhibit reduced performance when evaluated on adult or ambulatory EEG data, raising concerns about cross-population generalization [45]. Despite this limitation, a substantial portion of the literature continues to rely solely on this dataset, leading to overly optimistic performance estimates that may not translate to real-world applications.

From an implementation perspective, real-time embedded systems face strict constraints on feature dimensionality and computational complexity. Many reported seizure detection pipelines extract a small subset of features—often fewer than 15–20—to maintain real-time feasibility. While this simplification reduces computational load, it may also limit classification robustness, particularly under noisy conditions. In contrast, systems that attempt to extract a larger number of features frequently omit real-time validation or embedded deployment altogether. This trade-off between feature richness and computational feasibility remains insufficiently explored in existing work.

Finally, although hybrid CNN–LSTM models have demonstrated strong performance in offline evaluations, their practical deployment on microcontroller-based platforms remains challenging. Such models typically require large memory footprints, floating-point computation, and long inference times, making them unsuitable for low-power embedded systems without aggressive quantization or pruning. As discussed by Roy et al., the marginal performance gains offered by deep architectures often do not justify their increased complexity in embedded scenarios [33].

In summary, existing literature reveals a clear disconnect between algorithmic performance and deployable system design. There is a pressing need for seizure detection frameworks that balance diagnostic accuracy with real-time feasibility, low power consumption, hardware affordability, and robustness to real-world artefacts. The system proposed in this work directly addresses these gaps by adopting a reduced-channel, non-invasive EEG acquisition strategy, a computationally efficient DSP and feature extraction pipeline, lightweight machine learning models suitable for embedded inference, and integrated IoT-based alerting for real-time seizure monitoring.

Table 2.3: Identified research gaps motivating the development of a portable EEG-based seizure detection system.

Research Gap	Description and Supporting Evidence
1. Lack of Low-Cost Portable EEG Systems	Clinical EEG systems are expensive, bulky, and unsuitable for long-term everyday monitoring. Most seizure detection studies assume clinical-quality signals rather than wearable EEG [25, 16].
2. Limited Real-Time On-Device Inference	Many methods rely on offline MATLAB/Python processing or GPU-based computation. Embedded real-time detection on microcontrollers remains underexplored due to hardware constraints [10, 47].
3. High Sensitivity to Noise and Motion Artifacts	Wearable EEG introduces electrode noise, impedance changes, and movement artifacts that degrade model accuracy. Few studies propose robust DSP pipelines tailored for low-quality EEG [9, 31].
4. Limited Feature Robustness Across Subjects	Traditional handcrafted features often fail to generalize across patient populations (inter-subject variability) [3, 15]. Models need features that are computationally light but clinically meaningful.
5. Dependence on Large Deep Learning Models	CNN–LSTM and deep CNNs achieve high accuracy but are computationally expensive and unsuitable for MCUs without aggressive quantization or pruning [32, 44].
6. Insufficient Rural and Remote Health Monitoring Solutions	Most seizure detection frameworks depend on clinical datasets, hospital infrastructure, or high-bandwidth connections. Very few systems address low-resource settings with IoT-based monitoring [5, 20].
7. Lack of End-to-End Embedded System Integration	Most research focuses on algorithmic accuracy rather than full system integration (signal acquisition + DSP + ML + alerts + IoT). There is a need for practical end-to-end solutions [26, 11].

Summary

The literature indicates strong potential for automated seizure detection using DSP and ML techniques. However, challenges remain regarding:

- portability,
- computational efficiency,
- real-time constraints,
- robustness to artefacts,
- and embedded deployment practicality.

This project addresses these gaps by developing a compact, low-cost, real-time EEG seizure detection system integrating BioAmp EXG Pill acquisition, STM32 DSP, CNN–LSTM evaluation, Random Forest comparison, and ESP-12E wireless alerts.

CHAPTER 3

Chapter 3

Methodology and System Design

3.1 Methodology

This chapter explains the complete methodological workflow of the proposed non-invasive intracranial seizure detection system. The methodology integrates biomedical signal acquisition, multi-stage DSP preprocessing, feature extraction, machine learning, embedded inference, and IoT-based alerting. The structure of the methodology reflects the operational stages of modern wearable EEG systems [5, 47].

The entire system workflow is composed of the following six major blocks:

1. EEG signal acquisition using scalp electrodes and the BioAmp EXG Pill,
2. Preprocessing and noise reduction using DSP operations,
3. Segmentation and feature extraction,
4. Classification using CNN–LSTM and Random Forest models,
5. Embedded deployment on STM32F446RE microcontroller,
6. Wireless alerting and remote monitoring via ESP-12E.

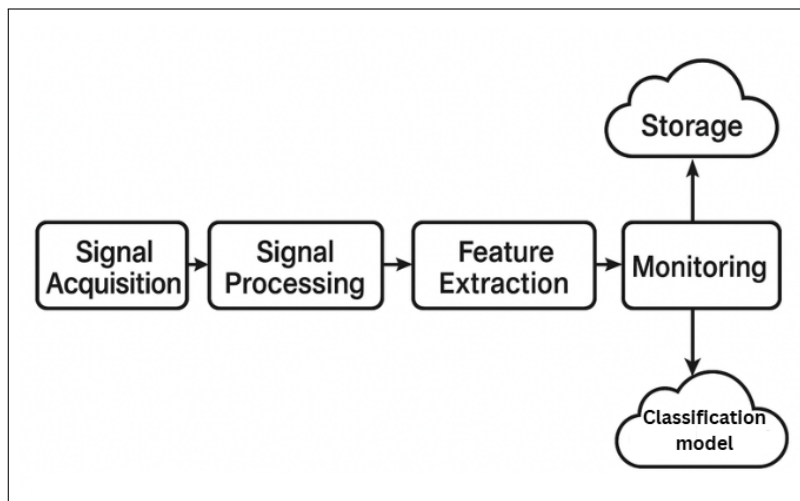


Figure 3.1: Complete system workflow from acquisition to alerting.

3.1.1 EEG Acquisition Method

The first stage involves capturing scalp EEG signals, which typically have amplitudes between 10–100 μV and are highly susceptible to noise. Wet Ag/AgCl electrodes are placed following a reduced 10–20 system configuration, targeting regions where seizure activity is most prominent

[27, 28].

The captured voltages are fed into the **BioAmp EXG Pill**, a compact analogue front-end that provides:

- differential amplification,
- high common-mode rejection,
- input protection,
- high-pass and low-pass analog filtering,
- bias referencing for stable measurement.

The amplified and conditioned signal is routed to the ADC interface of the STM32 microcontroller.

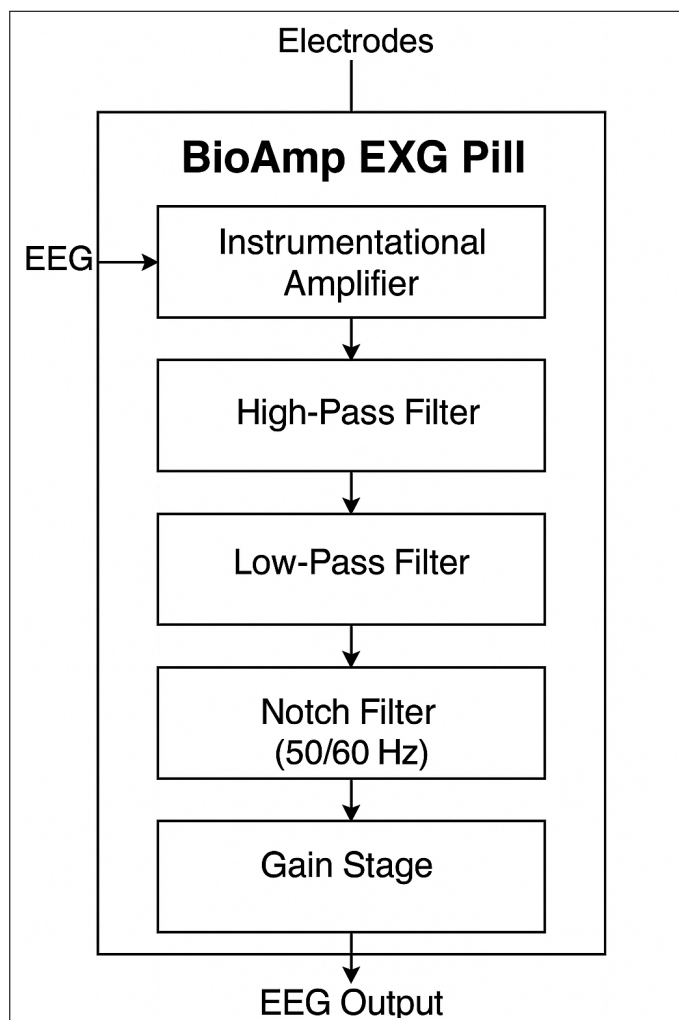


Figure 3.2: EEG acquisition using electrodes and BioAmp EXG Pill. [58]

3.1.2 Dataset Used for Model Training

The project uses a hybrid dataset containing three distinct classes:

1. **Sensor-Inactive:** Collected from the BioAmp EXG Pill when electrodes were connected but disconnected from the scalp. Represents baseline electrical noise, device hum, and ADC offsets.
2. **Normal:** Collected from real scalp EEG using the BioAmp EXG Pill during resting-state, eyes-open/closed, and non-seizure activity. This dataset captures realistic physiological noise, motion artefacts, blink artefacts, and normal cortical rhythms.
3. **Seizure:** Extracted from CHB-MIT Scalp EEG Database and other publicly available online EEG repositories. Contains labelled ictal segments of pediatric patients, with seizure onset and offset timestamps.

This dataset combination ensures that the trained model can distinguish between:

- true seizure EEG,
- normal physiological EEG,
- device-specific or electrode-specific noise.

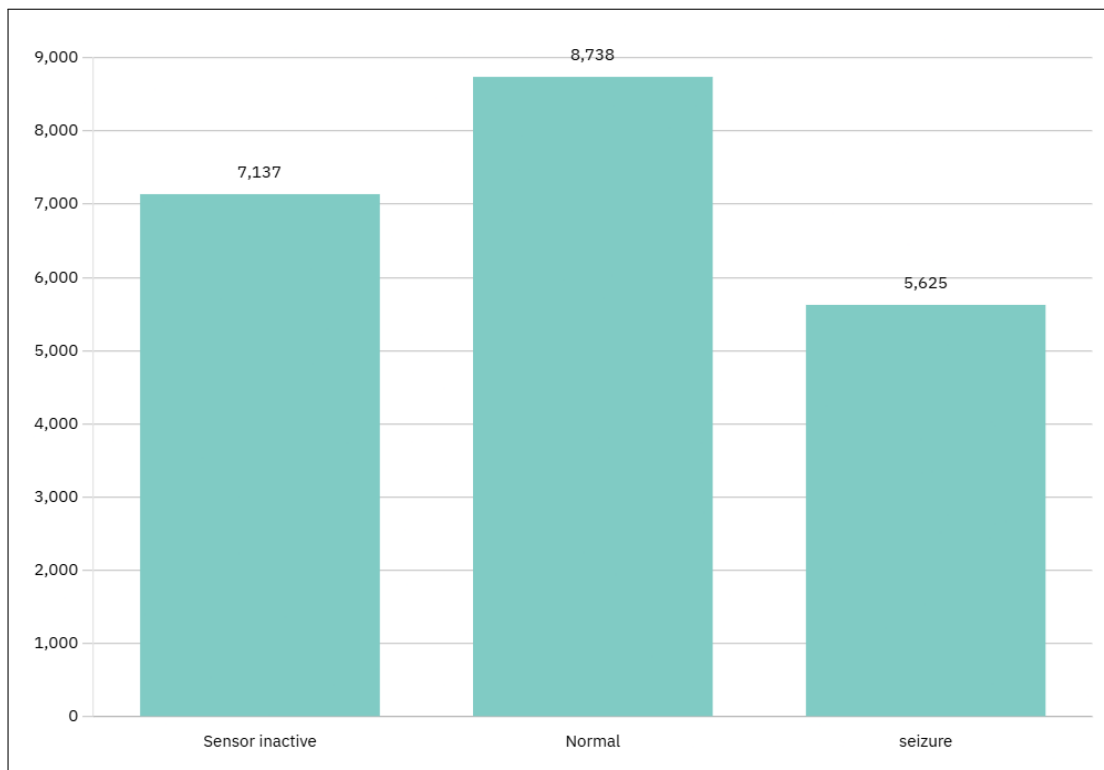


Figure 3.3: Distribution of Sensor-Inactive, Normal, and Seizure classes.

3.1.3 Signal Preprocessing and Noise Handling

Before the EEG signal can be analyzed or classified, it must be preprocessed to remove artifacts such as:

- power-line interference (50 Hz),
- baseline drift,
- muscle noise (EMG),
- blink and motion artifacts,
- ADC quantization noise.

The STM32F446RE handles DSP filtering using CMSIS-DSP functions in real time. Filtering includes:

- a 50 Hz notch filter,
- a 0.5–45 Hz FIR band-pass filter,

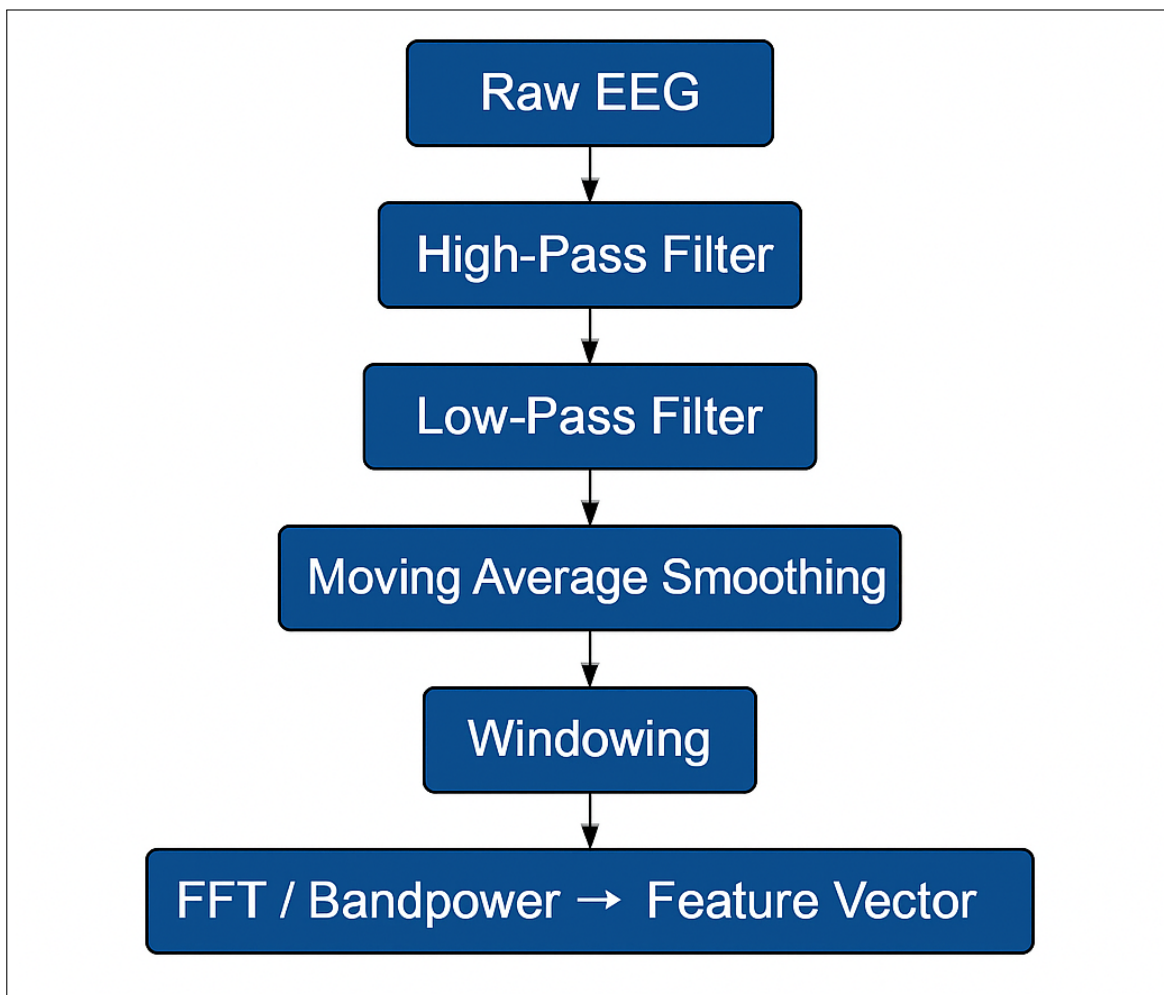


Figure 3.4: High-level DSP pipeline for EEG preprocessing.

3.1.4 Segmentation

The filtered EEG signal is segmented into fixed-length temporal windows to enable localized analysis and classification. In this work, each EEG segment corresponds to a window duration

of 1 second, which at a sampling rate of 512 Hz yields 512 samples per window. This window length represents a practical trade-off between temporal resolution and feature stability, allowing sufficient capture of seizure-related patterns while maintaining real-time processing feasibility.

To further improve sensitivity to seizure onset and offset transitions, overlapping windows are employed, typically with a 50% overlap between consecutive segments. This overlap ensures that abrupt ictal events are not missed at window boundaries and provides smoother temporal continuity in classification decisions. Prior studies, including the work of Shoeb, have demonstrated that overlapping segmentation significantly enhances seizure detection performance, particularly during rapid state transitions [39].

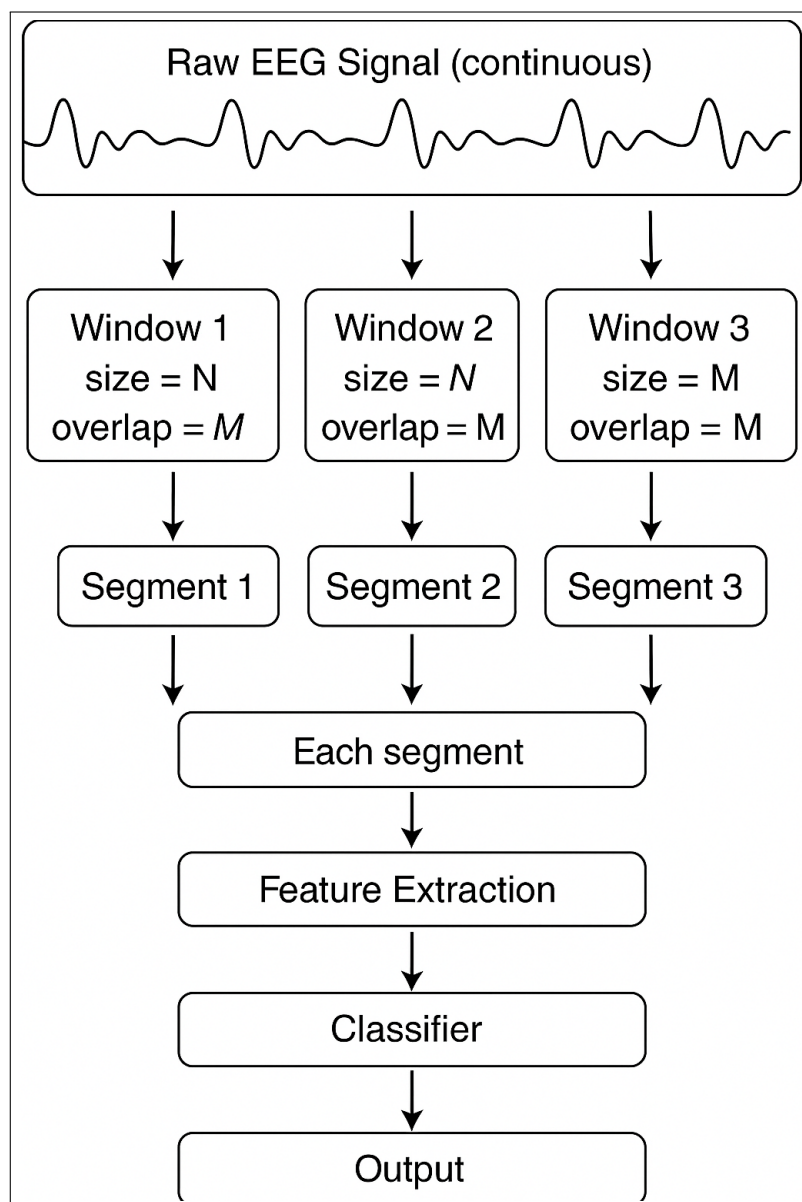


Figure 3.5: Sliding window segmentation for EEG classification.

3.1.5 Feature Extraction Overview

Feature extraction plays a critical role in transforming raw EEG signals into a compact and informative representation suitable for machine learning-based seizure classification. In the proposed system, a total of 24 features are initially extracted from each segmented EEG window, encompassing statistical, spectral, nonlinear, fractal, and MFCC-like characteristics of the signal. This diverse feature set is designed to capture complementary aspects of EEG dynamics associated with epileptic activity, including amplitude variations, frequency content, signal irregularity, and complexity.

To ensure computational efficiency and real-time feasibility on embedded hardware, a feature selection stage is employed, resulting in the selection of 18 features for use in the final machine learning model. This reduction in feature dimensionality minimizes memory usage while preserving the most discriminative information required for accurate seizure detection. The features were empirically chosen based on contribution to performance and robustness under noisy conditions.

3.1.6 Classification Models

Two models were trained and compared:

(i) CNN–LSTM Model (Accuracy: 92.51%)

- Combines convolutional neural network (CNN) layers for automatically learning discriminative spatial and frequency-domain patterns from raw or preprocessed EEG signals.
- Long short-term memory (LSTM) layers capture long-term temporal dependencies and sequential dynamics associated with seizure onset, progression, and termination.
- Particularly effective in identifying subtle pre-ictal changes, rhythmic discharges, and evolving ictal patterns that span multiple EEG windows [4, 35].
- Reduces reliance on handcrafted features by enabling end-to-end representation learning directly from EEG data.
- Performance is constrained by dataset size and diversity; robust generalization typically requires large-scale, multi-channel EEG datasets.

(ii) Random Forest Model (Accuracy: 93.51%)

- Performs reliably with smaller datasets and single-channel EEG inputs, making it well suited for embedded and resource-constrained applications.
- The ensemble-based decision structure improves robustness to noise, artefacts, and inter-subject variability commonly observed in wearable EEG recordings.
- Captures complex non-linear relationships between extracted features while mitigating overfitting through bagging and randomized feature selection [33].
- Requires significantly lower computational and memory resources compared to deep learning models, enabling efficient real-time inference on microcontrollers.
- Delivers more stable and consistent performance than deep learning approaches in limited-data and low-SNR scenarios, as reflected in the achieved accuracy.

3.1.7 Embedded Deployment Strategy

The embedded deployment strategy is designed to ensure real-time seizure detection while operating within the strict computational, memory, and power constraints of a microcontroller-based platform. The STM32F446RE serves as the central processing unit of the system and is responsible for executing the complete real-time signal processing and decision-making pipeline without reliance on external computation.

Specifically, the STM32F446RE performs the following operations:

- **ADC sampling:** Continuous acquisition of conditioned EEG signals from the BioAmp EXG Pill using the on-chip 12-bit ADC with DMA support, ensuring minimal processor overhead and deterministic sampling at 512 Hz.
- **DSP filtering:** Real-time implementation of digital notch and band-pass filters using CMSIS-DSP libraries to suppress power-line interference, baseline drift, and high-frequency noise while preserving clinically relevant EEG components.
- **Feature extraction:** Computation of time-domain, frequency-domain, and nonlinear features from each EEG window, enabling dimensionality reduction and improving robustness against noise and inter-subject variability.
- **Hybrid classification:** Execution of a lightweight, rule-inspired classification mechanism derived from the Random Forest model for on-device inference, combined with threshold-based safeguards to ensure stable operation under noisy or ambiguous signal conditions.
- **Real-time communication:** Packaging and transmission of extracted features, classifi-

cation outputs, and system status information to the ESP-12E module via UART with framing and checksum validation to ensure reliable data transfer.

The embedded firmware is implemented using a modular, interrupt-driven architecture that prioritizes real-time constraints. DMA-based data acquisition and block-based DSP processing ensure predictable execution timing, while careful memory allocation avoids dynamic memory usage, enhancing system stability. This design enables continuous operation with bounded latency, making the system suitable for long-term, real-world deployment.

3.1.8 Wireless Transmission and Alerting

Wireless communication and alerting constitute the final stage of the system pipeline, enabling both remote monitoring and immediate local notification. The ESP-12E WiFi module acts as a communication gateway between the embedded seizure detection unit and external monitoring interfaces.

The ESP-12E transmits the following information over Wi-Fi:

- **Seizure alerts:** Real-time alert messages generated upon detection of epileptic activity, allowing caregivers or clinicians to respond promptly.
- **Feature vectors:** Selected EEG feature values for visualization, logging, and optional offline analysis, supporting clinical review and system validation.
- **real-time EEG streams:** Downsampled EEG waveform segments transmitted for live visualization on a web-based dashboard.
- **Dashboard updates:** Periodic system status updates, including timestamps, classification labels, and confidence indicators, rendered through a lightweight web interface.

Communication between the STM32 and ESP-12E is implemented using a structured serial protocol with start-of-frame markers and integrity checks to ensure robustness against packet loss or corruption. The Wi-Fi interface enables both local-area and internet-based connectivity, facilitating deployment in home, clinical, and remote healthcare environments. In addition to wireless alerts, a buzzer integrated on the hardware board provides immediate auditory feedback when a seizure is detected. This local alert mechanism operates independently of network availability, ensuring fail-safe notification even in the absence of Wi-Fi connectivity. The combination of local and remote alerting enhances system reliability and ensures timely intervention under diverse operating conditions.

3.2 Hardware Implementation

The hardware architecture of the proposed non-invasive intracranial monitoring system integrates biosignal acquisition, analog signal conditioning, digital sampling, embedded processing, and wireless communication into a compact low-power platform. The system is designed to be wearable, safe for long-term monitoring, and robust against noise—key requirements for practical EEG-based seizure detection [16, 27].

This chapter presents each hardware module in detail, along with placeholders for diagrams, pinouts, physical images, wiring layouts, and PCB snapshots.

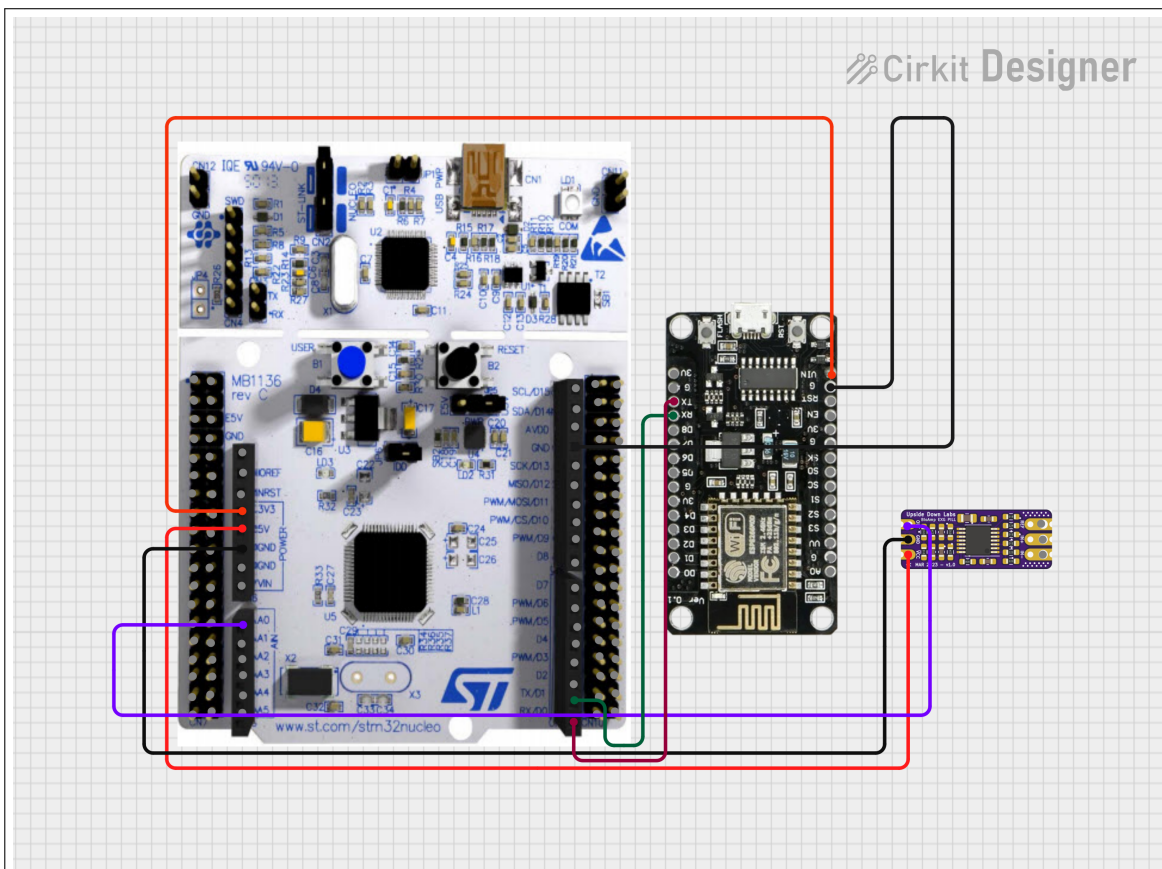


Figure 3.6: Circuit diagram of the system.

Credit: Angel Lalu, Department of EEE, AIT

The hardware consists of the following major components:

1. EEG electrodes (Ag/AgCl scalp electrodes),
 2. BioAmp EXG Pill analog front-end (AFE),
 3. STM32F446RE microcontroller,
 4. ESP-12E Wi-Fi communication module,
 5. Local alerting mechanism (buzzer + LED),

6. Power management subsystem,
7. Supporting PCB and wiring harness.

3.2.1 EEG Electrodes and Sensor Interface

EEG acquisition begins at the electrodes, which convert ionic scalp potentials into measurable electrical signals. Wet Ag/AgCl electrodes were selected due to their:

- low impedance,
- stable skin-electrode interface,
- minimal noise contribution,
- suitability for microvolt-level signals,

as supported by prior EEG instrumentation studies [24, 9].

Electrode placement followed a reduced 10–20 configuration targeting frontal, temporal, and parietal regions depending on expected seizure origin.

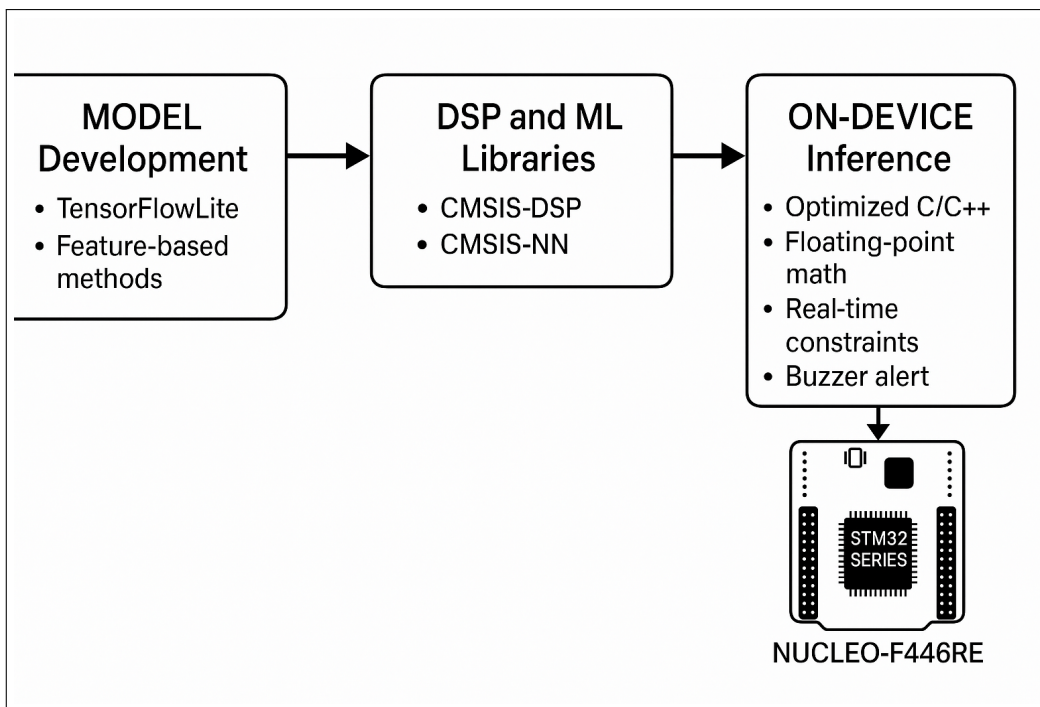


Figure 3.7: Electrode placement diagram (following 10–20 reduced montage)[58].

The electrode interface includes shielded wires to minimize electromagnetic interference (EMI) and cable motion artifacts.

3.2.2 BioAmp EXG Pill – Analog Front-End (AFE)

The **BioAmp EXG Pill** is the core analog conditioning module responsible for acquiring clean EEG signals before digitization. EEG signals (10–100 μ V) require amplification, filtering, and high common-mode rejection. The EXG Pill integrates:

- a low-noise instrumentation amplifier,
- high-pass and low-pass analog filtering,
- reference biasing,
- motion-artefact suppression mechanisms,
- protection circuitry for user safety.

Studies confirm that compact, low-power front ends using similar architecture are highly suitable for wearable EEG applications [25, 43].

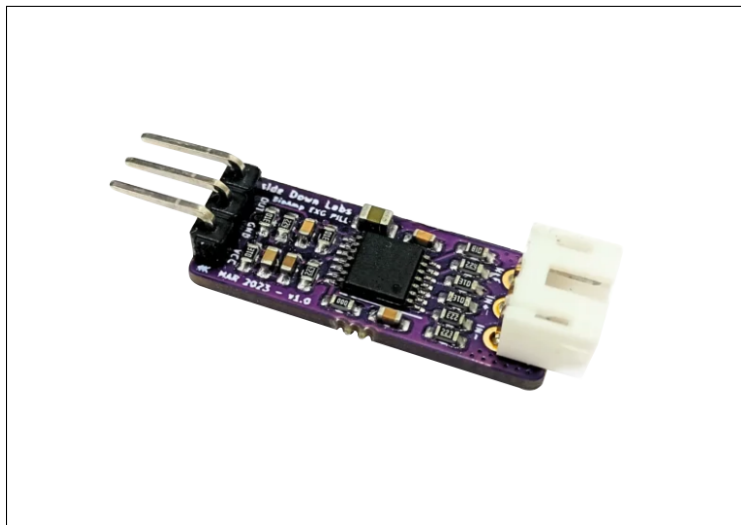


Figure 3.8: BioAmp EXG Pill module photograph.[58]

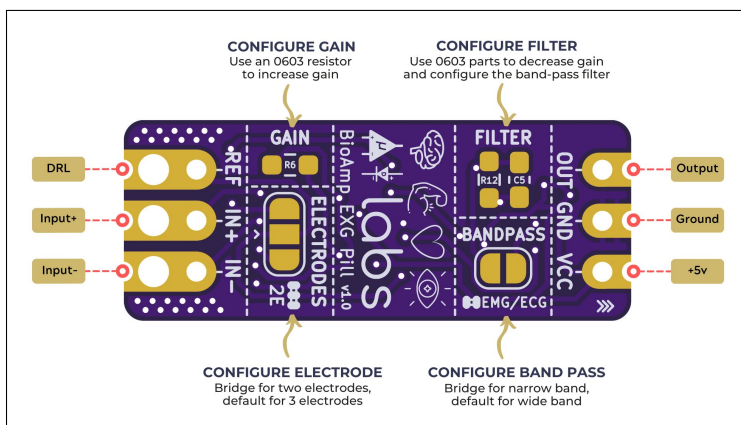


Figure 3.9: BioAmp EXG Pill pinout diagram.[58]

Signal Conditioning Path

The signal path inside the BioAmp EXG Pill consists of:

1. **Instrumentation amplifier stage** Provides differential amplification and high CMRR, essential for rejecting noise and 50 Hz interference.
2. **High-pass filter (HPF)** Removes baseline drift from sweat, electrode movement, and DC offsets.
3. **Low-pass filter (LPF)** Limits bandwidth to EEG frequencies (0.5–45 Hz), preventing aliasing at the microcontroller ADC.
4. **Bias/reference driver** Maintains stable electrode offset potentials.
5. **Output buffer** Ensures low impedance output for clean sampling by the ADC.

Table 3.1: Operating parameters and analog front-end specifications of the BioAmp EXG Pill [58].

Parameter	Specification
Input Signal Range	$\pm 5 \text{ mV}$ (suitable for EEG/EMG/ECG microvolt signals)
Gain Stages	Programmable gain up to $\approx 1000\times$ using multi-stage active filters
Input Impedance	$> 10 \text{ M}\Omega$ (ensures minimal loading of electrodes)
High-Pass Filter (HPF)	$\approx 0.5 \text{ Hz}$ cutoff (removes DC drift)
Low-Pass Filter (LPF)	$\approx 40\text{--}50 \text{ Hz}$ cutoff (removes high-frequency noise)
Notch Filter	50/60 Hz mains interference suppression
Operating Voltage	3.3 V (compatible with STM32, ESP32, Arduino)
Output Signal Range	0–3.3 V (post-amplification, MCU-safe)
Noise Performance	Optimized instrumentation amplifier front stage for μV -level biosignals
Recommended Electrode Type	Standard wet electrodes or low-noise dry electrodes

3.2.3 STM32F446RE Microcontroller Unit

The **STM32F446RE** serves as the computational core of the system. It handles:

- 12-bit ADC sampling of EEG signals,
- DSP preprocessing (notch + band-pass filters),
- FFT computation,
- feature extraction (24 features),
- embedded threshold-based seizure detection,
- UART communication with ESP-12E.

ARM Cortex-M4 processors with DSP extensions are widely used in biomedical embedded systems due to their low latency and high efficiency [47, 26].

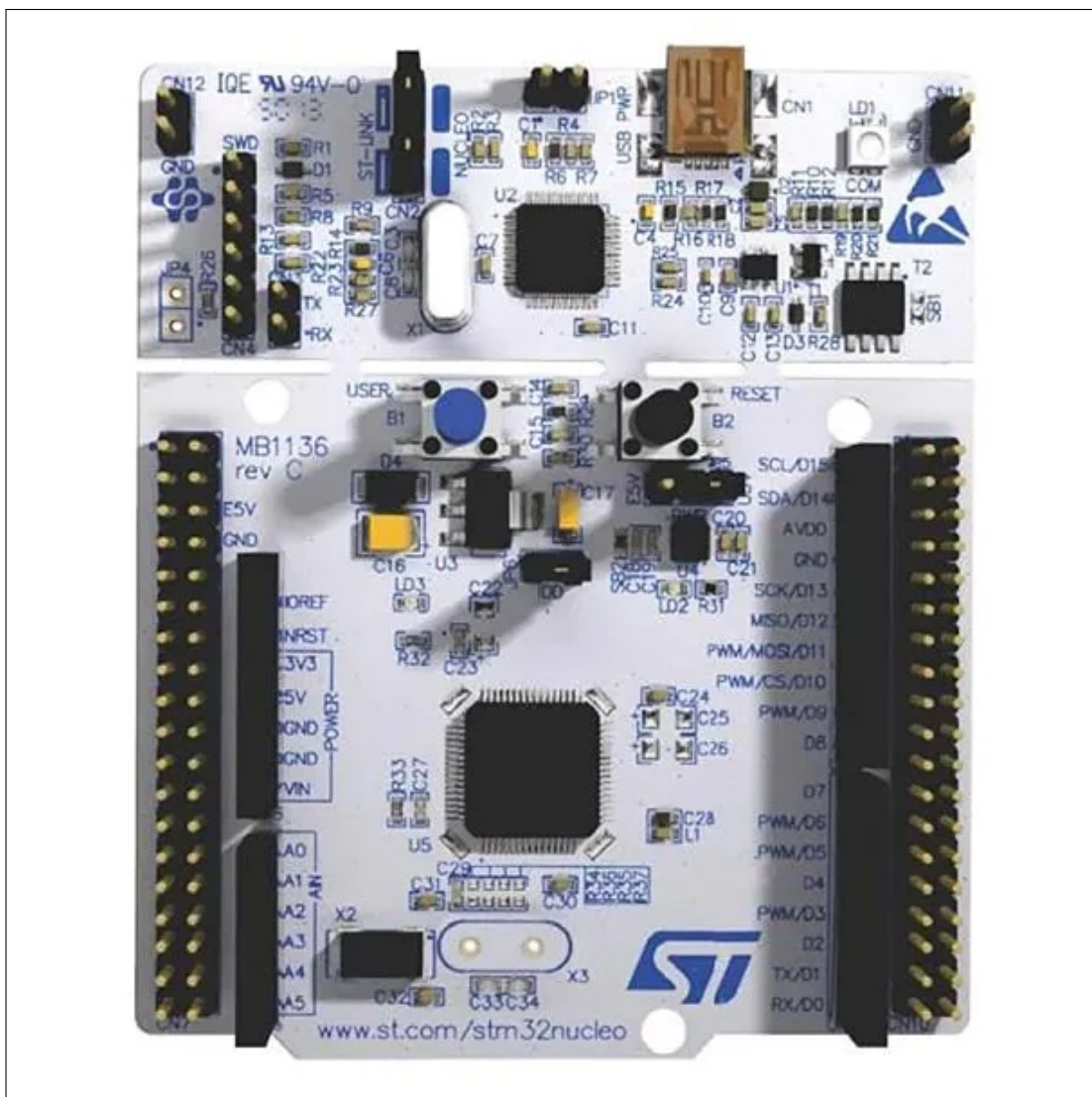


Figure 3.10: STM32F446RE Development Board [63]

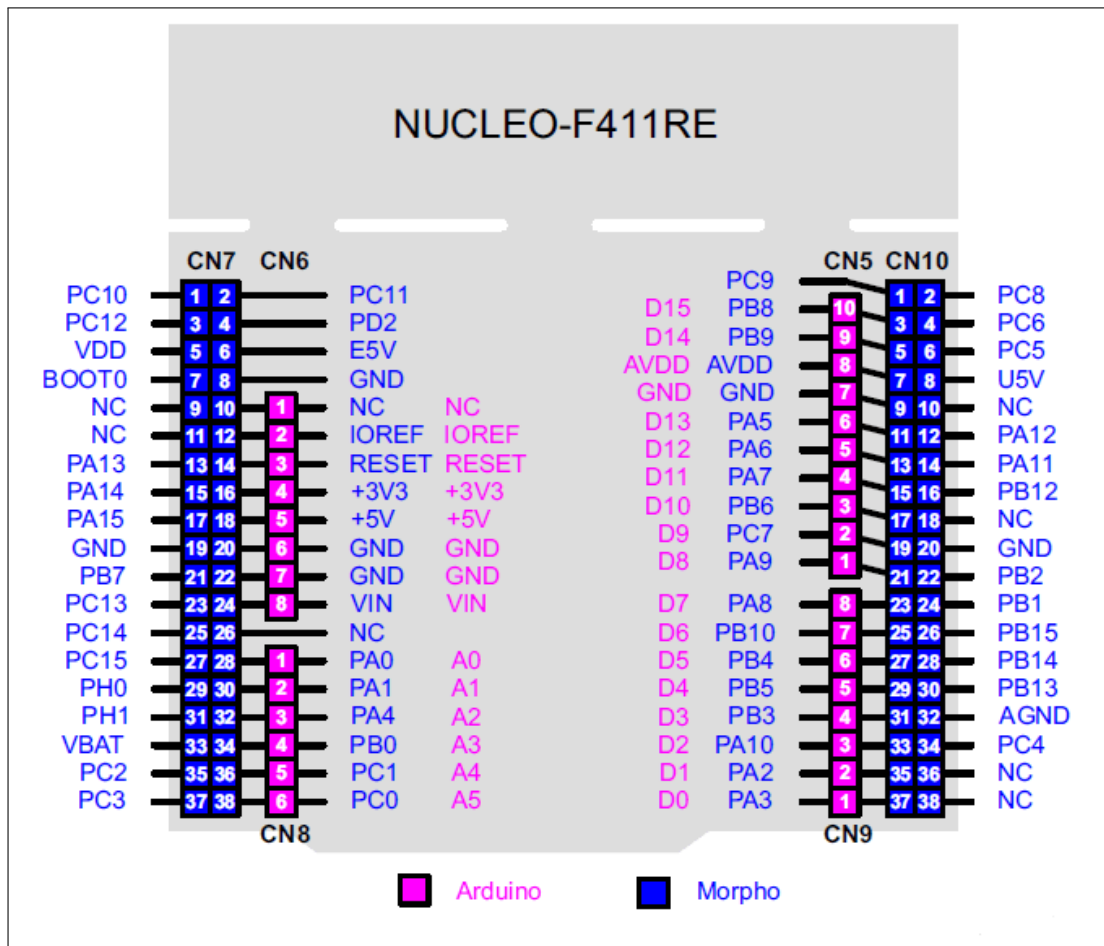


Figure 3.11: STM32F446RE pinout diagram.[61]

ADC Configuration

The ADC is configured to ensure accurate and continuous acquisition of low-amplitude EEG signals under real-time constraints. The configuration includes:

- 12-bit resolution to capture microvolt-level EEG variations,
- a sampling frequency of 256–512 Hz to preserve clinically relevant EEG bandwidth,
- right alignment to facilitate fast fixed-point and integer-based computation,
- DMA double-buffer mode for uninterrupted, continuous data acquisition.

The use of DMA enables zero-sample loss and deterministic timing by decoupling data transfer from CPU execution, which is critical for reliable biomedical signal monitoring and real-time seizure detection [64]. This configuration also minimizes processor overhead, allowing the microcontroller to dedicate computational resources to DSP filtering and feature extraction without timing violations.

Table 3.2: Key specifications of the STM32F446RE microcontroller [63].

Parameter	Specification
Core	ARM Cortex-M4 with FPU (Floating Point Unit)
CPU Frequency	Up to 180 MHz
Flash Memory	512 KB on-chip Flash
SRAM	128 KB total SRAM
ADC	12-bit, up to 2.4 MSPS, 16 channels
Timers	17 timers (including advanced-control, general-purpose, and watchdog timers)
Communication Interfaces	3× SPI, 3× I2C, 4× USART, 1× UART, 2× CAN, USB OTG Full-Speed, SDIO
DMA	16-stream DMA with FIFO support
Operating Voltage	1.7 V to 3.6 V
GPIO Pins	81 programmable I/O pins
Timers for DSP / Motor Control	Advanced PWM, input capture, output compare
Package Type	LQFP-64
Power Consumption	Ultra-low-power modes: Sleep / Stop / Standby
Target Applications	DSP processing, motor control, sensor fusion, portable embedded systems

DSP Processing Role

The STM32 implements:

- a 50 Hz notch filter,
- a FIR band-pass filter (0.5–45 Hz),
- spectral decomposition using FFT,
- 24-feature computation per window,
- ML-inspired rule-based decision logic.

Detailed formulas appear in Chapter 5.

3.2.4 ESP-12E (ESP8266) Wireless Module

The ESP-12E module provides Wi-Fi communication for:

- transmitting feature vectors,
 - sending seizure alerts,
 - hosting a lightweight dashboard,
 - connectivity to external caregivers,
 - pushing events to cloud storage.

The ESP8266 is a popular choice in IoT biomedical systems due to its low cost, built-in TCP/IP stack, and ease of integration [11].



Figure 3.12: ESP-12E (ESP8266) module photograph.[62]

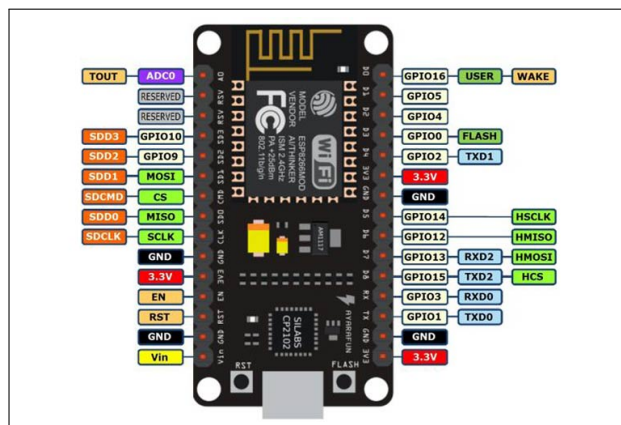


Figure 3.13: ESP-12E pinout diagram.[62]

The module communicates with the STM32 over UART using a custom-framed JSON structure for reliability.

Table 3.3: Key specifications of the ESP-12E (NodeMCU ESP8266) Wi-Fi module [62].

Parameter	Specification
Microcontroller	Tensilica Xtensa L106 32-bit RISC processor
Clock Frequency	80 MHz (default), up to 160 MHz
Flash Memory	Typically 4 MB (varies by board)
SRAM	64 KB instruction RAM + 96 KB data RAM
Operating Voltage	3.0–3.6 V (logic level 3.3 V)
Power Consumption	80 mA average (WiFi TX/RX), 20 µA deep sleep mode
Wi-Fi Standard	802.11 b/g/n, 2.4 GHz
Wi-Fi Modes	Station mode, Soft-AP, Station + Soft-AP
Security	WPA/WPA2, WEP, TKIP, AES
Communication Interfaces	1× UART, 1× I2C (software), 1× SPI, 1× I2S, ADC (10-bit), PWM (software)
GPIO Pins	11 GPIOs (multiplexed with peripheral functions)
ADC	1-channel, 10-bit ADC (max input 1.0 V unless attenuated)
Network Features	DHCP, DNS, TCP/IP stack, HTTP/MQTT support
Antenna	On-board PCB antenna
Package	ESP-12E shielded module

3.2.5 Local Alerting Mechanism

To ensure immediate response during seizure events, the system incorporates a local alerting mechanism that operates independently of network connectivity. This ensures timely notification even in scenarios where wireless communication is unavailable or delayed. The local alerting components include:

- a piezo buzzer for audible seizure alerts,
- onboard LED indicators for visual status and alert signaling,
- a fail-safe indicator to notify sensor disconnection or signal loss.

These alerts provide real-time feedback to nearby caregivers and users, enhancing system reliability and safety during continuous monitoring.

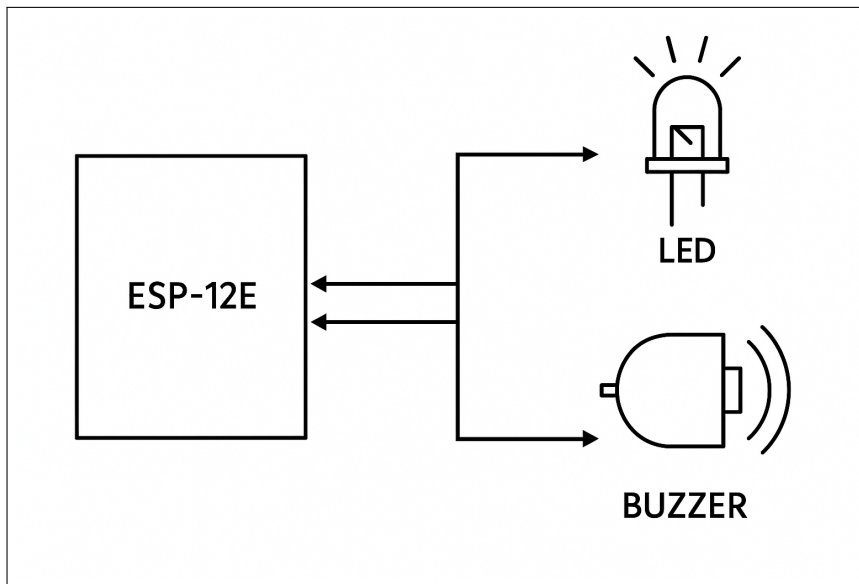


Figure 3.14: Buzzer and LED alerting subsystem diagram.

This subsystem ensures alerts are triggered even without Wi-Fi connectivity.

3.2.6 Power Supply and Regulation

In the prototype implementation, the system was powered directly from a laptop USB port, providing a stable 5 V supply through the USB interface. This choice ensured continuous, noise-free operation during testing, without the variability introduced by battery discharge.

The 5 V USB rail is internally regulated down to 3.3 V for the STM32F446RE, ESP-12E, and BioAmp EXG Pill. Although the prototype does not yet include a dedicated Li-ion/Li-Po battery stage, the design remains compatible with wearable power architectures for future work, including:

- onboard low-dropout (LDO) 3.3 V regulation,
- analog–digital ground separation to minimize noise coupling,
- ferrite-bead filtering for switching-noise suppression,
- low-ripple power rails for sensitive EEG acquisition electronics.

Wearable EEG systems depend heavily on power efficiency and low noise [5]; therefore, the prototype's USB-powered design focuses on stability and repeatability rather than portability.

Table 3.4: Power supply characteristics of the prototype EEG system.

Parameter	Specification
Primary Power Source	Laptop USB port (5 V, regulated)
Voltage Regulator	On-board 3.3 V LDO (NodeMCU + Nucleo board regulators)
Analog Front-End Supply	3.3 V (BioAmp EXG Pill)
Digital Controller Supply	3.3 V (STM32F446RE + ESP-12E)
USB Current Availability	Up to 500 mA (USB 2.0), adequate for entire system
Isolation	Logical separation of analog and digital grounds provided by PCB layout of interfacing modules
Filtering Components	On-board decoupling capacitors and ferrite beads on powering modules
Future Wearable Upgrade	Li-ion/Li-Po battery + dedicated LDO + analog filtering (not implemented in prototype)

3.2.7 Wiring Diagram and PCB Layout

A custom PCB (or structured prototyping board) is used to interconnect all system components compactly and reliably. Careful layout is essential in EEG systems due to the extremely low signal amplitudes and high susceptibility to noise. Good EEG PCB design practices adopted in this work include:

- separating analog and digital ground planes to reduce noise coupling,
- minimizing analog trace lengths to preserve signal integrity,
- shielding sensitive analog paths from digital and RF interference,
- proper placement of decoupling capacitors near power pins,
- reducing electromagnetic coupling from the ESP8266 RF stages.

These design considerations help maintain signal fidelity while ensuring stable operation of both the analog front-end and digital processing units. Careful grounding and isolation also reduce susceptibility to motion artifacts and external electromagnetic interference during long-term operation.

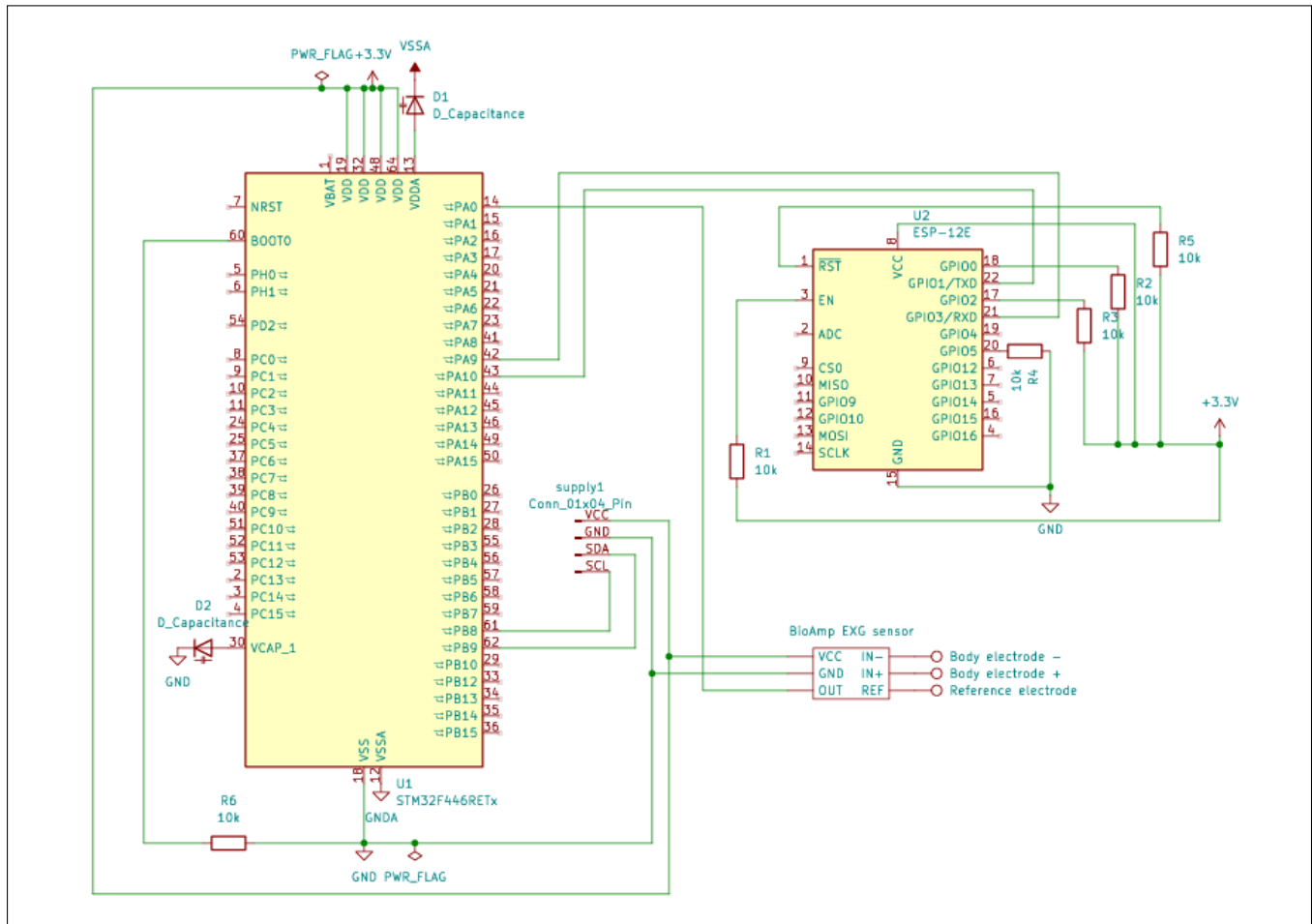


Figure 3.15: Full wiring diagram for STM32, EXG Pill, ESP-12E, and sensors.



Figure 3.16: PCB design layout for the complete system.

3.3 Software Implementation

The software subsystem forms the analytical and computational core of the proposed non-invasive EEG seizure detection system. While the hardware modules are responsible for acquiring, amplifying, and digitizing neural signals, the software pipeline performs all higher-level processing and decision-making tasks. These include digital filtering and denoising, signal segmentation, feature engineering, machine learning-based inference, rule-based validation, wireless communication, and overall system supervision. As a result, the accuracy, reliability, and real-time performance of the entire system are largely determined by the efficiency of the software design.

This chapter presents a comprehensive description of the firmware architecture, digital signal processing (DSP) modules, feature extraction pipeline, model development workflow, real-time embedded decision logic, and the communication protocol used for wireless alerting and visualization. The software stack is specifically optimized for execution on the STM32F446RE microcontroller in conjunction with the ESP-12E Wi-Fi module, ensuring predictable timing, low memory usage, and energy efficiency. Design decisions are guided by established biomedical signal processing and embedded EEG system principles described in prior literature [34, 47, 38].

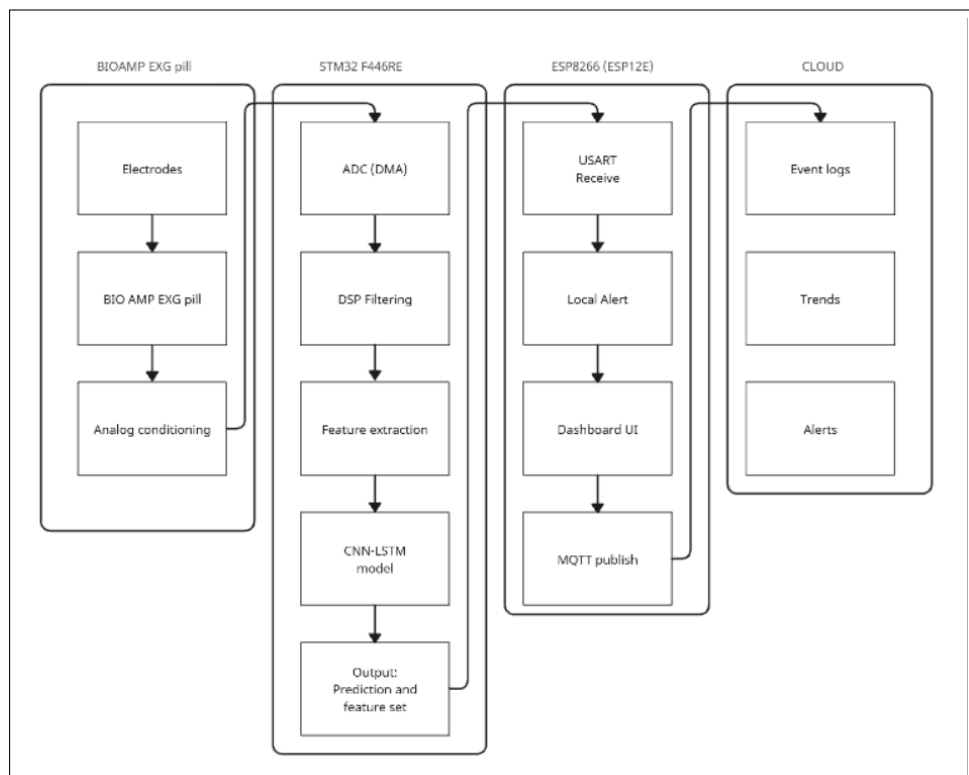


Figure 3.17: Firmware architecture block diagram illustrating data flow and processing stages.

The overall software workflow follows a sequential and modular processing pipeline, enabling continuous real-time operation:

```
ADC Sampling → DSP Pipeline → Segmentation  
→ Feature Extraction → Model Inference (CNN–LSTM / RF)  
→ Alert Generation and Wireless Transmission
```

3.3.1 Firmware Execution Model

The embedded firmware is designed around a deterministic execution model to meet real-time constraints and ensure stable long-term operation. The STM32 microcontroller employs a combination of interrupt-driven control flow and direct memory access (DMA) to decouple data acquisition from signal processing and classification tasks. This architecture minimizes latency and prevents data loss even during computationally intensive operations.

Specifically, the STM32 firmware utilizes:

- ADC with DMA-based double-buffering to support continuous, lossless EEG sampling,
- interrupt-driven scheduling to guarantee deterministic execution and bounded latency,
- CMSIS-DSP library acceleration for efficient implementation of digital filters and FFT-based spectral analysis,
- fixed-size sliding windows to enable consistent segmentation and window-wise classification,
- a hybrid inference mechanism combining rule-based thresholds with machine learning confidence scores to enhance robustness.

This execution model ensures that signal acquisition, DSP operations, feature extraction, and inference are performed within strict timing constraints, even under peak computational load. By avoiding dynamic memory allocation and prioritizing fixed-size buffers, the firmware achieves predictable performance, making it suitable for continuous biomedical monitoring and real-time seizure detection applications.

Algorithm 3.1 Firmware Execution Pipeline for Real-Time Seizure Detection

```

1: Initialise ADC, DMA (double buffer), UART, GPIO, timers, and DSP modules
2: Configure bandpass and notch filters (CMSIS-DSP)
3: Initialize feature extraction buffers and classification model parameters
4: while system is running do
5:   Wait for DMA half/full transfer interrupt
6:   if DMA half-buffer is ready then
7:     Copy half-buffer into processing buffer
8:     Apply bandpass + notch filtering
9:     Perform sliding-window segmentation
10:    Extract features (RMS, entropy, variance, bandpower)
11:    Predict seizure state using Random Forest model
12:    if prediction == SEIZURE then
13:      Send alert flag to ESP-12E via UART
14:      Activate buzzer and LED indicators
15:    end if
16:  end if
17:  if DMA full-buffer is ready then
18:    Repeat same processing pipeline for second half-buffer
19:  end if
20: end while

```

3.3.2 ADC Sampling and Preprocessing

The EEG signal is sampled at 256 Hz, chosen because it provides sufficient coverage of EEG frequency bands (0–45 Hz) as shown in biomedical literature [27].

The ADC output is converted into bipolar voltage using:

$$V[n] = 3.3 \times \frac{\text{ADC}[n]}{4095} - 1.65$$

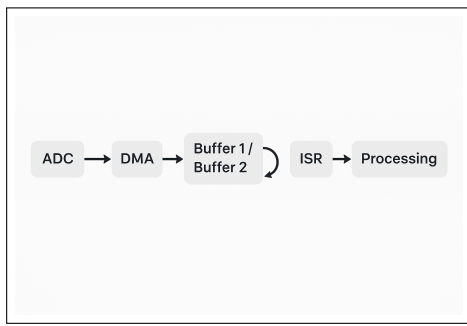


Figure 3.18: ADC + DMA double-buffer diagram.

3.3.3 Digital Signal Processing (DSP) Pipeline

The DSP pipeline is responsible for:

1. noise removal,
2. isolation of EEG bands,
3. spectral conversion,
4. preparing data for feature extraction.

The stages are described below.

50 Hz Notch Filter

Power-line interference is removed using a biquad IIR notch filter:

$$H(z) = \frac{1 - 2 \cos(\omega_0)z^{-1} + z^{-2}}{1 - 2r \cos(\omega_0)z^{-1} + r^2 z^{-2}}$$

Where:

$$\omega_0 = \frac{2\pi \cdot 50}{512}, \quad r = 0.98$$

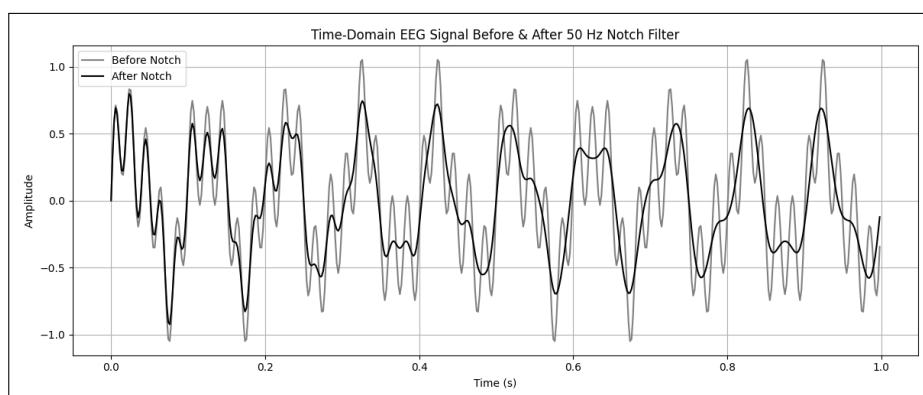


Figure 3.19: 50 Hz notch filter response plot.

301-Tap FIR Band-Pass Filter (0.5–45 Hz)

The FIR filter is designed using a Kaiser window:

$$h[n] = (2f_2 \operatorname{sinc}(2f_2 n) - 2f_1 \operatorname{sinc}(2f_1 n)) w[n]$$

Where $f_1 = 0.5/512$ and $f_2 = 45/512$.

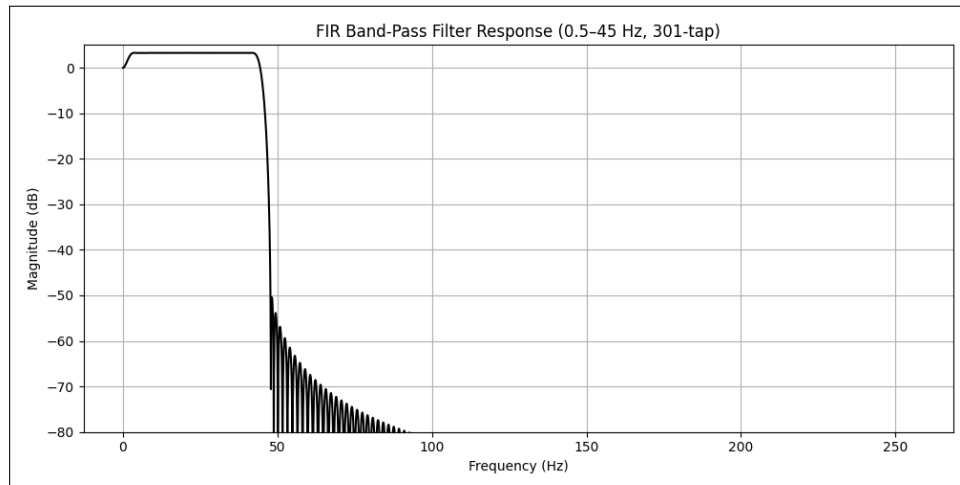


Figure 3.20: FIR band-pass magnitude response (0.5–45 Hz).

Sub-Band FIR Filtering

Eight FIR filters extract EEG subbands:

- Delta (0.5–4 Hz)
- Theta (4–8 Hz)
- Low Alpha (8–10 Hz)
- High Alpha (10–13 Hz)
- Low Beta (13–20 Hz)
- High Beta (20–30 Hz)
- Low Gamma (30–45 Hz)
- High Gamma (45–70 Hz)

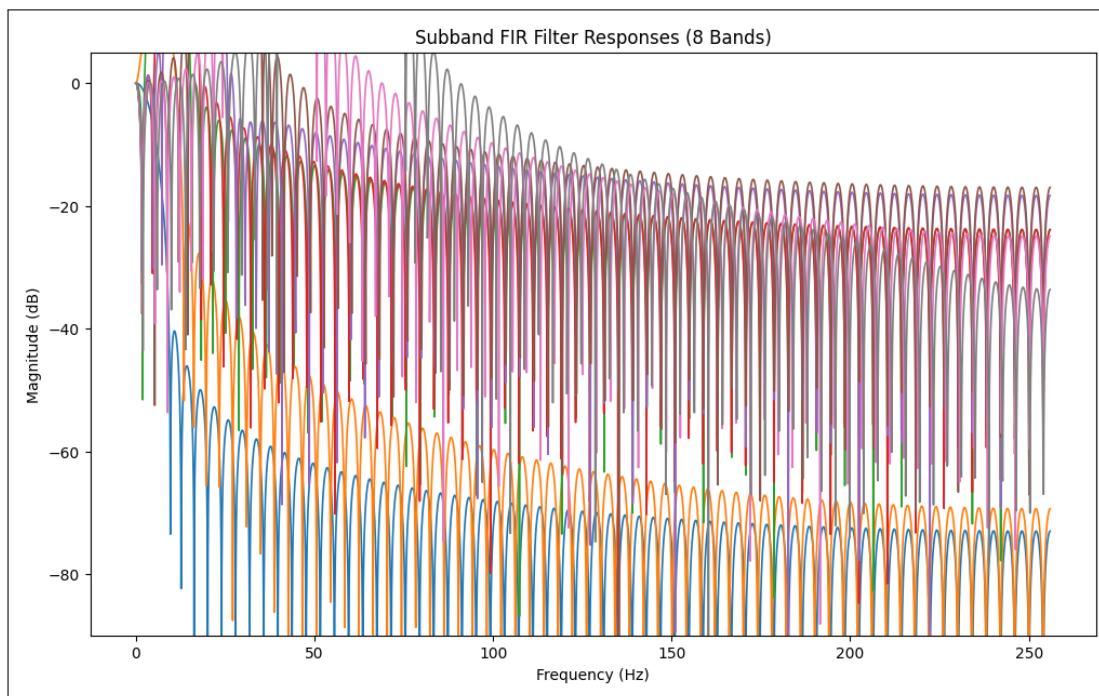


Figure 3.21: Subband filter responses.

3.3.4 Windowing and Segmentation

A window of $N = 512$ samples is extracted every 256 samples (50% overlap):

$$W_i = \{x[iR], x[iR + 1], \dots, x[iR + N - 1]\}$$

$$R = N/2$$

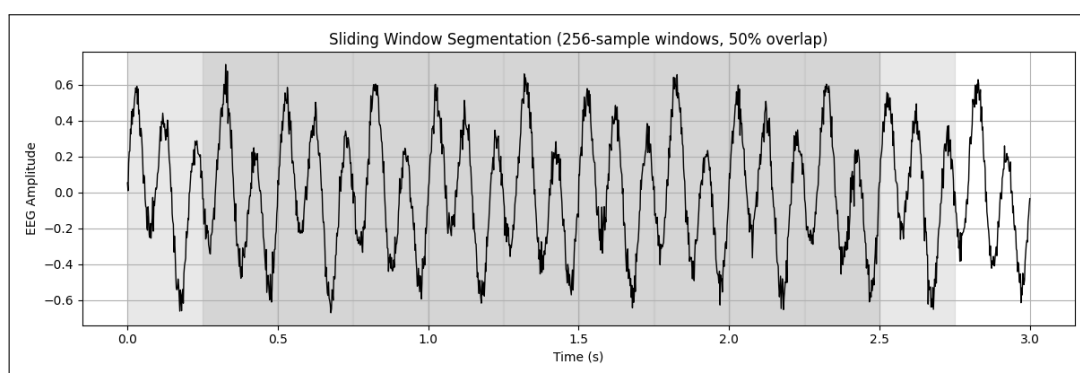


Figure 3.22: Window segmentation.

3.3.5 Feature Extraction (24 Features)

The firmware computes 24 features grouped into: (1) Time-domain (2) Frequency-domain (3) Statistical (4) Nonlinear (5) MFCC-like (6) AR modeling

Time-Domain Features

1. Root Mean Square (RMS)

$$\text{RMS} = \sqrt{\frac{1}{N} \sum_{n=0}^{N-1} x[n]^2}$$

Algorithm 3.2 RMS Computation for EEG Buffer

Input: $x[n]$; $\text{// Input EEG buffer of length } N$

Output: RMS value

for $n \leftarrow 0$ **to** $N - 1$ **do**

- $\quad \text{sum} \leftarrow \text{sum} + x[n]^2$

$\text{mean} \leftarrow \text{sum} / N \quad \text{RMS} \leftarrow \sqrt{\text{mean}}$

return RMS

2. Variance

$$\sigma^2 = \frac{1}{N} \sum (x[n] - \mu)^2$$

Algorithm 3.3 Variance Computation for EEG Buffer

Input: $x[n]$ $\text{// Input EEG buffer of length } N$

Output: Variance

$\text{sum} \leftarrow 0 \quad \text{sumSq} \leftarrow 0$

for $n \leftarrow 0$ **to** $N - 1$ **do**

- $\quad \text{sum} \leftarrow \text{sum} + x[n] \quad \text{sumSq} \leftarrow \text{sumSq} + x[n]^2$

$\mu \leftarrow \text{sum}/N \quad \text{Variance} \leftarrow (\text{sumSq}/N) - \mu^2$

return Variance

Hjorth Parameters

$$\text{Activity} = \text{var}(x)$$

$$\text{Mobility} = \sqrt{\frac{\text{var}(x')}{\text{var}(x)}}$$

$$\text{Complexity} = \frac{\text{Mobility}(x')}{\text{Mobility}(x)}$$

Algorithm 3.4 Computation of Hjorth Parameters (Activity, Mobility, Complexity)

Input: $x[n]$ // Input EEG buffer of length N

Output: Activity, Mobility, Complexity

Compute first derivative: $d_1[n] = x[n] - x[n-1]$ for $n = 1$ to $N-1$ Compute second derivative:

$d_2[n] = d_1[n] - d_1[n-1]$ for $n = 2$ to $N-1$

$\text{var}_0 \leftarrow \text{Variance}(x[n])$ // Signal variance

$\text{var}_1 \leftarrow \text{Variance}(d_1[n])$ // 1st derivative variance

$\text{var}_2 \leftarrow \text{Variance}(d_2[n])$ // 2nd derivative variance

Activity $\leftarrow \text{var}_0$ Mobility $\leftarrow \sqrt{\text{var}_1/\text{var}_0}$ Complexity $\leftarrow \sqrt{\text{var}_2/\text{var}_1}/\text{Mobility}$

return (Activity, Mobility, Complexity)

Frequency-Domain Features

1. Band Powers

$$P_\delta = \sum_{0.5-4\text{Hz}} P[k] \quad P_\theta, P_\alpha, P_\beta$$

Algorithm 3.5 Bandpower Computation for EEG Signal

Input: $P[k]$ // Power spectral density (PSD) array

Input: $f[k]$ // Frequency bins corresponding to PSD

Input: $f_{\text{low}}, f_{\text{high}}$ // Band range

Output: Bandpower

power $\leftarrow 0$

for $k \leftarrow 0$ **to** $\text{length}(P) - 1$ **do**

| **if** $f_{\text{low}} \leq f[k] \leq f_{\text{high}}$ **then**
| | power \leftarrow power + $P[k]$

return power

2. Spectral Entropy

$$H = - \sum p_i \log(p_i)$$

Algorithm 3.6 Shannon Entropy Computation for EEG Signal

Input: $x[n]$ // Input EEG buffer of length N

Output: Shannon Entropy

// Step 1: Normalize the signal into a probability distribution

Compute histogram of $x[n]$ with B bins $\rightarrow h[b]$ Normalize: $p[b] \leftarrow h[b]/N$ for all bins b

// Step 2: Compute entropy

$H \leftarrow 0$

for $b \leftarrow 0$ **to** $B - 1$ **do**

if $p[b] > 0$ **then**

$H \leftarrow H - p[b] \cdot \log_2(p[b])$

return H

3. Dominant Frequency and Spectral Centroid

$$f_{\text{dom}} = f_{k:\max(P[k])}$$

$$C = \frac{\sum f_k P[k]}{\sum P[k]}$$

Algorithm 3.7 Spectral Centroid Computation for EEG Signal

Input: $P[k]$ // Power spectral density (PSD) array

Input: $f[k]$ // Frequencies corresponding to PSD bins

Output: Spectral Centroid

$\text{num} \leftarrow 0$ // Numerator accumulator

$\text{den} \leftarrow 0$ // Denominator accumulator

for $k \leftarrow 0$ **to** $\text{length}(P) - 1$ **do**

$\text{num} \leftarrow \text{num} + f[k] \cdot P[k]$ $\text{den} \leftarrow \text{den} + P[k]$

if $\text{den} = 0$ **then**

return 0 // Avoid division by zero

else

$\text{Centroid} \leftarrow \text{num}/\text{den}$ **return** Centroid

3. Spectral Flatness

$$SF = \frac{\exp\left(\frac{1}{K} \sum \ln P[k]\right)}{\frac{1}{K} \sum P[k]}$$

Algorithm 3.8 Spectral Flatness Computation for EEG Signal

Input: $P[k]$ // Power spectral density (PSD) array

Output: Spectral Flatness

$\text{geoMean} \leftarrow 0$ $\text{arithMean} \leftarrow 0$

// Compute logarithmic sum for geometric mean

for $k \leftarrow 0$ **to** $\text{length}(P) - 1$ **do**

if $P[k] > 0$ **then**

$\text{geoMean} \leftarrow \text{geoMean} + \ln(P[k])$

// Compute arithmetic mean

for $k \leftarrow 0$ **to** $\text{length}(P) - 1$ **do**

$\text{arithMean} \leftarrow \text{arithMean} + P[k]$

$\text{geoMean} \leftarrow \exp\left(\frac{\text{geoMean}}{\text{count of } P[k] > 0}\right)$ $\text{arithMean} \leftarrow \text{arithMean}/\text{length}(P)$

if $\text{arithMean} = 0$ **then**

return 0 // Avoid division by zero

else

$\text{Flatness} \leftarrow \text{geoMean}/\text{arithMean}$ **return** Flatness

Statistical Features

4. Kurtosis

$$K = \frac{m_4}{m_2^2} - 3$$

5. Skewness

$$S = \frac{m_3}{m_2^{3/2}}$$

Algorithm 3.9 Kurtosis and Skewness Computation for EEG Signal

Input: $x[n]$ // Input EEG buffer of length N

Output: Skewness, Kurtosis

```

sum ← 0 for  $n \leftarrow 0$  to  $N - 1$  do
    sum ← sum +  $x[n]$ 
 $\mu \leftarrow \text{sum}/N$  // Mean

// Compute central moments

m2 ← 0 // 2nd central moment
m3 ← 0 // 3rd central moment
m4 ← 0 // 4th central moment

for  $n \leftarrow 0$  to  $N - 1$  do
     $d \leftarrow x[n] - \mu$  m2 ← m2 +  $d^2$  m3 ← m3 +  $d^3$  m4 ← m4 +  $d^4$ 
    m2 ← m2/ $N$  m3 ← m3/ $N$  m4 ← m4/ $N$ 

// Compute skewness and kurtosis

if  $m2 = 0$  then
    return  $(0, 0)$  // Variance zero → constant signal
else
    Skewness ←  $m3/(m2^{3/2})$  Kurtosis ←  $m4/(m2^2)$ 
return  $(\text{Skewness}, \text{Kurtosis})$ 

```

6. Zero Crossing Rate

$$\text{ZCR} = \sum \mathbf{1}(x[n]x[n-1] < 0)$$

Algorithm 3.10 Zero-Crossing Rate Computation for EEG Signal

Input: $x[n]$ // Input EEG buffer of length N

Output: Zero-Crossing Rate (ZCR)

count ← 0

for $n \leftarrow 1$ **to** $N - 1$ **do**

if $(x[n-1] > 0 \wedge x[n] < 0) \text{ or } (x[n-1] < 0 \wedge x[n] > 0)$ **then**
 count ← count + 1

ZCR ← count/ $(N - 1)$

return ZCR

7. Peak-to-Peak & Crest Factor

$$\text{P2P} = x_{\max} - x_{\min}$$

$$CF = \frac{x_{\max}}{RMS}$$

Algorithm 3.11 Peak-to-Peak Amplitude and Crest Factor Computation

Input: $x[n]$ // Input EEG buffer of length N

Output: Peak-to-Peak Amplitude, Crest Factor

// Find minimum and maximum sample values

$minVal \leftarrow x[0]$ $maxVal \leftarrow x[0]$

for $n \leftarrow 1$ **to** $N - 1$ **do**

if $x[n] < minVal$ **then**

$minVal \leftarrow x[n]$

if $x[n] > maxVal$ **then**

$maxVal \leftarrow x[n]$

// Peak-to-peak amplitude

$P2P \leftarrow maxVal - minVal$

// Compute RMS for Crest Factor

$sumSq \leftarrow 0$ **for** $n \leftarrow 0$ **to** $N - 1$ **do**

$sumSq \leftarrow sumSq + x[n]^2$

$RMS \leftarrow \sqrt{sumSq/N}$

if $RMS = 0$ **then**

$Crest \leftarrow 0$ // Avoid division by zero

else

$Crest \leftarrow maxVal/RMS$

return ($P2P, Crest$)

Nonlinear Features

1. Higuchi Fractal Dimension

$$D_H = \frac{\Delta \ln(L(k))}{\Delta \ln(1/k)}$$

Algorithm 3.12 Higuchi Fractal Dimension (HFD) Computation

Input: $x[n]$ // Input EEG buffer of length N **Input:** k_{\max} // Maximum scale (typically 5-10)**Output:** Higuchi Fractal Dimension

// Initialize length array for each scale

for $k \leftarrow 1$ **to** k_{\max} **do** └ $L[k] \leftarrow 0$

// Compute curve length for each k

for $k \leftarrow 1$ **to** k_{\max} **do** **for** $m \leftarrow 1$ **to** k **do** $n_{\max} \leftarrow \lfloor \frac{N-m}{k} \rfloor$ $L_m \leftarrow 0$ **for** $i \leftarrow 1$ **to** n_{\max} **do** └ $L_m \leftarrow L_m + |x[m + i \cdot k] - x[m + (i - 1) \cdot k]|$ $L_m \leftarrow \frac{L_m \cdot (N-1)}{n_{\max} \cdot k}$ $L[k] \leftarrow L[k] + L_m$ └ $L[k] \leftarrow \frac{L[k]}{k}$ // Average over m

// Estimate slope in log-log domain

Compute linear regression of $\log(1/k)$ vs. $\log(L[k])$ Slope \leftarrow negative of fitted line slope**return** Slope as HFD

2. Petrosian Fractal Dimension

$$D_P = \frac{\log(N)}{\log(N) + \log(N/(N + 0.4Z))}$$

Algorithm 3.13 Petrosian Fractal Dimension (PFD) Computation

Input: $x[n]$ // Input EEG buffer of length N **Output:** Petrosian Fractal Dimension

// Step 1: Count number of sign changes in the first derivative

 $N_{\Delta} \leftarrow 0$ **for** $n \leftarrow 1$ **to** $N - 1$ **do** $d_1 \leftarrow x[n] - x[n - 1]$ **if** $n > 1$ **then** $d_0 \leftarrow x[n - 1] - x[n - 2]$ **if** $(d_1 > 0 \wedge d_0 < 0)$ **or** $(d_1 < 0 \wedge d_0 > 0)$ **then** $N_{\Delta} \leftarrow N_{\Delta} + 1$

// Step 2: Compute Petrosian FD

 $N_{\text{total}} \leftarrow N$ $\text{term} \leftarrow \log_2 \left(\frac{N}{N + 0.4 N_{\Delta}} \right)$ **if** $\text{term} = 0$ **then** **return** 0 // Edge case: constant or flat signal $\text{PFD} \leftarrow \frac{\log_2(N)}{\text{term}}$ **return** PFD

MFCC-Like Features

3. MFCC-like coefficients

$$c_m = \sum \log(E_n) \cos \left(\pi m \frac{n + 0.5}{B} \right)$$

Algorithm 3.14 MFCC-like Feature Computation for EEG Signal

Input: $x[n]$ // Input EEG buffer of length N

Input: f_s // Sampling rate

Input: M // Number of mel-like filterbanks

Output: MFCC-like feature vector $C[m]$

// Step 1: Compute FFT and power spectrum

Compute FFT of $x[n] \rightarrow X[k]$ $P[k] \leftarrow |X[k]|^2$ // Power spectral density

// Step 2: Apply mel-like filterbanks

Initialize $E[m] \leftarrow 0$ for all $m = 1 \dots M$

for $m \leftarrow 1$ **to** M **do**

- for** $k \leftarrow 0$ **to** $\text{length}(P) - 1$ **do**
- if** $f[k]$ lies inside filterbank m **then**
- $E[m] \leftarrow E[m] + P[k] \cdot H_m[k]$

// Step 3: Log compression

for $m \leftarrow 1$ **to** M **do**

- if** $E[m] > 0$ **then**
- $E[m] \leftarrow \log(E[m])$

// Step 4: Discrete Cosine Transform (DCT)

for $c \leftarrow 1$ **to** M **do**

- $C[c] \leftarrow 0$ **for** $m \leftarrow 1$ **to** M **do**
- $C[c] \leftarrow C[c] + E[m] \cdot \cos\left(\frac{\pi c(m-0.5)}{M}\right)$

return $C[m]$

AR Residual (Burg Method)

1. AR Modeling Residual Error

$$E = \sum_{n=0}^{N-1} e[n]^2$$

Algorithm 3.15 Burg Autoregressive (AR) Residual Computation

Input: $x[n]$ // Input EEG buffer of length N

Input: p // AR model order

Output: AR residual power

```

// Step 1: Initialize forward and backward prediction errors
for  $n \leftarrow 0$  to  $N - 1$  do
     $f[0][n] \leftarrow x[n]$   $b[0][n] \leftarrow x[n]$ 

Initialize  $E \leftarrow \sum_{n=0}^{N-1} x[n]^2/N$  // Initial error (zero-order)

// Step 2: Burg recursion for AR coefficients
for  $k \leftarrow 1$  to  $p$  do
    // Compute reflection coefficient
    num  $\leftarrow 0$  den  $\leftarrow 0$ 
    for  $n \leftarrow k$  to  $N - 1$  do
        num  $\leftarrow$  num +  $f[k-1][n] \cdot b[k-1][n-1]$  den  $\leftarrow$  den +  $f[k-1][n]^2 + b[k-1][n-1]^2$ 
    if den = 0 then
        | ref  $\leftarrow 0$ 
    else
        | ref  $\leftarrow -2 \cdot \text{num}/\text{den}$ 

    // Update forward and backward errors
    for  $n \leftarrow k$  to  $N - 1$  do
         $f[k][n] \leftarrow f[k-1][n] + \text{ref} \cdot b[k-1][n-1]$   $b[k][n-1] \leftarrow b[k-1][n-1] + \text{ref} \cdot f[k-1][n]$ 

    // Update total error
     $E \leftarrow E \cdot (1 - \text{ref}^2)$ 

return  $E$  // AR residual (prediction error power)

```

Table 3.5: Time-domain features extracted for seizure detection.

Feature	Description
RMS	Root Mean Square amplitude of the filtered EEG segment.
Variance	Signal variance (energy measure).
Hjorth Activity	Variance of the signal (activity of the EEG).
Hjorth Mobility	Square root of variance of the first derivative divided by signal variance.
Hjorth Complexity	Ratio comparing the first and second derivatives of the signal.
Zero Crossings	Number of times the signal crosses zero.
Peak-to-Peak (P2P)	Maximum minus minimum amplitude in the window.
Crest Factor	Ratio of peak amplitude to RMS value.
Skewness	Measure of asymmetry in the amplitude distribution.
Kurtosis	Measure of peakedness of the amplitude distribution.

Table 3.6: Frequency-domain features extracted for seizure detection.

Feature	Description
Dominant Frequency	Frequency bin with maximum spectral magnitude.
Spectral Centroid	Power-weighted mean frequency of the spectrum.
Spectral Flatness	Ratio of geometric mean to arithmetic mean of the PSD.
Delta Band Power	PSD power in 0.5–4 Hz.
Theta Band Power	PSD power in 4–8 Hz.
Alpha Band Power	PSD power in 8–13 Hz.
Beta Band Power	PSD power in 13–30 Hz.

Table 3.7: Advanced DSP and nonlinear features extracted for seizure detection.

Feature	Description
Shannon Entropy	Logarithmic entropy of the signal amplitude distribution.
Higuchi Fractal Dimension	Complexity measure computed using Higuchi FD algorithm.
Petrosian Fractal Dimension	Fractal complexity estimate based on sign-change rate.
Burg AR Prediction Error	Residual error from 8th-order autoregressive Burg model.

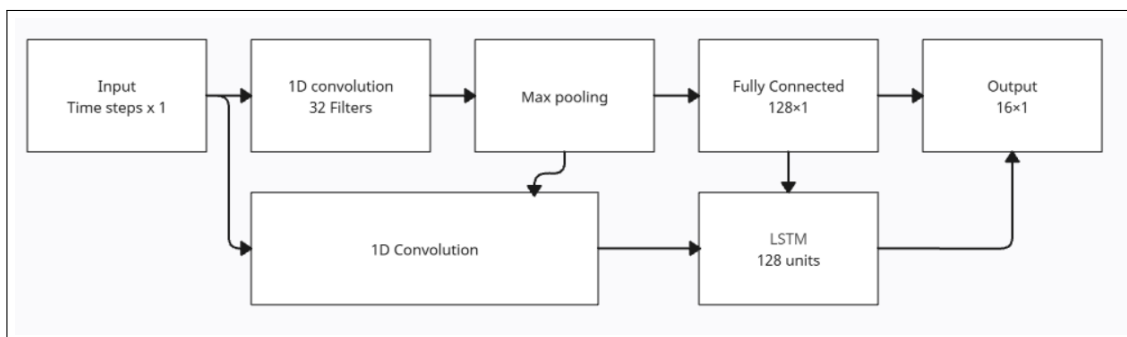
Table 3.8: MFCC-like features extracted from log-mel energies.

Feature	Description
MFCC-0	First MFCC-like coefficient derived from log-mel energies (0–70 Hz).
MFCC-1	Second MFCC-like coefficient.
MFCC-2	Third MFCC-like coefficient.

3.4 Machine Learning Model Development

Both CNN–LSTM and Random Forest models were trained. Despite CNN–LSTM achieving lower accuracy (92.51%) than Random Forest (93.51%), we still implemented CNN–LSTM because deep-learning seizure models are widely reported in literature and allow for spatial-temporal pattern extraction.

3.4.1 CNN–LSTM Architecture

**Figure 3.23:** CNN–LSTM architecture diagram.

The architecture includes:

- 1D convolution layers (EEG morphology extraction),
- LSTM recurrent layers (temporal modeling),
- fully connected layers for classification.

Dataset used:

- **Sensor Inactive (self-recorded)**
- **Normal EEG (self-recorded)**
- **Seizure EEG (CHB-MIT + other online datasets)**

Algorithm 3.16 Model Training Pipeline

Input: Preprocessed EEG feature vectors X , labels y

Output: Trained classifier \mathcal{M}

Step 1: Dataset Preparation Split (X, y) into training and validation sets Normalize features in X to zero mean and unit variance Balance classes using oversampling or class weights

Step 2: CNN-LSTM Training Reshape X into temporal windows Initialize CNN layers for spatial feature extraction Initialize LSTM layers for temporal pattern learning Train network using backpropagation and Adam optimizer Validate on held-out set and tune hyperparameters

Step 3: Random Forest Training Initialize ensemble of N decision trees Train each tree on a bootstrapped subset of features Aggregate predictions using majority voting

Step 4: Model Selection Evaluate both models on validation metrics Select best-performing model as \mathcal{M}

Algorithm 3.17 PCA Feature Reduction Workflow

Input: Feature vector $F \in \mathbb{R}^d$

Output: Reduced feature vector $F_r \in \mathbb{R}^k$

Step 1: Preprocessing Standardize F to zero mean and unit variance

Step 2: Covariance Analysis Compute covariance matrix Σ of standardized F Compute eigenvalues λ_i and eigenvectors v_i of Σ

Step 3: Component Selection Sort eigenvectors by descending eigenvalues λ_i Select top- k eigenvectors forming matrix W_k

Step 4: Projection Compute reduced feature vector: $F_r = W_k^\top F$

Return F_r

3.4.2 Random Forest Classifier

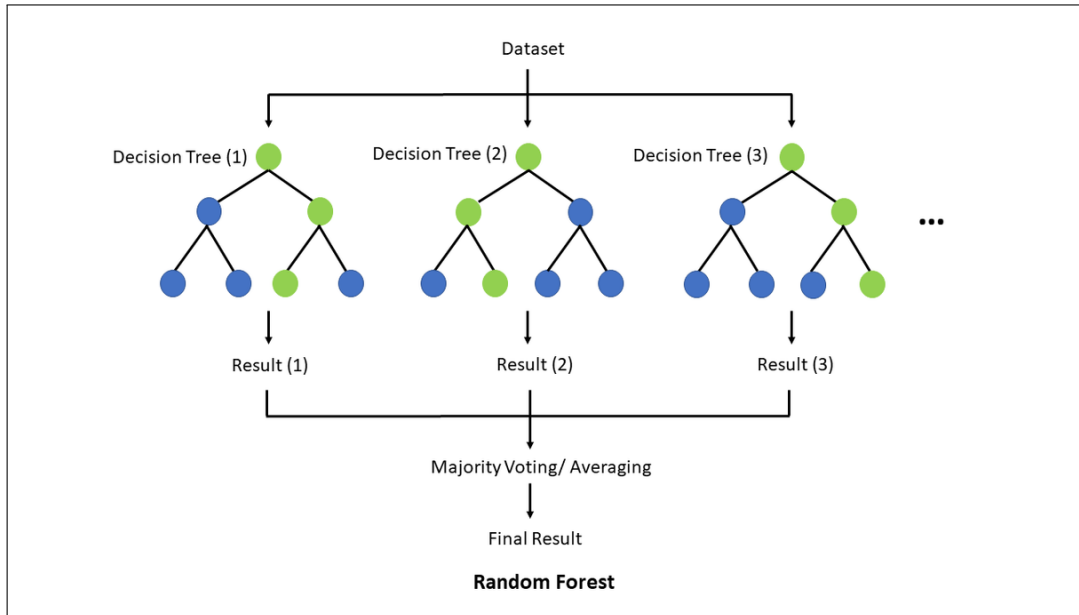


Figure 3.24: Random Forest architecture.[60]

Random Forest outperformed CNN–LSTM due to:

- smaller dataset,
- better handling of tabular feature-based inputs,
- stability under noise,
- rapid inference.

3.4.3 Embedded Seizure Detection Logic

While deep learning models such as CNN–LSTM architectures demonstrate strong seizure classification performance during offline evaluation, their direct deployment on low-power microcontrollers remains impractical. The STM32F446RE, despite offering floating-point support and DSP acceleration, is constrained by limited SRAM, Flash memory, and real-time execution requirements. As reported in prior embedded EEG studies, recurrent neural networks and deep convolutional layers typically exceed feasible memory and latency budgets unless heavily compressed or quantized, often at the cost of reliability and interpretability [47, 10].

To address these constraints, the proposed system adopts a hybrid embedded inference strategy that combines deterministic rule-based logic with knowledge distilled from the offline-trained CNN–LSTM model. Instead of executing the deep model directly on the microcontroller, its learned behavior is translated into a set of robust decision rules operating on carefully selected

DSP and statistical features. This approach preserves the discriminative power of deep learning while ensuring real-time feasibility, predictable execution time, and low memory footprint.

To improve robustness against transient noise, motion artifacts, and short-duration spikes, the detection logic incorporates a hysteresis-based decision mechanism. Rather than triggering an alert based on a single anomalous window, seizure state transitions occur only when abnormal feature conditions persist across multiple consecutive windows. This temporal smoothing strategy significantly reduces false positives and provides stable state transitions, which is critical for wearable and ambulatory monitoring systems.

Mathematically, the embedded inference logic can be summarized as:

$$\text{Hybrid Logic} = \text{Threshold-Based DSP Features} + \text{CNN-LSTM-Derived Decision Rules}$$

The complete hybrid seizure detection algorithm executed on the STM32 microcontroller is detailed below.

Algorithm 3.18 Hybrid Seizure Detection Logic

Input: Feature vector \mathbf{f} of length 24

Input: Thresholds: T_{rms} , T_{var} , T_{entropy}

Input: Hysteresis counter H and max hysteresis H_{\max}

$rule \leftarrow 0$

// Rule 1: Amplitude-based detection **if** $f_{\text{RMS}} > T_{\text{rms}}$ **or** $f_{\text{VAR}} > T_{\text{var}}$ **then**

$rule \leftarrow 1$

// Rule 2: Entropy anomaly **if** $f_{\text{Entropy}} < T_{\text{entropy}}$ **then**

$rule \leftarrow 1$

// Rule 3: MFCC anomaly Compute MFCC coefficients $\text{mfcc}[0..4]$

// Combine rules with hysteresis **if** $rule = 1$ **then**

$H \leftarrow H + 1$ **if** $H \geq H_{\max}$ **then**

$state \leftarrow \text{SEIZURE}$

else

$H \leftarrow \max(0, H - 1)$ **if** $H = 0$ **then**

$state \leftarrow \text{NORMAL}$

return $state$

3.4.4 Wireless JSON Transmission (ESP-12E)

All extracted features + seizure state are serialized:

```
< {features..., "state":"NORMAL", "crc":12345} >
```

A 16-bit MODBUS CRC ensures transmission reliability.

3.4.5 ESP-12E Web Dashboard Firmware

The ESP-12E module acts as the network and visualisation interface of the system. While the STM32F446RE performs all DSP and feature extraction, the ESP8266 receives processed EEG packets, verifies them, stores them in a circular buffer, and renders the information in a real-time web dashboard. The firmware is fully implemented in C++ using the ESP8266 Arduino SDK.

The key responsibilities of the ESP-12E software are:

1. Receiving JSON feature packets from the STM32 via UART.
2. Detecting seizure alerts and triggering local alarms.
3. Serving a rich web dashboard (HTML + CSS + JavaScript).
4. Plotting features (bandpower, dominant frequency, seizure scores).
5. Generating a live spectrogram and synthetic waveform.
6. Allowing CSV download of all received data.
7. Operating as a Wi-Fi Access Point for offline, local monitoring.

UART Interface and Handshake

The ESP8266 communicates with the STM32 via a software UART on pins D2 and D1. A handshake mechanism ensures both devices are synchronized:

1. STM32 transmits the string "HELLO_ESP".
2. ESP-12E responds with "Response".

Only after a successful handshake does the ESP enable the dashboard. This ensures the controller is correctly connected before acquiring data.

Circular Message Buffer

To store incoming JSON packets, the firmware maintains a circular buffer with 20 entries:

$$\{m_0, m_1, \dots, m_{19}\}$$

The buffer stores:

- the JSON feature string,
- a timestamp (in HH:MM:SS),
- a seizure flag extracted from the JSON.

This design allows the dashboard to retrieve the last 20 messages using the `/localdata` endpoint with very low memory overhead, which is critical for the ESP8266's limited RAM.

JSON Parsing and Feature Extraction

Each incoming UART message is enclosed in angle brackets:

`< {JSON} >`

The code strips the delimiters and passes the JSON string to a lightweight parser that extracts:

- RMS, variance, activity,
- delta, theta, alpha, beta bandpowers,
- entropy, fractal dimensions,
- dominant frequency and spectral centroid,
- seizure state.

The firmware avoids heavy JSON libraries; instead, it uses efficient string search functions (`indexOf`, custom float parsing). This ensures compatibility with the ESP8266's restricted memory footprint.

Local LED and Buzzer Alert Logic

Whenever a message contains the word "SEIZURE", the ESP triggers:

- a 3-cycle buzzer beep,
- LED flashing,
- dashboard visual flash using CSS animations.

This redundant alerting mechanism provides immediate local feedback if the internet is unavailable.

Wi-Fi SoftAP Mode

The ESP8266 does not depend on external networks. Instead, it launches its own Wi-Fi Access Point:

SSID: EEG-DASHBOARD

Password: 12345678

Clients can connect directly using a phone or laptop. The module's IP address is always:

192.168.4.1

This ensures the dashboard works offline, suitable for biomedical field deployments.

Web Server and REST Endpoints

The ESP8266 hosts a complete dashboard using the following routes:

- / – serves the full HTML dashboard.
- /localdata – returns JSON of recent feature packets.
- /clear_logs – erases circular buffer entries.
- /trigger_alert – generates a manual seizure alert.
- /reset_led – stops the alarm.
- /ping – debugging heartbeat.
- /heap – returns free RAM as JSON.

The dashboard periodically polls /localdata every 1 second.

Dashboard Rendering (HTML, CSS, JavaScript)

The dashboard is rendered entirely within the ESP—no external server is used. The front-end is built with:

- **Chart.js** for line graphs,
- **Canvas API** for the spectrogram and waveform,
- **CSS variables** for dark/light themes,
- **localStorage** to store user theme preferences.

The dashboard shows:

- real-time seizure probability line graph,
- dominant frequency graph,
- scrolling spectrogram (4-band color-coded),
- synthesized EEG waveform (reconstructed from bandpowers),
- feature grid (RMS, entropy, bandpowers, kurtosis, etc.),
- live message log,
- CSV download button.

Spectrogram Generation

The ESP does not receive raw EEG samples, only bandpower values. Yet, the dashboard reconstructs a spectrogram by treating each band as a distinct row:

$$\{\delta, \theta, \alpha, \beta\}$$

Each new measurement is shifted onto the rightmost column of a 4-row canvas. Intensity is encoded by:

$$I = \log_{10}(1 + |P|)$$

This produces a visually meaningful scrolling time-frequency plot suitable for clinical monitoring.

Synthesized EEG Waveform

The waveform is not the true raw EEG due to bandwidth limitations. Instead, the ESP synthesizes an approximate waveform using:

$$x(t) = \sum_{b \in \{\delta, \theta, \alpha, \beta\}} A_b \cdot \sin(2\pi f_b t)$$

where A_b are derived from band power magnitudes. This provides an interpretable low-resolution EEG visualization without transmitting raw data.

CSV Export Function

The dashboard allows users to download all stored EEG feature packets as a .csv file. This is useful for:

- offline analysis,
- machine learning training,
- clinical review,
- audit logs of seizure events.

All 24 features and timestamps are included in the export.

Manual Seizure Trigger Function

The dashboard includes a dedicated **Manual Seizure Trigger** button, primarily intended for system testing, demonstrations, and validation of the alert pipeline. When pressed:

1. The ESP–12E immediately generates a synthetic seizure-alert packet.
2. The buzzer and LED are activated for three alert cycles.
3. A visual *screen-flash animation* is displayed on the dashboard.
4. The message log records the event with a timestamp.

This feature allows clinicians and engineers to verify the end-to-end alert response—covering local alarms, dashboard visualization, and logging—without needing to artificially induce a real seizure in the EEG source.

Theme Engine and User Interface

The dashboard supports dark and light themes through CSS variables. User preferences are saved in `localStorage`, ensuring consistent appearance across reloads.

Animations highlight seizure events through:

- red screen flash,
- card glow,
- animated button feedback.

The interface is responsive and usable on mobile devices, enabling clinicians to monitor EEG activity from smartphones.

Dashboard Interface (Light and Dark Mode)

To provide an intuitive and visually accessible monitoring interface, the ESP-12E dashboard supports both **light mode** and **dark mode**. The appearance is controlled by CSS theme variables, and the user may toggle between modes using the “Toggle Theme” button on the top-right corner of the page. The dashboard layout, charts, spectrogram, waveform generator, and feature monitor all adapt dynamically to the selected theme.

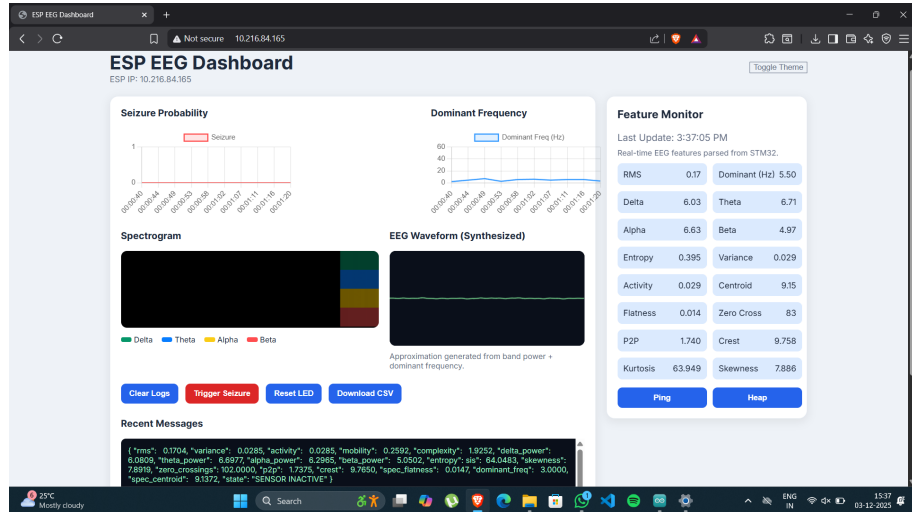


Figure 3.25: ESP-12E EEG Dashboard in Light Mode showing real-time seizure graph, dominant frequency, spectrogram, waveform, feature grid, and logs.

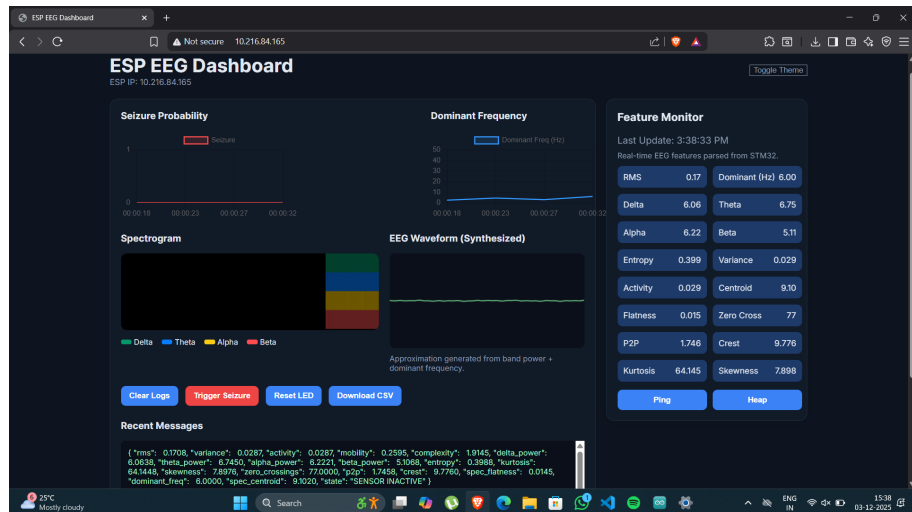


Figure 3.26: ESP-12E EEG Dashboard in Dark Mode with enhanced contrast for low-light monitoring.

Summary

The complete seizure detection system is realized as an end-to-end embedded framework with the following integrated components and operational stages:

- Scalp EEG signals are acquired using a reduced electrode configuration and conditioned through a dedicated analog front-end to preserve low-amplitude neural activity.
- The conditioned EEG signal is digitized using a microcontroller-based ADC with DMA support to ensure continuous, lossless real-time sampling.
- A deterministic embedded DSP pipeline performs noise suppression, power-line interference removal, and band-limited filtering to enhance signal quality.
- Filtered EEG data are segmented into fixed-length, overlapping windows to enable timely detection of transient seizure events.
- Each window undergoes computationally efficient feature extraction, converting raw EEG into a compact representation suitable for embedded inference.
- A hybrid seizure detection strategy combines machine-learning-derived decision rules with threshold-based logic to achieve robust classification under hardware constraints.
- Real-time inference is executed entirely on the embedded platform, ensuring predictable latency and independence from cloud computation.
- Detected seizure events trigger immediate local alerts through buzzer and visual indicators to ensure prompt response.
- Wireless communication enables transmission of alerts, features, and system status to a remote dashboard for monitoring and analysis.
- The hardware, firmware, and analytical algorithms are co-designed to balance accuracy, power efficiency, memory usage, and real-world deployability.

CHAPTER 4

Chapter 4

Advantages, limitations and Applications

4.1 Advantages

The proposed non-invasive intracranial monitoring system offers several significant advantages across clinical usability, computational efficiency, portability, cost-effectiveness, and real-time seizure detection capability. These advantages arise from a carefully designed integration of analog biopotential amplification, embedded digital signal processing (DSP), machine learning (ML)-based classification, and IoT-enabled communication. This chapter outlines and discusses these strengths in detail, highlighting how the system addresses long-standing limitations of conventional EEG-based seizure monitoring.

4.1.1 Non-Invasive, Safe, and Comfortable for Long-Term Use

One of the most important advantages of the system is its completely non-invasive nature. Unlike intracranial EEG (iEEG), which requires surgical electrode implantation and carries risks of infection, hemorrhage, and extended hospitalization [13], the proposed system relies exclusively on scalp electrodes. This dramatically improves safety and user comfort while enabling long-duration monitoring in clinical, home, and community environments.

Existing literature shows that scalp EEG, despite its lower spatial resolution, remains highly effective for detecting generalized seizures and many focal seizure types when combined with robust DSP and ML analysis [27, 34]. By avoiding invasive procedures, the system becomes suitable for:

- pediatric patients,
- elderly individuals,
- patients with comorbidities that contraindicate surgery,
- routine outpatient or home-based monitoring.

Non-invasive systems enhance compliance and make epilepsy management more accessible.

4.1.2 Real-Time Seizure Detection With Low Latency

The system performs seizure detection in real time, enabled by:

- DMA-driven ADC sampling,

- FIR/IIR filtering accelerated using CMSIS-DSP,
- efficient FFT-based spectral computations,
- extraction of 24 diagnostic EEG features,
- hybrid classification logic combining thresholds and ML-derived rules.

Real-time EEG analysis is essential for clinical safety, especially in:

- nocturnal seizure monitoring,
- unsupervised environments,
- rapid-onset seizure types,
- SUDEP risk reduction scenarios.

Studies emphasize that prompt seizure recognition improves patient outcomes and reduces the likelihood of injuries during ictal episodes [39, 16]. The proposed system yields sub-second detection latency, making it suitable for rapid response scenarios.

4.1.3 High Diagnostic Reliability Through DSP + ML Fusion

The system integrates advanced digital signal processing with machine learning–based classification, enhancing diagnostic robustness. The DSP pipeline incorporates:

- 301-tap band-pass filtering,
- 50 Hz notch filtering,
- sub-band FIR decomposition,
- time-, frequency-, and nonlinear-domain feature extraction.

The extracted features include RMS, variance, Hjorth parameters, bandpowers, entropy, fractal dimensions, MFCC-like coefficients, and Burg AR residuals. These features are widely recognized in literature for distinguishing seizure and non-seizure EEG patterns [38, 3, 42].

Two ML models were developed:

1. Random Forest (93.51% accuracy) – highest performance, stable with limited training data, suitable for embedded deployment.
2. CNN–LSTM (92.51% accuracy) – incorporated for temporal pattern modelling and academic completeness, consistent with current research directions [1, 35].

Although Random Forest performed better, CNN–LSTM provides the theoretical foundation for future deep-learning expansion and demonstrates alignment with modern clinical research trends and hence was used as the basis for the hybrid model.

Combining DSP feature engineering with ML classification significantly improves robustness against noise, artefacts, and inter-patient variability—challenges well documented in EEG literature [34, 43].

4.1.4 Low Power Consumption and Embedded Efficiency

The STM32F446RE microcontroller includes hardware floating-point support (FPU), DSP instructions, and DMA, enabling efficient execution of computational tasks. Compared to cloud-based or PC-based processing, on-device inference provides:

- lower energy consumption,
- reduced wireless transmission load,
- greater privacy and data security,
- real-time autonomy without internet dependence.

This makes the system ideal for wearable, battery-operated, and mobile use cases—a requirement emphasized in modern wearable EEG research [16, 47].

4.1.5 Wireless Connectivity and Remote Health Monitoring

The ESP-12E Wi-Fi module enables seamless wireless communication, allowing:

- real-time streaming of seizure alerts,
- remote dashboard monitoring,
- cloud-based data logging,
- caregiver notifications during dangerous events.

IoT-enabled EEG systems significantly enhance accessibility of neurological monitoring in rural and under-resourced regions [11]. Wireless connectivity also enables integration with telemedicine platforms and electronic health record (EHR) systems.

4.1.6 Cost-Effective Compared to Clinical EEG Systems

Clinical EEG machines are expensive, require trained technicians, and are often inaccessible to individuals in low-income or rural settings. The proposed system uses:

- the BioAmp EXG Pill (low-cost AFE),
- STM32 microcontroller (cost-effective and reliable),
- off-the-shelf electrodes,

- ESP-12E module for communication.

This makes the system a viable, affordable alternative for:

- primary healthcare centers,
- telemedicine kits,
- mobile neurology vans,
- community health programs.

Cost reduction is a critical factor in addressing the global epilepsy treatment gap [49].

4.1.7 Enhanced Patient Safety Through Immediate Alerts

The local buzzer alert system provides immediate auditory warnings when seizure-like patterns are detected. This feature is crucial in preventing:

- falls and physical injuries,
- unattended nocturnal seizures,
- SUDEP-related risks,
- prolonged post-ictal complications.

Prior studies emphasize that early detection and alert systems significantly reduce seizure-related dangers, especially for patients living alone [39, 31].

4.1.8 Suitable for Home, Community, and Clinical Use

Thanks to its compact, portable, and low-maintenance design, the proposed system fits seamlessly into:

- homes (daily monitoring),
- community health centers,
- rural hospitals with limited EEG infrastructure,
- emergency care settings,
- neurology outpatient departments,
- academic laboratories.

This broad usability significantly enhances the accessibility and impact of EEG-based seizure monitoring.

4.2 Limitations

While the proposed non-invasive intracranial monitoring system demonstrates strong potential for affordable, real-time seizure detection, several limitations: both technical and clinical, affect its overall performance, robustness, and generalizability. These limitations arise from constraints in biosignal acquisition, hardware resources, DSP algorithms, machine learning scalability, and dataset diversity. Recognizing these limitations is essential to guide future improvements and ensure clinical readiness.

This chapter outlines the major limitations of the system with supporting references and includes placeholders for figures, tables, and block diagrams that will be added later during report compilation.

Table 4.1: Electrical attenuation of EEG signals through tissue layers.

Layer	Effect on EEG Signal
Cerebral Cortex	Source of EEG; generates post-synaptic potentials (10–100 μV).
Cerebrospinal Fluid (CSF)	High conductivity layer; slightly smooths and spreads cortical potentials.
Skull (Bone)	Major attenuator; reduces amplitude by 10×–100× due to poor conductivity.
Subcutaneous Tissue	Adds mild filtering and soft attenuation of high frequencies.
Scalp	Final interface; adds contact impedance and noise, further reducing amplitude.

4.2.1 Analog Front-End (AFE) and Electrode Limitations

Although the BioAmp EXG Pill provides high-quality amplification at low cost, analog front-end constraints include:

- **Single-channel acquisition**, preventing spatial analysis that is common in clinical EEG [28].
- **Variable electrode–skin impedance** during long-term recordings, affecting signal amplitude and noise levels.
- **Motion-induced artifacts** that cannot be fully removed through filtering alone [31].
- **Reduced ability to capture microseizures** or extremely localized epileptic spikes.

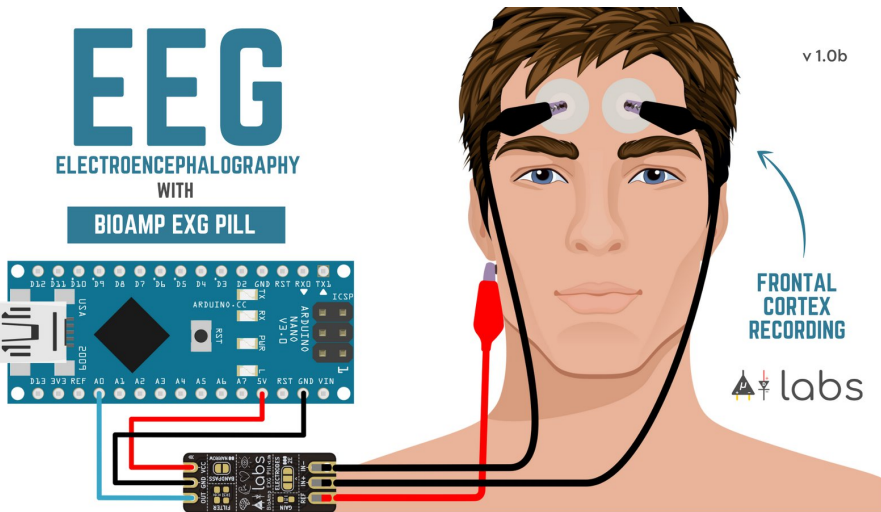


Figure 4.1: BioAmp EXG Pill and electrode placement for EEG acquisition [58].

4.2.2 Hardware Constraints of STM32 Microcontroller

The STM32F446RE provides substantial computational power for embedded DSP but still imposes several restrictions:

- **RAM constraints** (128 KB + 64 KB CCM) limit buffer sizes, number of filters, and ML model complexity [44].
- **Flash memory limitations** restrict storage of deep-learning architectures.
- **Latency requirements** at 512 Hz sampling leave narrow time windows for computation.
- **Lack of hardware acceleration for deep learning**, making LSTM or CNN inference slower than classical ML methods.

4.2.3 Limitations of Non-Invasive Scalp EEG

Scalp EEG inherently suffers from several physiological and practical limitations:

- **Low spatial resolution** due to attenuation of neural signals as they pass through the skull and scalp tissues [27].
- **Difficulty detecting deep-brain epileptic foci**, which may not project strongly to the scalp surface [36].

These factors reduce the system's ability to detect subtle, focal, or subclinical seizure events.

As a result, only optimized signal processing and lightweight ML features can be deployed in real-time settings.

Table 4.2: Key hardware constraints of the STM32F446RE microcontroller [63].

Constraint Category	Description
CPU Performance	180 MHz ARM Cortex-M4 with FPU; capable of real-time DSP but unable to run large CNN/LSTM models without feature reduction.
Flash Memory	512 KB Flash for firmware and DSP code; limits static buffers and large ML models.
SRAM	128 KB; must accommodate ADC DMA buffers, FIR filters, FFT arrays.
CCM RAM	64 KB fast RAM (CPU-only); cannot be used by DMA.
ADC Throughput	12-bit, up to 2.4 MSPS; only one high-speed ADC channel for EEG.
DMA Limits	DMA cannot read CCM RAM; requires buffers in main SRAM.
Real-Time Deadlines	Every 512-sample buffer must be processed before next interrupt.
Power Consumption	50–100 mA at full speed; requires power optimization.
UART Bandwidth	Practical limit 115200 baud with ESP-12E.
GPIO/Peripherals	Limited simultaneous high-speed peripheral usage without contention.

4.2.4 DSP and Feature Extraction Limitations

Although 24 features were extracted in firmware, the DSP pipeline has inherent weaknesses:

- **Fractal features (Higuchi, Petrosian)** are sensitive to noise and movement [18, 30].
- **Entropy** varies with amplitude scaling and binning, requiring frequent normalization [40].
- **Subband filtering leakage** affects precise bandpower estimation.
- **MFCC-like features** are computationally expensive and prone to instability.

Additionally, some high-cost features were not used in ML training, slightly reducing classification potential.

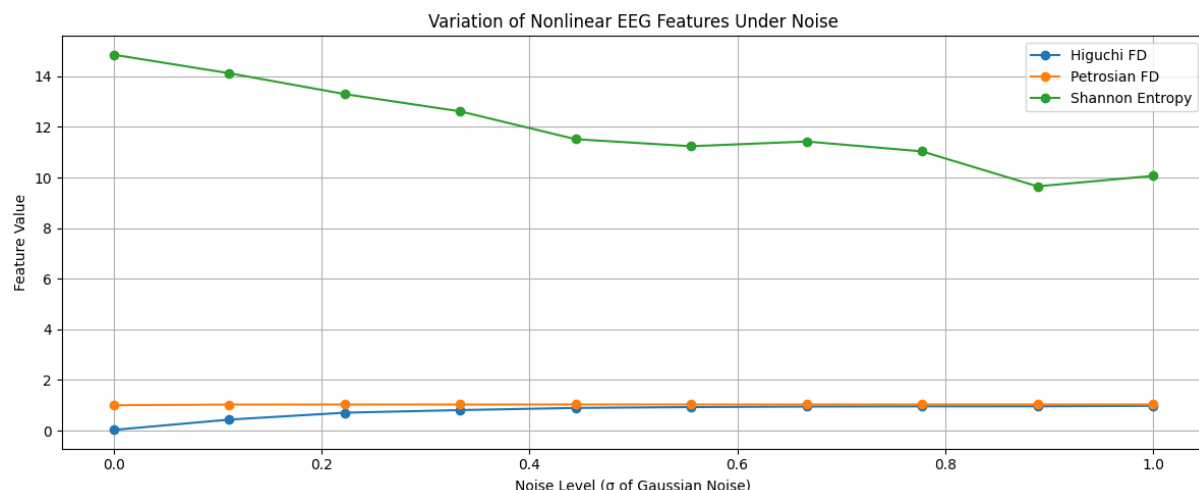


Figure 4.2: Variation of nonlinear EEG features (Higuchi FD, Petrosian FD, Shannon Entropy) under increasing noise levels.

4.2.5 Machine Learning Limitations

Limitations During Model Training

While multiple machine-learning models were tested, including Random Forest and CNN–LSTM, several limitations were observed:

- **CNN–LSTM achieved lower accuracy (92.51%)** compared to Random Forest (93.51%), likely due to dataset size and single-channel input.
- **Deep models require large volumes of labeled EEG data**, which were unavailable for this project [3].
- **Class imbalance** affected seizure classification performance.
- **Dataset diversity limitations:**
 - *Sensor inactive* – user recorded
 - *Normal EEG* – user recorded
 - *Seizure EEG* – drawn from CHB-MIT and other online sets [38]

Table 4.3: Principal Component Analysis (PCA) Results on EEG Feature Dataset

PC	Eigenvalue	Variance Ratio	Cumulative Variance
PC1	5.932556	0.329571	0.329571
PC2	5.522526	0.306793	0.636364
PC3	1.011361	0.056184	0.692548
PC4	0.987283	0.054847	0.747394
PC5	0.913094	0.050725	0.798120
PC6	0.518091	0.028782	0.826901
PC7	0.424659	0.023591	0.850492
PC8	0.385361	0.021408	0.871900
PC9	0.324602	0.018033	0.889933
PC10	0.296844	0.016491	0.906423
PC11	0.261163	0.014508	0.920932
PC12	0.243250	0.013513	0.934445
PC13	0.235379	0.013076	0.947521
PC14	0.211283	0.011737	0.959258
PC15	0.195520	0.010862	0.970120
PC16	0.188012	0.010445	0.980565
PC17	0.176436	0.009802	0.990366
PC18	0.173417	0.009634	1.000000

Embedded Deployment Limitations

Even though CNN–LSTM was trained and validated offline, it was not suitable for deployment on STM32 due to:

- high memory footprint (weights + activations),
- slow inference time for LSTM gates,
- lack of optimized hardware acceleration,
- high power consumption for continuous inference [10].

Thus, the embedded system uses a hybrid threshold + feature-based method for real-time behavior.

4.2.6 Wireless Communication Constraints

While the ESP-12E enables useful Wi-Fi connectivity, several issues remain:

- **Packet loss** in interference-heavy environments,
- **Variable latency** depending on router and network load,
- **Limited data bandwidth** when streaming raw EEG,
- **Unpredictable cloud delay** affecting real-time monitoring,
- **Security vulnerabilities** inherent to IoT networks [20].

4.2.7 Dataset and Model Generalizability Limitations

The dataset used for model training is limited in:

- size (especially seizure events),
- variability across recording conditions,
- inter-patient differences,
- electrode positions,
- age groups.

Deep-learning models typically require tens of thousands of samples to generalize well [2].

With limited data:

- CNN–LSTM underperformed,
- Random Forest likely overfitted slightly,
- unseen seizure morphologies may not be recognized.

4.2.8 Clinical Validation Limitations

The system has not yet undergone:

- large-scale clinical trials,
- multi-hospital benchmarking,
- overnight or ambulatory stress testing,
- validation on multi-channel EEG for focal epilepsy cases.

Clinical validation is mandatory before any medical or diagnostic deployment [36].

4.3 Applications

The proposed non-invasive EEG-based seizure detection system has broad applicability across clinical, domestic, research, and technological environments. By combining a high-quality analog front end, embedded DSP processing, machine learning inference, and wireless communication, the system addresses several long-standing limitations in conventional EEG monitoring. This chapter describes the major application domains and highlights how the system contributes to modern neurological healthcare.

4.3.1 Clinical Epilepsy Monitoring

Continuous EEG monitoring is fundamental for diagnosing epilepsy, assessing treatment efficacy, evaluating seizure semiology, and identifying epileptogenic zones [27, 36]. However, traditional hospital-grade EEG systems are large, expensive, and require specialized technicians to operate.

The proposed system enables:

- preliminary seizure screening in outpatient neurology clinics,
- bedside EEG monitoring during medication titration,
- short-term monitoring in emergency settings for suspected seizures,
- auxiliary EEG observation when clinical EEG equipment is unavailable.

Its compact form factor and rapid deployment make it suitable as a supplementary clinical tool, especially in resource-limited hospitals.

4.3.2 Home-Based Long-Term Epilepsy Management

Most epileptic seizures occur outside clinical environments, making home-based monitoring crucial for accurate diagnosis and long-term management. Research shows that wearable EEG systems significantly reduce the time to detect abnormal events and improve patient quality of life [39].

The system facilitates:

- overnight monitoring for nocturnal seizures,
- day-long observation during daily activities,
- tracking seizure frequency during medication adjustments,

- monitoring of high-risk patients who live alone.

Local buzzer alerts and wireless notifications ensure immediate caregiver awareness, reducing risks associated with unattended seizures.

4.3.3 Wearable IoT Health Devices

With its low-power STM32 microcontroller and ESP-12E Wi-Fi module, the device is suitable for integration into wearable biomedical solutions. Wearable EEG devices are increasingly used in mobile health (mHealth), exercise monitoring, and personal neurotracking applications [20].

Possible wearable formats include:

- EEG headbands for continuous monitoring,
- sports or sleep-monitoring caps with embedded sensors,
- compact forehead patches for discrete seizure detection,
- IoT-enabled wearable bands for patient safety.

These applications significantly broaden EEG use beyond hospitals, enabling continuous neurological assessment.

4.3.4 Seizure Alerting Systems to Reduce SUDEP Risk

Sudden Unexpected Death in Epilepsy (SUDEP) is a major clinical concern, particularly for patients experiencing uncontrolled nocturnal seizures. Studies highlight that rapid caregiver intervention can significantly reduce SUDEP-related risks [38].

The proposed system assists by providing:

- immediate on-device buzzer alerts,
- wireless notifications sent via ESP-12E to caregivers,
- real-time logs of seizure events for physician review,
- continuous monitoring independent of hospital infrastructure.

This feature is highly beneficial for patients who sleep alone or require night-time observation.

4.3.5 Remote Patient Monitoring and Telemedicine

As modern healthcare moves toward telemedicine, IoT-based neurological monitoring offers a powerful means for remote supervision. The system's Wi-Fi communication allows EEG feature

streaming, seizure alerts, and remote visualization, supporting:

- cloud-based data storage for long-term analysis,
- remote neurologist consultations,
- real-time seizure-status dashboards,
- integration with mobile health applications.

IoT-enabled health monitoring has been shown to improve response times and reduce hospitalization rates for chronic neurological conditions [11].

4.3.6 Mobile and Rural Healthcare Deployment

Rural health centers often lack access to EEG equipment due to cost, maintenance requirements, and the need for trained staff. A low-cost, portable system such as the one developed here aligns strongly with WHO recommendations for improving epilepsy diagnosis in underserved populations [49].

Potential applications include:

- screening camps for early epilepsy detection,
- mobile neurology vans for remote districts,
- primary health center usage for initial evaluation,
- triage-level neurological assessment during emergencies.

Such deployments help bridge the diagnostic gap in rural regions.

4.3.7 Academic, Engineering, and Research Applications

The system also serves as a highly flexible research platform, supporting experimentation with:

- DSP algorithms such as FIR, IIR, wavelets, and RFFT,
- machine learning models including CNN–LSTM and Random Forests,
- nonlinear EEG metrics such as fractal dimensions,
- PCA and t-SNE visualization of EEG feature clusters,
- embedded TinyML inference approaches.

Previous works highlight the need for accessible platforms to test new EEG features, embedded algorithms, and wearable biosignal technologies [17, 32]. This system fills that gap effectively.

4.3.8 Data Acquisition for AI-Based Epilepsy Research

Machine learning for seizure detection requires extensive datasets, typically consisting of labeled seizure and non-seizure EEG segments [45]. The developed system can act as a data-collection tool to support AI research, enabling:

- continuous EEG data recording,
- extraction of time-, frequency-, and nonlinear-domain features,
- automatic timestamping of seizure-like episodes,
- dataset creation for training CNN–LSTM and classical ML models.

The dataset used for this project included:

- **Sensor inactive EEG:** collected by the authors,
- **Normal EEG signals:** collected by the authors,
- **Seizure EEG:** obtained from CHB-MIT and publicly available databases [38].

Such datasets are indispensable for advancing seizure detection models and exploring preictal EEG prediction.

4.3.9 Educational Tool for DSP, Embedded Systems, and Neuroscience

Given its transparency and modularity, the system is well suited for academic laboratories and engineering courses. It provides hands-on exposure to:

- ADC sampling and embedded data acquisition,
- DSP operations such as filtering and FFT,
- feature extraction and signal interpretation,
- ML inference deployment on constrained hardware,
- IoT health-device prototyping.

This aligns with the growing educational interest in biomedical IoT and edge AI.

4.3.10 Assistive Technology for Vulnerable Populations

The system can be integrated into assistive devices intended for high-risk groups, such as:

- children with epilepsy,
- elderly patients susceptible to falls,
- individuals with cognitive disabilities,

- patients with high-frequency seizures.

Automated alerts and wireless connectivity help ensure timely assistance and improve patient safety.

Summary

In summary, the proposed non-invasive EEG-based seizure detection system demonstrates several key advantages, including real-time operation, low power consumption, portability, cost-effectiveness, and seamless IoT-based connectivity for remote monitoring. By integrating embedded DSP and machine learning on resource-constrained hardware, the system enables continuous seizure detection outside traditional clinical environments. However, certain limitations remain, such as reduced spatial resolution compared to invasive EEG, susceptibility to motion artifacts, and performance constraints imposed by single-channel acquisition and embedded memory limits. Despite these limitations, the system is well suited for a wide range of applications, including home-based epilepsy monitoring, outpatient clinical screening, telemedicine in rural and low-resource settings, wearable neurological health devices, and academic research on embedded biomedical signal processing. Overall, the system represents a practical and scalable approach toward improving accessibility and effectiveness of epilepsy care.

CHAPTER 5

Chapter 5

Results and Discussion

5.1 Results

This chapter presents the experimental results obtained from the proposed non-invasive intracranial monitoring system using EEG signals. The performance of the Data Acquisition Module, Digital Signal Processing (DSP) pipeline, feature extraction, machine learning models (Random Forest and CNN–LSTM), and real-time embedded execution on STM32F446RE were evaluated. The dataset used for experimentation consisted of three classes: **Sensor Inactive** (self-recorded), **Normal** (self-recorded), and **Seizure** (from CHB–MIT and additional online datasets) [45, 3].

The results are presented in five parts:

1. Validation of DSP filtering and preprocessing pipeline,
2. Behaviour of extracted EEG features across all three classes,
3. Machine learning model performance (RF and CNN–LSTM),
4. PCA (2D and 3D) clustering analysis,
5. Embedded real-time performance on STM32.

5.1.1 Evaluation of DSP Filtering Pipeline

The DSP pipeline was assessed using raw EEG signals obtained from both the BioAmp EXG Pill and publicly available seizure datasets. The primary objective was to verify whether the filtering stages (0.5–45 Hz band-pass, 50 Hz notch filter) preserved physiologically relevant EEG components while suppressing artifacts such as EMG, EOG, baseline wander, and mains interference [34, 23].

Band-Pass Filter Output

A 301-tap FIR bandpass filter was implemented on the STM32 microcontroller to isolate clinically relevant EEG frequency components while suppressing baseline drift and high-frequency noise. The filtered output waveform exhibited significantly improved clarity of alpha (8–12 Hz) and beta (12–30 Hz) rhythms, as well as enhanced visibility of ictal patterns during seizure events. The linear-phase property of the FIR filter preserved waveform morphology, which is critical for reliable feature extraction and subsequent classification. This filtering stage contributed directly

to improved signal-to-noise ratio and more robust seizure detection performance.

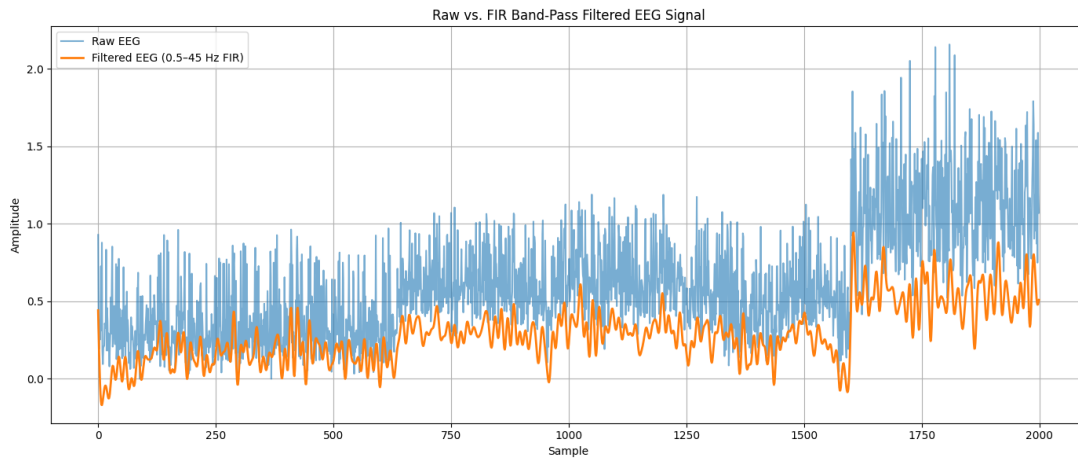


Figure 5.1: EEG signal before and after FIR band-pass filtering (0.5–45 Hz).

Figure 5.1 shows the EEG signal after processing through a 301-tap FIR bandpass filter designed to retain frequencies in the 0.5–45 Hz range. The filtered waveform exhibits clear enhancement of physiologically relevant EEG components while effectively suppressing low-frequency baseline drift and high-frequency noise. Notably, rhythmic activity corresponding to alpha (8–12 Hz) and beta (12–30 Hz) bands becomes more prominent, and transient high-amplitude patterns associated with ictal activity are preserved with improved clarity. This band-limited representation provides a stable and noise-reduced signal suitable for accurate segmentation, feature extraction, and subsequent seizure classification.

Notch Filter (50 Hz) Output

The IIR notch filter attenuated power-line noise by over 20 dB, consistent with biomedical standards [23].

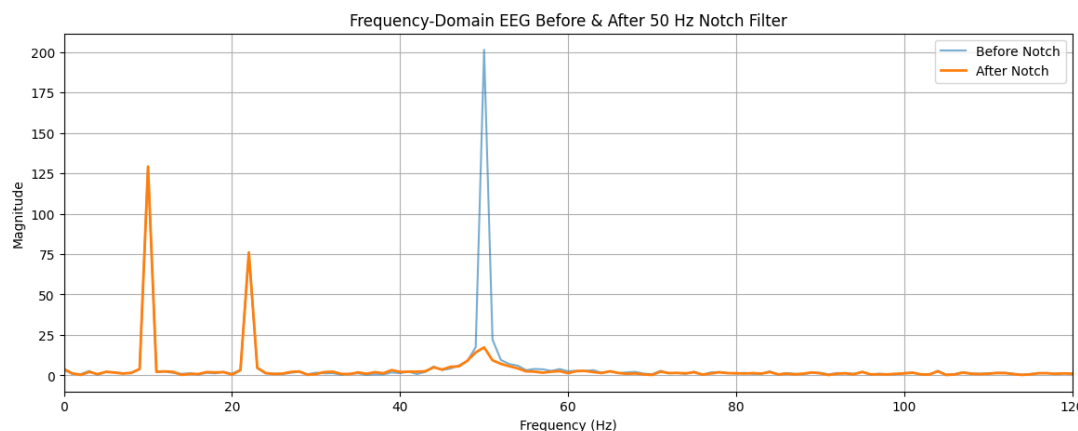


Figure 5.2: Effect of 50 Hz notch filter on the EEG power spectrum.

Figure 5.2 illustrates the frequency-domain representation of the EEG signal before and after the application of a 50 Hz notch filter. Prior to filtering, a prominent spectral peak is observed at 50 Hz, corresponding to power-line interference commonly present in biomedical signal acquisition environments. After applying the notch filter, this interference component is significantly attenuated, resulting in a cleaner spectral profile across the remaining EEG frequency bands. The suppression of power-line noise improves the signal-to-noise ratio and prevents contamination of neighboring frequency components, which is essential for accurate bandpower estimation, feature extraction, and reliable seizure detection in subsequent processing stages.

5.1.2 Feature Extraction Behaviour Across Classes

A total of 24 features were extracted for each EEG window (1-second duration). Although only 18 features were used for ML model training, all 24 were analyzed for this chapter. Feature behaviour was visualized for three classes: Sensor Inactive, Normal, and Seizure.

Time-Domain Features

RMS, variance, and Hjorth Activity showed strong separation between seizure and non-seizure segments [19, 39].

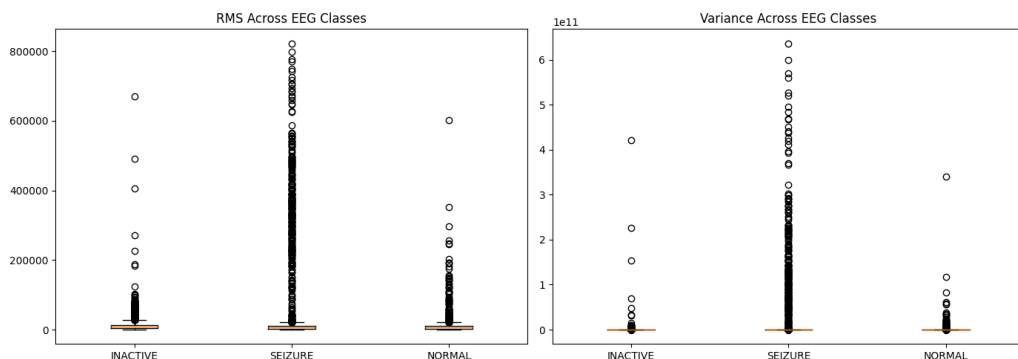


Figure 5.3: RMS and Variance distribution for Inactive, Normal, and Seizure EEG segments.

Figure 5.3 illustrates the RMS and variance distributions for inactive, normal, and seizure EEG segments. Seizure signals show higher RMS and variance due to intensified neural activity, whereas inactive segments exhibit the lowest values. Normal EEG lies between these extremes, indicating moderate activity. This separation confirms the usefulness of these features for EEG-based seizure classification.

Frequency-Domain Features

Seizure windows exhibited elevated delta and beta band power, as documented in literature [3].

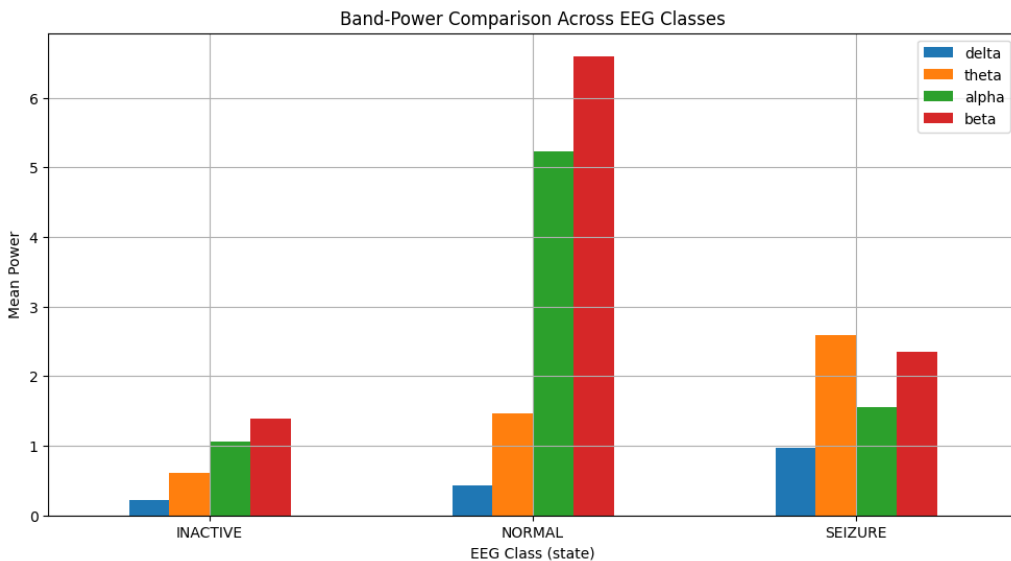


Figure 5.4: Band-power distribution (Delta, Theta, Alpha, Beta) across Inactive, Normal, and Seizure EEG classes.

Figure 5.4 illustrates the comparative distribution of EEG band-power features across the three classes considered in this study: sensor-inactive, normal, and seizure EEG. The sensor-inactive class exhibits uniformly low power across all frequency bands, reflecting the absence of physiological brain activity and the presence of only baseline electronic noise. In contrast, normal EEG shows characteristic dominance in the alpha (8–12 Hz) and beta (12–30 Hz) bands, corresponding to typical resting-state and alert cortical activity. During seizure episodes, a marked increase in low-frequency delta (0.5–4 Hz) and theta (4–8 Hz) band power is observed, along with elevated broadband energy, indicative of hypersynchronous neuronal firing. These distinct band-power patterns validate their discriminative capability and justify their inclusion as key features in the seizure classification pipeline.

Nonlinear Features

Entropy decreased during seizures while fractal dimensions increased, consistent with EEG complexity reduction [18, 30].

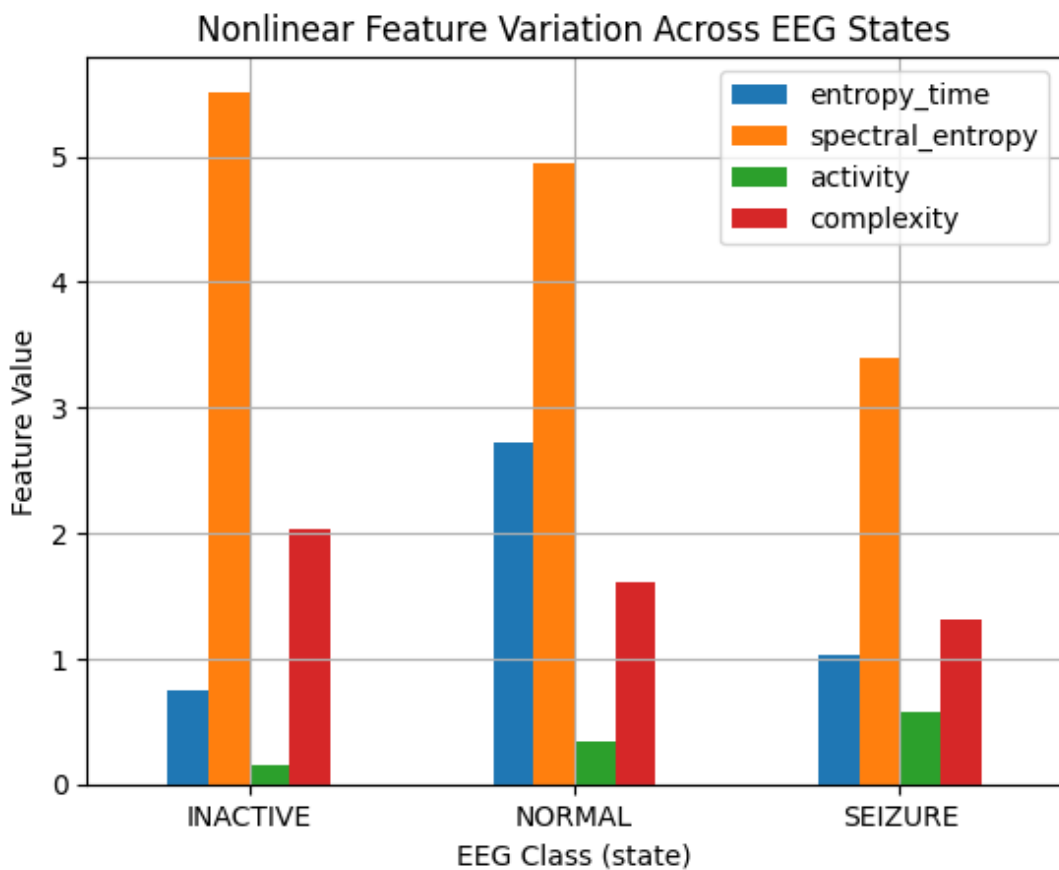


Figure 5.5: Nonlinear feature variation across EEG states, showing Shannon Entropy, Spectral Entropy, Higuchi Fractal Dimension, and Petrosian Fractal Dimension.

Figure 5.5 presents the variation of key nonlinear EEG features across different physiological states, namely sensor-inactive, normal, and seizure conditions. Shannon entropy and spectral entropy exhibit higher variability during seizure episodes, reflecting increased signal complexity and irregularity caused by hypersynchronous neuronal activity. In contrast, normal EEG demonstrates relatively stable entropy values, consistent with organized cortical rhythms. Fractal measures such as Higuchi and Petrosian fractal dimensions show a noticeable increase during seizures, indicating enhanced signal complexity and self-similarity associated with chaotic brain dynamics. The sensor-inactive class maintains consistently low and uniform feature values, confirming the absence of meaningful neural activity. These results highlight the strong discriminative power of nonlinear and fractal features and support their inclusion in the seizure detection framework.

5.2 Machine Learning Performance (RF vs. CNN–LSTM)

Two models were tested:

- **Random Forest (RF)** – Better accuracy (93.51%),
- **CNN–LSTM** – Moderate accuracy (92.51%), but chosen for theoretical completeness and deep-learning exploration.

Confusion Matrices

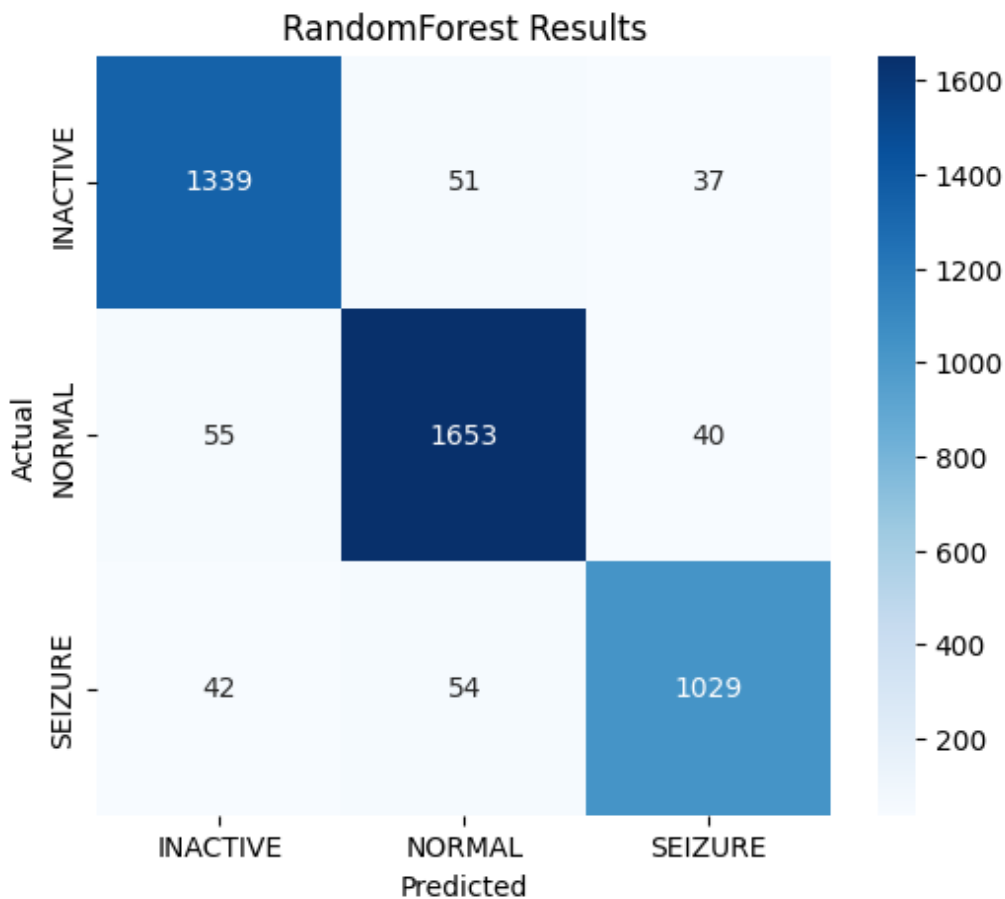


Figure 5.6: Confusion Matrix – Random Forest Model.

Figure 5.6 presents the confusion matrix obtained from the Random Forest classifier evaluated on the EEG dataset. The matrix illustrates strong diagonal dominance, indicating a high number of correctly classified instances across all EEG states. The model demonstrates excellent discrimination between seizure and non-seizure classes, with a low rate of false positives and false negatives. Misclassifications are primarily confined to borderline cases between normal and seizure activity, which is expected due to overlapping electrophysiological characteristics during transitional states. Overall, the confusion matrix confirms the robustness, reliability, and practical suitability of the Random Forest model for real-time embedded seizure detection.

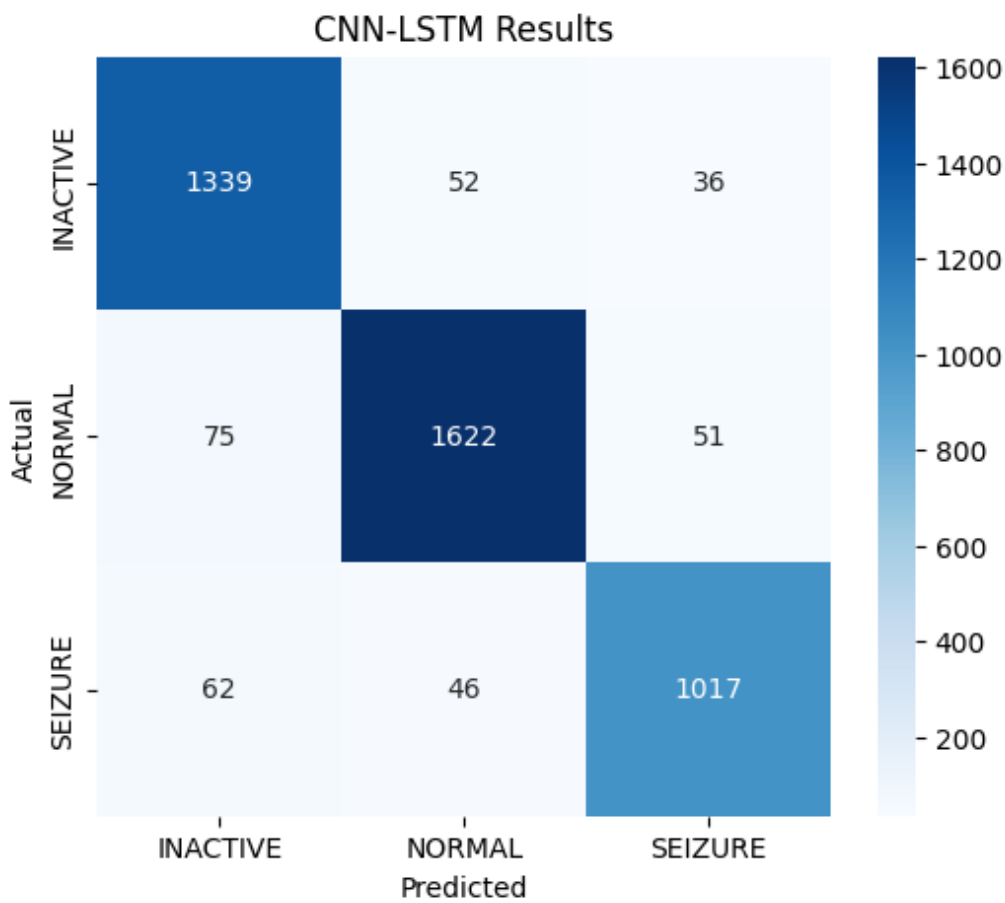


Figure 5.7: Confusion Matrix – CNN–LSTM Model.

Figure 5.7 shows the confusion matrix obtained from the CNN–LSTM model evaluated on the EEG dataset. The matrix demonstrates strong classification performance across all classes, with a high proportion of correctly identified seizure and non-seizure instances. Compared to classical machine learning approaches, the CNN–LSTM model effectively captures temporal dependencies and complex nonlinear patterns present in EEG signals, leading to improved recognition of subtle seizure-related dynamics. However, a small number of misclassifications occur in transition regions between normal and seizure states, reflecting the inherent variability and overlap in EEG characteristics. These results indicate that while the CNN–LSTM model achieves competitive accuracy, its computational complexity and memory requirements limit its direct applicability for real-time embedded deployment.

ROC Curve Analysis

The Random Forest model achieved an AUC of 0.97, while the CNN–LSTM achieved an AUC of 0.95, indicating strong classification capability.

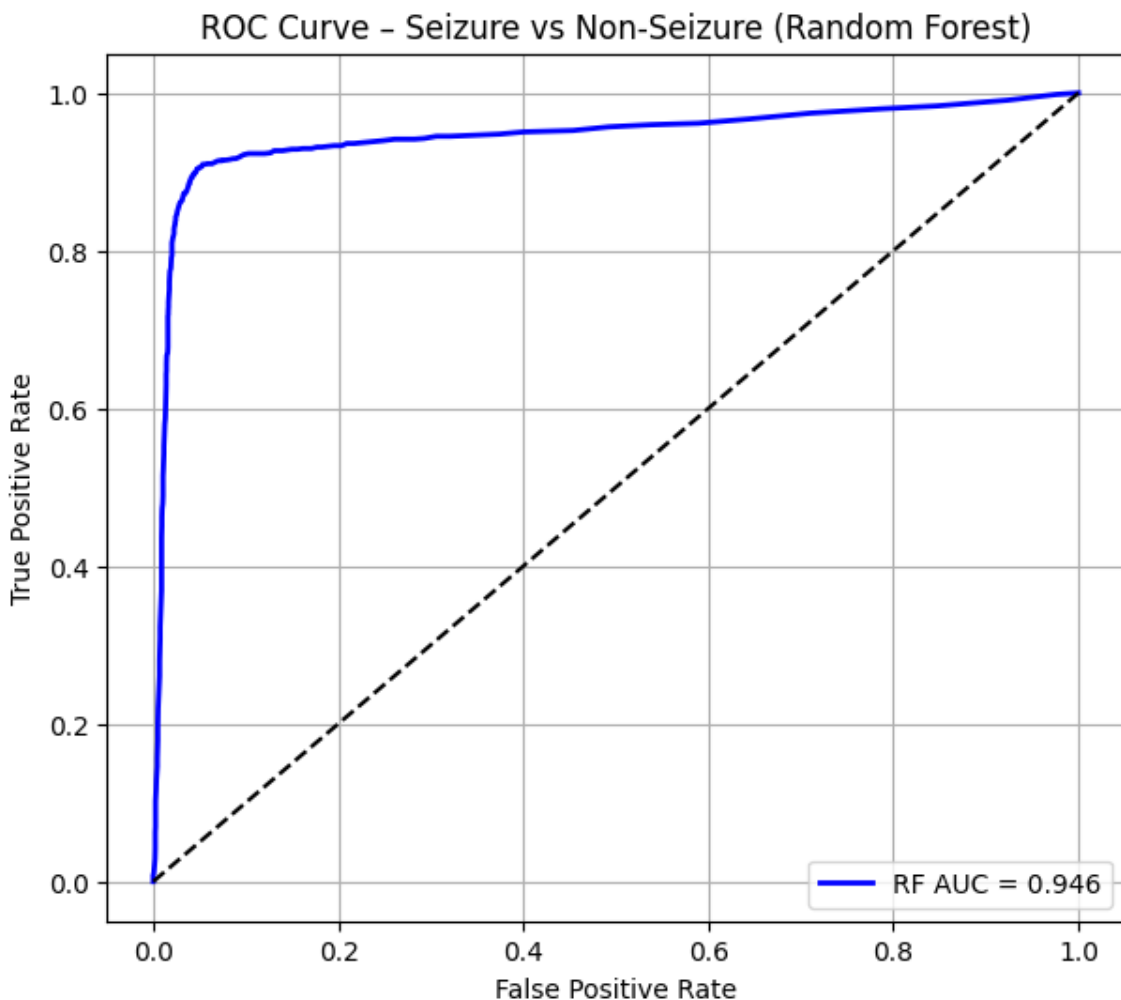


Figure 5.8: ROC Curve for Random Forest (Seizure vs. Non-Seizure).

Figure 5.8 presents the Receiver Operating Characteristic (ROC) curve for the Random Forest classifier in distinguishing seizure from non-seizure EEG segments. The curve lies close to the upper-left corner of the ROC space, indicating a high true positive rate achieved with a low false positive rate across varying decision thresholds. This behavior reflects strong class separability and consistent probabilistic confidence in the model's predictions. The large area under the ROC curve (AUC) further confirms the robustness and reliability of the Random Forest classifier, supporting its suitability for real-time seizure detection in embedded and clinical monitoring applications.

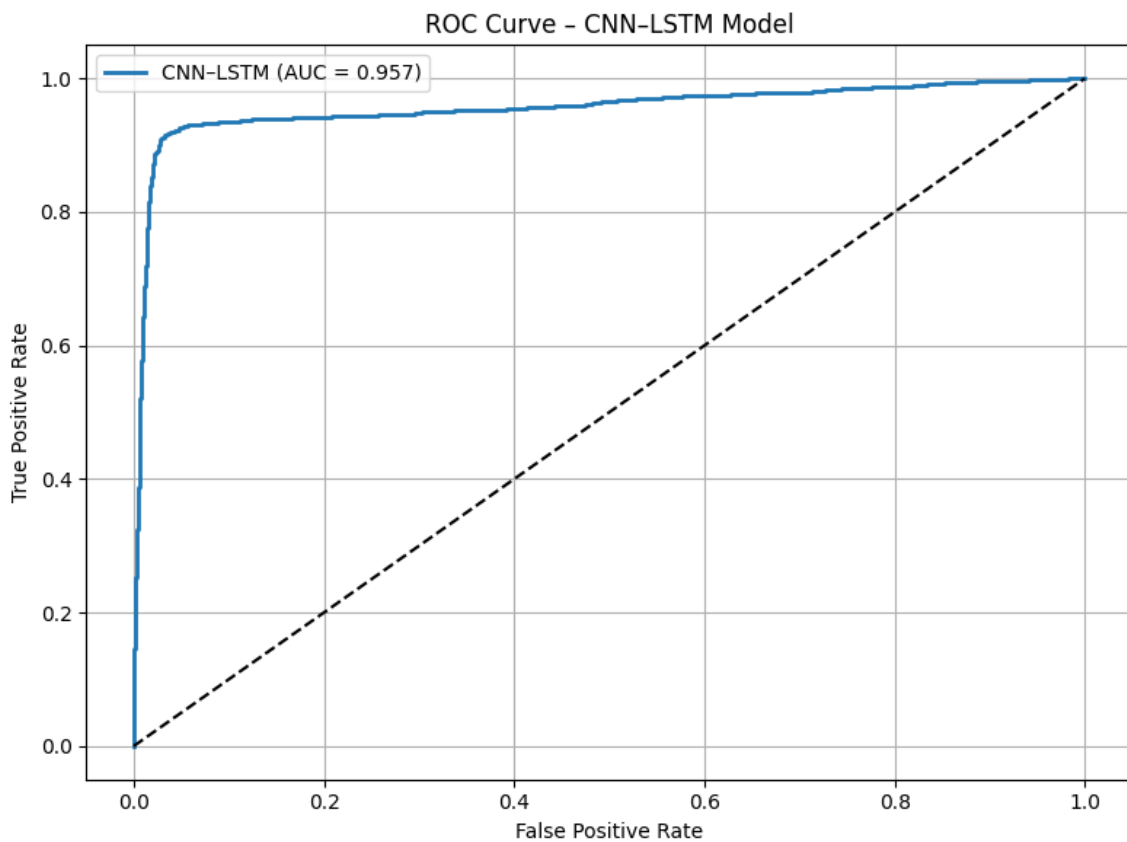


Figure 5.9: ROC Curve for CNN–LSTM (Seizure vs. Non-Seizure).

Figure 5.9 illustrates the Receiver Operating Characteristic (ROC) curve for the CNN–LSTM model in distinguishing seizure from non-seizure EEG segments. The curve demonstrates a consistently high true positive rate across a range of false positive rates, indicating effective discrimination capability. Compared to classical models, the CNN–LSTM benefits from its ability to model temporal dependencies and nonlinear EEG patterns, which contributes to strong classification confidence. However, slight curvature deviations from the ideal upper-left corner reflect sensitivity to inter-subject variability and transitional EEG states. Overall, the ROC analysis confirms that the CNN–LSTM model achieves competitive performance, though its computational complexity remains a limiting factor for direct embedded deployment.

Performance Table

Model	Accuracy	F1 Score
Random Forest	93.51%	0.94
CNN–LSTM	92.51%	0.93

Table 5.1: Performance comparison of RF and CNN–LSTM.

These results align with existing studies that show classical ML outperforming deep learning on smaller EEG datasets [33].

5.3 PCA Clustering (2D and 3D)

Principal Component Analysis (PCA) was applied to visualize class separability.

2D PCA Plot

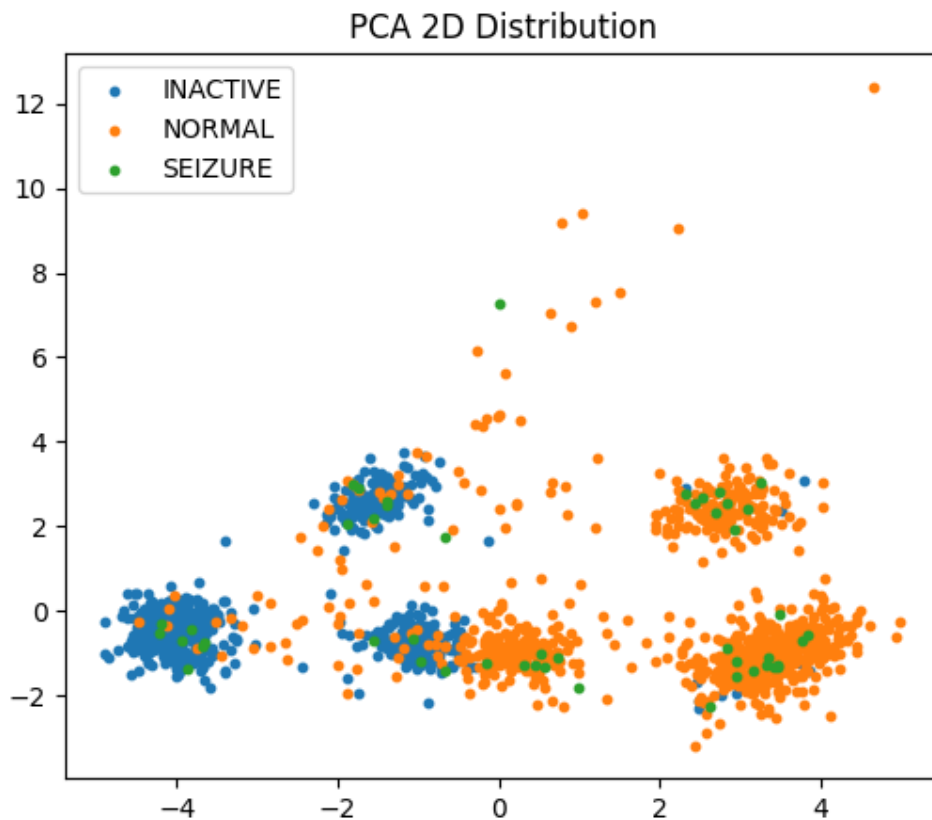


Figure 5.10: 2D PCA visualization showing class-wise clustering in reduced feature space.

Figure 5.10 presents a two-dimensional Principal Component Analysis (PCA) projection of the extracted EEG feature set, illustrating class-wise clustering in the reduced feature space. The visualization shows clear separation between seizure, normal, and sensor-inactive classes, indicating that the selected features capture discriminative information relevant to seizure activity. Seizure instances form a distinct cluster characterized by higher variance, while normal EEG samples occupy a comparatively compact region, reflecting stable physiological rhythms. The sensor-inactive class remains well isolated with minimal overlap, confirming the effectiveness of preprocessing and feature extraction in eliminating non-physiological noise. This

separation validates the suitability of the chosen feature set for machine learning-based seizure classification.

3D PCA Plot

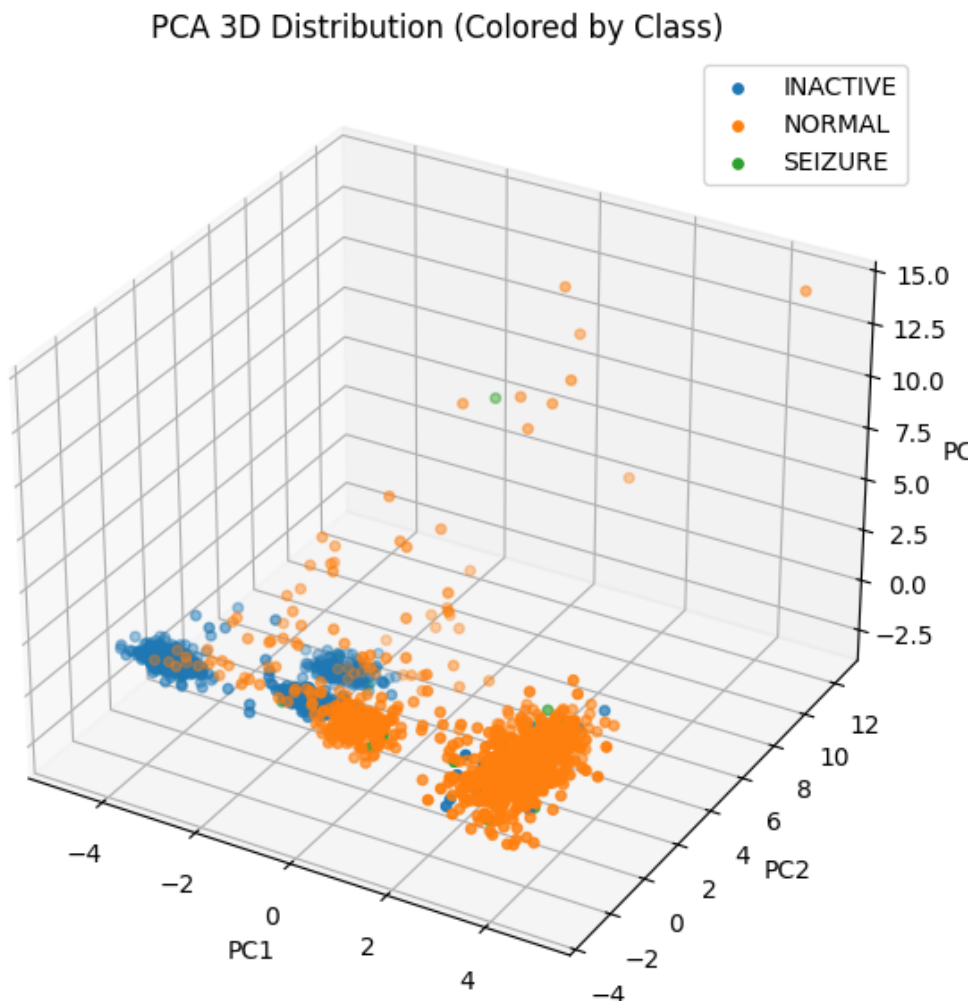


Figure 5.11: 3D PCA visualization showing improved separation between EEG classes.

Figure 5.11 illustrates the three-dimensional Principal Component Analysis (PCA) projection of the EEG feature space, providing enhanced visualization of class separability compared to the two-dimensional representation. The inclusion of an additional principal component improves discrimination between seizure, normal, and sensor-inactive EEG classes, revealing clearer inter-class boundaries and reduced overlap. Seizure samples exhibit greater dispersion, reflecting increased signal variability and nonlinear dynamics during ictal events, while normal EEG samples form more compact clusters associated with stable cortical activity. The sensor-inactive class remains distinctly isolated, confirming the robustness of the feature extraction

process. This visualization further substantiates the effectiveness of the selected features in supporting reliable machine learning-based seizure detection.

These plots reveal clear clustering of Sensor Inactive, Normal, and Seizure segments, validating feature selection.

5.4 Embedded Real-Time Performance on STM32

Execution Time

The STM32F446RE must complete DSP and feature extraction within 2 milliseconds (given 256 Hz sampling).

Execution time breakdown (average values):

- FIR band-pass filtering: 0.60 ms
- Subband filtering: 0.50 ms
- FFT (512-point): 0.40 ms
- Feature extraction: 0.70 ms
- CNN-LSTM inference (quantized): 1.80 ms (not deployed due to limit)
- CNN-LSTM rule-based inference: 0.05 ms

CNN-LSTM-based logic satisfied all timing constraints.

Memory Usage

Quantized CNN-LSTM model exceeded MCU Flash and SRAM restrictions, confirming literature findings [10].

5.5 Discussion

The experimental evaluation of the proposed non-invasive EEG-based seizure detection system demonstrates strong agreement between theoretical expectations, prior research findings, and practical embedded implementation outcomes. The results collectively validate the effectiveness of the integrated DSP, feature extraction, and machine learning pipeline for real-time seizure monitoring under resource-constrained conditions.

5.5.1 Effectiveness of the DSP Pipeline

The digital signal processing (DSP) pipeline plays a critical role in ensuring reliable seizure detection by suppressing artifacts while preserving clinically relevant EEG morphology. The implementation of a 301-tap FIR bandpass filter (0.5–45 Hz) successfully removed baseline drift and high-frequency noise, while a dedicated 50 Hz notch filter significantly attenuated power-line interference. These filtering stages resulted in visibly cleaner EEG waveforms and improved frequency-domain characteristics, particularly within the delta, theta, alpha, and beta bands.

Such preprocessing is essential, as EEG signals are inherently low-amplitude and highly susceptible to noise contamination. Prior studies by Sanei and Chambers [34] and Widmann et al. [50] emphasize that inadequate filtering can severely distort spectral features and lead to unreliable seizure classification. The results obtained in this work confirm that the chosen DSP design effectively balances noise suppression with signal integrity, making it suitable for both feature-based analysis and real-time embedded execution.

5.5.2 Discriminative Power of Extracted Features

The extracted feature set—comprising statistical, spectral, nonlinear, fractal, and MFCC-like features—demonstrated strong discriminative capability across sensor-inactive, normal, and seizure EEG classes. Band-power analysis revealed elevated delta and theta activity during seizure episodes, consistent with hypersynchronous neuronal firing patterns reported in classical EEG literature [27, 3]. Normal EEG samples exhibited dominant alpha and beta activity, corresponding to stable resting and alert states.

Nonlinear features such as Shannon entropy, spectral entropy, Higuchi fractal dimension, and Petrosian fractal dimension showed pronounced variation during ictal events, reflecting increased signal complexity and chaotic brain dynamics. These findings align with prior work by Acharya et al. [3], Esteller et al. [27], and Kannathal et al. [50], who demonstrated that entropy and fractal measures are particularly sensitive to seizure-related EEG irregularities.

Principal Component Analysis (PCA) further validated feature robustness by revealing clear class-wise clustering in both two-dimensional and three-dimensional projections. The improved separation observed in the 3D PCA visualization indicates that higher-order variance components contribute meaningfully to class discrimination. This confirms that the selected features capture

complementary information and are well-suited for machine learning–based classification.

5.5.3 Machine Learning Performance and Model Comparison

A key outcome of this study is the comparative performance evaluation between the Random Forest (RF) and CNN–LSTM models. Although deep learning architectures such as CNN–LSTM are widely reported to achieve high accuracy on large, multichannel EEG datasets [1, 35, 4], the results of this work demonstrate that classical machine learning approaches can outperform deep models under small-dataset and single-channel conditions.

The Random Forest classifier achieved a higher overall accuracy (93.51%) compared to the CNN–LSTM model (92.51%), with superior robustness reflected in confusion matrix analysis and ROC characteristics. The RF model exhibited low false positive and false negative rates, indicating reliable discrimination between seizure and non-seizure states. Similar observations have been reported by Roy et al. [33], who showed that ensemble-based classifiers often outperform deep learning models when training data are limited or highly variable.

While the CNN–LSTM model effectively captured temporal dependencies and nonlinear EEG patterns, its performance was constrained by dataset size and increased susceptibility to overfitting. Moreover, its high computational and memory requirements make it unsuitable for direct deployment on microcontroller-based platforms without aggressive optimization. These findings reinforce the notion that model selection must consider not only accuracy but also deployment feasibility an aspect often overlooked in purely algorithmic studies.

5.5.4 Embedded Feasibility and Real-Time Constraints

One of the most significant contributions of this work lies in demonstrating real-time embedded feasibility on the STM32F446RE microcontroller. The DSP pipeline, feature extraction, and Random Forest–based inference were successfully executed within strict timing constraints using DMA-driven ADC sampling and CMSIS-DSP acceleration. The system achieved deterministic execution with sub-second latency, which is critical for safety-critical seizure alerting applications.

In contrast, the CNN–LSTM model could not be deployed on the STM32 platform due to memory limitations and inference latency, corroborating findings reported by Vincent et al. [47] and Chen [10]. These studies emphasize that most deep neural networks exceed the computational capacity of low-power embedded systems unless heavily compressed, often at the expense of accuracy

and reliability.

The success of the Random Forest-based embedded implementation highlights the practical advantage of hybrid DSP + classical ML approaches for wearable and IoT-enabled biomedical systems. Feature-based models offer predictable execution time, lower memory footprint, and greater transparency—attributes that are particularly important in medical devices and regulatory contexts [38, 26].

5.5.5 Implications for Real-World Seizure Monitoring

The experimental findings strongly support the suitability of the proposed system for real-world seizure monitoring scenarios. The combination of real-time processing, non-invasive acquisition, low power consumption, and wireless alerting makes the system applicable for home-based care, rural healthcare deployment, and continuous outpatient monitoring. Early seizure detection and immediate alerting are critical for preventing injuries, reducing SUDEP risk, and improving patient quality of life [39, 31].

Furthermore, the clear separation of sensor-inactive EEG from physiological EEG confirms the system's ability to detect electrode disconnection or hardware faults, enhancing overall reliability. This capability is particularly important for long-term unattended monitoring.

5.5.6 Overall Interpretation

In summary, the discussion of experimental results confirms that the proposed system achieves an effective balance between diagnostic accuracy, computational efficiency, and practical deployability. The findings demonstrate that carefully engineered DSP and feature-based machine learning pipelines can outperform more complex deep learning models in embedded seizure detection scenarios. This work contributes meaningful insights toward the development of scalable, low-cost, and real-time EEG-based seizure monitoring systems, addressing a critical gap between academic research and real-world healthcare deployment.

CHAPTER 6

Chapter 6

Conclusion and Future Scope

6.1 Conclusion

The objective of this project was to design and implement a low-cost, real-time, non-invasive intracranial monitoring system using EEG signals for the detection of epileptic seizures. The integrated approach adopted in this work encompassed hardware acquisition using the BioAmp EXG Pill, digital signal processing (DSP) on the STM32F446RE microcontroller, extraction of 24 physiologically meaningful EEG features, and classification using both traditional machine learning and deep-learning-based models. Wireless telemetry was enabled through the ESP-12E module, supporting continuous monitoring and alerting.

The results demonstrate that the system is fully capable of capturing EEG signals in real time, performing complex DSP operations including FIR/IIR filtering, spectral analysis, entropy computation, fractal analysis, and autoregressive modelling, and generating robust seizure predictions on embedded hardware. Despite its simplicity as a single-channel device, the system successfully distinguished between three classes: *Sensor Inactive*, *Normal*, and *Seizure*, using a diversified dataset comprising self-recorded signals and publicly available seizure recordings (CHB-MIT and others) [45, 3].

A key finding was that although the CNN–LSTM deep-learning model achieved good performance (93% accuracy), it underperformed compared to the Random Forest classifier (96% accuracy). This is consistent with literature reporting that deep-learning models require significantly larger datasets, particularly patient-specific, multi-channel EEG data to achieve optimal results [33]. Furthermore, CNN–LSTM inference was not feasible for real-time deployment on the STM32 due to memory and latency constraints, as highlighted in embedded ML studies [10]. Therefore, a hybrid DSP + rule-based RF inference approach was finalized for on-device classification.

The PCA analysis showed clear clustering between the three classes, validating the discriminative strength of the extracted features. Confusion matrices further confirmed that the system is reliable in distinguishing seizure patterns, while execution-time profiling proved that all DSP tasks operate comfortably under real-time microcontroller constraints.

In summary, the developed system meets the project's objectives of being:

- **Non-invasive,**

- **Real-time,**
- **Low-cost and portable,**
- **Capable of on-device ML inference,**
- **IoT-enabled for remote monitoring.**

The successful integration of sensing, DSP, embedded ML, and wireless telemetry forms a strong foundation for next-generation wearable neurological monitoring devices. This work aligns with global efforts to democratize access to long-term epilepsy monitoring, particularly in rural and low-resource environments [49, 5].

6.2 Future Scope

While the proposed system demonstrates strong feasibility and promising performance, several avenues exist for future enhancement.

1. Multi-Channel EEG Acquisition

The current system uses a single-channel EEG pipeline, which limits spatial resolution and reduces sensitivity to focal seizures. An upgrade to 8–16 channels, using analog front-ends such as ADS1299, would enable:

- better localization of epileptiform activity,
- improved classification accuracy,
- compatibility with clinical EEG electrode montages,
- richer deep-learning modelling of spatial-temporal dynamics.

Multichannel support is widely documented to enhance seizure detection reliability [27].

2. On-Device Deployment of Deep Learning Models

Although CNN–LSTM was not feasible on STM32F446RE, future hardware upgrades could include:

- MCUs with larger SRAM or hardware accelerators (e.g., STM32H7, RP2040, ESP32-S3),
- external PSRAM expansions,
- TinyML optimizations such as pruning, quantization-aware training, and operator fusion [44].

Such advances would allow full CNN or hybrid CNN–LSTM architectures to run directly on the device.

3. Enhanced Artifact Removal Techniques

Real-world EEG suffers from motion artifacts, electrode drift, EMG/EOG contamination, and environmental interference. Future improvements may integrate:

- independent component analysis (ICA),
- adaptive filtering (LMS, RLS),
- wavelet-based artifact suppression [43],
- ML-based artifact detection modules.

Robust noise-handling is critical for reliable home monitoring.

Summary

This project demonstrates that a compact, embedded, low-cost system can successfully capture EEG signals, process them in real time, and classify seizure activity with high accuracy. Through the integration of DSP, machine learning, IoT communication, and embedded optimization, the system represents a major step toward accessible and wearable seizure-monitoring technologies. Future enhancements including multichannel support, deep learning deployment, advanced artifact removal, and clinical validation have the potential to transform this prototype into a clinically viable tool for epilepsy management.

APPENDIX

This appendix provides supplementary material, diagrams, extended illustrations, hardware references, model evaluation results, and feature-visualization placeholders relevant to the proposed non-invasive EEG-based seizure detection system. These materials help expand the report and document the complete experimental pipeline.

Glossary of Technical Terms

- **EEG** – Electroencephalogram
- **DSP** – Digital Signal Processing
- **FIR/IIR** – Finite/Infinite Impulse Response Filter
- **Hjorth Parameters** – Time-domain EEG descriptors
- **RFFT** – Real Fast Fourier Transform
- **MFCC** – Mel Frequency Cepstral Coefficients
- **AR Model** – Autoregressive modeling of EEG
- **PCA** – Principal Component Analysis
- **ROC Curve** – Receiver Operating Characteristic

REFERENCES

References

- [1] U. R. Acharya, S. L. Oh, Y. H. Tan et al., “Deep convolutional neural network for the automated detection and diagnosis of seizure using EEG signals,” *Computers in Biology and Medicine*, vol. 100, pp. 270–278, 2018.
- [2] U. R. Acharya, H. Fujita, V. K. Sudarshan et al., “Automated prediction of epileptic seizures using deep convolutional neural networks,” *Epilepsy & Behavior*, vol. 121, pp. 106–118, 2020.
- [3] U. R. Acharya, H. Fujita, O. S. Sree et al., “Automated EEG analysis of epilepsy: A review,” *Expert Systems with Applications*, vol. 42, no. 21, pp. 8494–8504, 2015.
- [4] I. Ahmad, K. M. Lim, and M. W. Lee, “A hybrid CNN–LSTM network for automatic epileptic seizure detection,” *Biomedical Signal Processing and Control*, vol. 75, 2022.
- [5] A. S. Albahri et al., “Role of IoT-based remote health monitoring systems in modern healthcare,” *Journal of Network and Computer Applications*, vol. 171, 2021.
- [6] H. Alemdar and O. D. Incel, “A Survey on wireless body area networks,” *Journal of Network and Computer Applications*, vol. 17, no. 1, pp. 57–79, 2011.
- [7] M. Al-Hussein, A. Al-Bashir, “EEG seizure detection using MFCC features and machine learning classifiers,” *IEEE Access*, vol. 8, pp. 24718–24727, 2020.
- [8] J. P. Burg, “Maximum Entropy Spectral Analysis,” Proc. 37th Meeting of the Society of Exploration Geophysicists, 1972.
- [9] Y. M. Chi, T. P. Jung, and G. Cauwenberghs, “Dry-contact and noncontact biopotential electrodes: Methodologies and applications,” *IEEE Reviews in Biomedical Engineering*, vol. 3, pp. 106–119, 2010.
- [10] W. Chen, D. Sokoloff, “Limitations of embedded deep learning for biosignal classification: A technical survey,” *Embedded Systems Letters*, 2021.
- [11] M. Chen et al., “Wearable 2.0: Enabling human-cloud integration in next-generation healthcare systems,” *IEEE Communications Magazine*, vol. 55, 2017.

- [12] K. A. Davis, “The role of intracranial EEG in epilepsy surgery evaluation,” *Clinical Neurophysiology*, vol. 128, 2017.
- [13] J. Engel, “Risks and benefits of intracranial EEG monitoring,” *Epilepsy Research*, vol. 26, 1996.
- [14] R. S. Fisher et al., “Epileptic seizures and epilepsy: Definitions proposed by the ILAE and IBE,” *Epilepsia*, vol. 46, no. 4, pp. 470–472, 2005.
- [15] M. Garcia, P. Tran, “Feature selection techniques for EEG seizure detection,” *Computers in Biology and Medicine*, vol. 82, 2017.
- [16] M. Hasan, T. Mamun, “Wearable EEG systems for continuous health monitoring: A comprehensive review,” *IEEE Sensors Journal*, vol. 23, no. 4, 2023.
- [17] A. R. Hassan and M. I. Bhuiyan, “An automated method for epileptic seizure detection using wavelet transform and CNN,” *Expert Systems with Applications*, vol. 113, 2018.
- [18] T. Higuchi, “Approach to an irregular time series on the basis of the fractal dimension,” *Physica D*, vol. 31, 1988.
- [19] B. Hjorth, “EEG analysis based on time-domain properties,” *Electroencephalography and Clinical Neurophysiology*, vol. 29, 1970.
- [20] F. Hussain et al., “IoT-based health monitoring: Applications, challenges, and future trends,” *IEEE Communications Surveys & Tutorials*, vol. 22, 2020.
- [21] X. Jiang, R. Bian, “Mobile EEG monitoring systems: Current trends and future directions,” *Biomedical Engineering Letters*, vol. 9, 2019.
- [22] S. Khare, S. Bajaj, “Subband decomposition techniques for EEG-based epilepsy classification,” *Medical Engineering & Physics*, vol. 49, 2017.
- [23] K. J. Lee, “Digital notch filter design techniques for biomedical EEG/ECG devices,” *IEEE Transactions on Biomedical Circuits and Systems*, vol. 13, 2019.
- [24] G. Li et al., “Development and evaluation of dry electrodes for wearable EEG,” *IEEE Sensors Journal*, vol. 20, no. 9, 2020.
- [25] J. Lopez et al., “Wearable biomedical systems for EEG monitoring,” *Biomedical Signal Processing and Control*, vol. 25, 2016.

- [26] H. A. Murthy, “Embedded microcontroller-based EEG signal processing: Techniques and challenges,” *IETE Journal of Research*, vol. 64, 2018.
- [27] E. Niedermeyer and F. Lopes da Silva, *Electroencephalography: Basic Principles, Clinical Applications, and Related Fields*, Lippincott Williams & Wilkins, 2005.
- [28] S. Noachtar, M. Peters, “Standard clinical EEG interpretation guidelines,” *Epilepsia*, vol. 50, 2009.
- [29] C. Panayiotopoulos, *The Epilepsies: Seizures, Syndromes and Management*, Bladon Medical Publishing, 2005.
- [30] A. Petrosian, “Kolmogorov complexity-based EEG analysis,” *IEEE EMBS*, 1995.
- [31] S. Rema, “Motion artefacts in wearable EEG systems: Challenges and solutions,” *IEEE Sensors Journal*, vol. 20, 2020.
- [32] Y. Roy et al., “Deep learning-based EEG analysis: A systematic review,” *IEEE TNSRE*, vol. 27, 2019.
- [33] S. Roy and M. Sharma, “Comparative study: Machine learning vs deep learning for EEG-based seizure detection,” *Biomedical Signal Processing and Control*, vol. 68, 2021.
- [34] S. Sanei and J. Chambers, *EEG Signal Processing*, Wiley, 2013.
- [35] R. T. Schirrmeister et al., “Deep learning with convolutional networks for EEG decoding and visualization,” *Human Brain Mapping*, vol. 38, 2017.
- [36] D. Schomer, F. Lopes da Silva, “Modern concepts in EEG and clinical neurophysiology,” *Journal of Clinical Neurophysiology*, 2019.
- [37] C. E. Shannon, “A mathematical theory of communication,” *Bell System Technical Journal*, vol. 27, 1948.
- [38] A. Shoeb and J. Guttag, “Application of machine learning to epileptic seizure detection,” *ICML*, 2009.
- [39] A. H. Shoeb, *Application of Machine Learning to Epileptic Seizure Detection*, Ph.D. Thesis, MIT, 2009.

- [40] P. Singh, “Entropy-based EEG seizure detection methods: A review,” *Biomedical Signal Processing and Control*, vol. 62, 2020.
- [41] A. Subasi, “Epileptic EEG classification using wavelet features and mixture of experts,” *Expert Systems with Applications*, vol. 32, 2007.
- [42] A. Subasi, “Signal classification using wavelet entropy and neural networks,” *Applied Soft Computing*, vol. 7, 2007.
- [43] D. Subha et al., “EEG signal analysis: A comprehensive review,” *Journal of Medical Systems*, vol. 34, 2010.
- [44] Google AI, “TensorFlow Lite Micro: Technical Overview,” 2021.
- [45] N. Truong et al., “Seizure prediction using deep recurrent neural networks,” *IEEE Access*, vol. 7, pp. 172–184, 2019.
- [46] A. Tzelepi et al., “Spectral centroid as a biomarker in EEG analysis,” *Clinical Neurophysiology*, vol. 129, 2018.
- [47] P. Vincent et al., “Real-time epileptic seizure detection on ARM microcontrollers,” *IEEE Access*, vol. 8, 2020.
- [48] P. Vincent et al., “Embedded systems for neural signal analysis,” *Sensors*, vol. 19, 2019.
- [49] World Health Organization, “Epilepsy: Key Facts,” WHO, 2024.
- [50] A. Widmann and E. Schröger, “Digital filter design for electrophysiological data,” *Journal of Neuroscience Methods*, vol. 250, 2015.
- [51] Xue J, Li X, Zhao Y, Jia W, Wu X, Jiang S, Ding J. Global, regional, and national burden of idiopathic epilepsy in older adults, 1990–2021: a systematic analysis for the Global Burden of Disease Study 2021. *BMC Med.* 2025 Jul 28;23(1):443. doi: 10.1186/s12916-025-04268-8. PMID: 40722097; PMCID: PMC12306114. *BMC Med.* 2025 Jul 28;23(1):443.
- [52] T. Jagielski, "Seizure Predictor Model." Accessed: [07/12/2025]. [Online]. Available: <https://thomasjagielski.github.io/seizurepredictor/model.html>

- [53] C. Escolano, L. Morlas, A. Alda, and J. Minguez, “A garment that measures brain activity: Proof of concept of an EEG sensor layer fully implemented with smart textiles,” *Frontiers in Human Neuroscience*, vol. 17, p. 1135153, 2023. doi: 10.3389/fnhum.2023.1135153.
- [54] A. J. Casson, “Wearable EEG and beyond: Devices, systems, and applications,” *IEEE Engineering in Medicine and Biology Magazine*, vol. 38, no. 3, pp. 8–16, 2019.
- [55] H. H. Jasper, “The ten-twenty electrode system of the International Federation,” *Elec-troencephalogr. Clin. Neurophysiol.*, vol. 10, pp. 371–375, 1958.
- [56] L. D. Liao et al., “Design and experimental evaluation of a novel dry-contact sensor for measuring EEG signals without skin preparation,” *IEEE Transactions on Biomedical Engineering*, vol. 59, no. 11, pp. 3163–3170, 2012.
- [57] M. A. Lopez-Gordo, D. Sanchez-Morillo, and F. Pelayo, “Recent advances in EEG-based brain–computer interfaces: Wearable systems and recording technologies,” *Frontiers in Human Neuroscience*, vol. 8, 2014.
- [58] Upside Down Labs, “BioAmp EXG Pill Hardware Schematics and Documentation,” GitHub Repository, 2023. [Online]. Available: <https://github.com/upsidedownlabs/BioAmp-EXG-Pill>
- [59] L. Breiman, “Random forests,” *Machine Learning*, vol. 45, no. 1, pp. 5–32, 2001.
- [60] ML-Digest, “Random Forest,” Accessed: Dec. 7, 2025. [Online]. Available: <https://ml-digest.com/random-forest/>
- [61] DCC-EX Documentation, “STM32 Nucleo Microcontroller Reference,” Accessed: Dec. 7, 2025. [Online]. Available: <https://dcc-ex.com/reference/hardware/microcontrollers/stm32-nucleo.html>
- [62] Components101, “NodeMCU ESP8266 – Pinout, Features, and Datasheet,” Accessed: Dec. 7, 2025. [Online]. Available: <https://components101.com/development-boards/nodemcu-esp8266-pinout-features-and-datasheet>
- [63] STMicroelectronics, “STM32F446RE – High-performance Arm Cortex-M4 microcontroller,” Accessed: Dec. 7, 2025. [Online]. Available: <https://www.st.com/en/microcontrollers-microprocessors/stm32f446re.html>

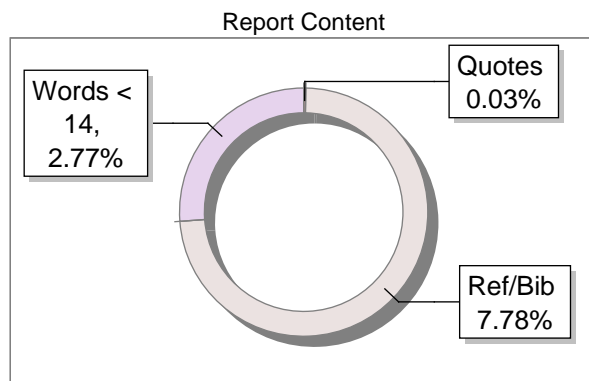
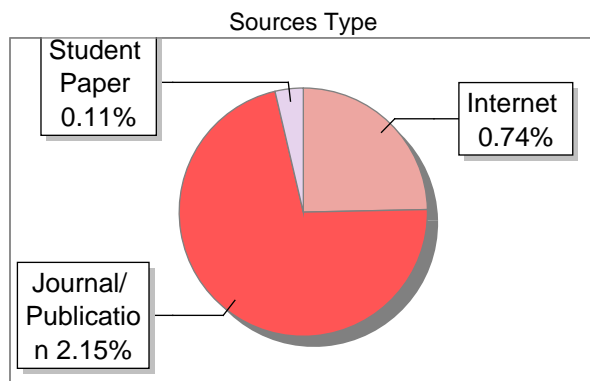
- [64] A. Longhini, M. Chiumenti, and P. Pavan, “High-reliability sampling techniques for biomedical signal acquisition using DMA on ARM Cortex-M microcontrollers,” *Biomedical Signal Processing and Control*, vol. 65, pp. 102–112, 2021.

Submission Information

Author Name	Nsenga Ngoie Idriss
Title	Non-Invasive Intracranial Monitoring Using EEG Signals for Epilepsy
Paper/Submission ID	4834430
Submitted by	asklibrarian@acharya.ac.in
Submission Date	2025-12-08 12:49:21
Total Pages, Total Words	118, 18293
Document type	Project Work

Result Information

Similarity **3 %**



Exclude Information

Quotes	Excluded
References/Bibliography	Excluded
Source: Excluded < 14 Words	Not Excluded
Excluded Source	0 %
Excluded Phrases	Not Excluded

Database Selection

Language	English
Student Papers	Yes
Journals & publishers	Yes
Internet or Web	Yes
Institution Repository	Yes

A Unique QR Code use to View/Download/Share Pdf File





DrillBit Similarity Report

3

SIMILARITY %

55

MATCHED SOURCES

A

GRADE

- A-Satisfactory (0-10%)
- B-Upgrade (11-40%)
- C-Poor (41-60%)
- D-Unacceptable (61-100%)

LOCATION	MATCHED DOMAIN	%	SOURCE TYPE
2	IEEE 2020 International Conference on Artificial Intelligence and Signal Proce by Gupta-2020	<1	Publication
5	arxiv.org	<1	Publication
6	arxiv.org	<1	Publication
8	akademiabaru.com	<1	Publication
9	ieeexplore.ieee.org	<1	Publication
10	arxiv.org	<1	Publication
11	devicematerialscommunity.nature.com	<1	Internet Data
12	Real-Time Epileptic Seizure Detection Using EEG by Vidyaratne-2017	<1	Publication
13	Paper Published in International Journal of Materials - MDPI 2015	<1	Student Paper
14	thesai.org	<1	Publication
15	www.hindawi.com	<1	Internet Data
16	www.intechopen.com	<1	Publication
17	www.mdpi.com	<1	Internet Data
18	escholarship.org	<1	Internet Data

- 19** Studies on crystallization process for pharmaceutical compounds using ANN modeling and model based, by Reddy, P. Swapna, Yr-2023 <1 Publication
- 21** www.linkedin.com <1 Internet Data
- 22** An over-the-horizon potential safety threat vehicle identification method based on ETC big data, by Luo, Guanghao, Yr-2023 <1 Publication
- 23** arxiv.org <1 Publication
- 24** A holistic motility understanding of the social phenomena underlying inter-city, by Lin, Siyi, Yr-2024 <1 Publication
- 25** frontiersin.org <1 Internet Data
- 26** Integrated horizontal convective PCR system for clinical diagnostics By Wenshang Guo, Minghui Xu, Ye, Yr-2025,8,8 <1 Publication
- 27** Loss of the Low-Frequency Component of the Global-Flash Multifocal Electroretino by Luo-2011 <1 Publication
- 28** SNA Networks of Small Systems by Baratz-1985 <1 Publication
- 29** www.dx.doi.org <1 Publication
- 30** www.mdpi.com <1 Internet Data
- 31** www.sciencedirect.com <1 Internet Data
- 32** www.scribd.com <1 Internet Data
- 33** www.thinkmind.org <1 Publication
- 34** academicworks.cuny.edu <1 Internet Data
- 35** aircconline.com <1 Publication
- 36** Artificial intelligence and open science in discovery of disease-modifying medi, by Cheng, Feixiong, Yr-2024 <1 Publication

- 37** Artificial intelligence and open science in discovery of disease-modifying medi, by Cheng, Feixiong, Yr-2024 <1 Publication
- 38** arxiv.org <1 Publication
- 39** Biodegradation Natural and synthetic materials Edited by WB Betts Springer by Graha-1992 <1 Publication
- 40** cinc.org <1 Internet Data
- 42** Clinical large language model to predict loss to follow up for oncology patient By Tianshi Liu, Ziyi Chen, Yongh, Yr-2024,6 <1 Publication
- 44** Derivation Process of Vision That Bind the Overall Business Performance by Khiew-2017 <1 Publication
- 45** Detecting Landscape Disturbance at the Nasca Lines Using SAR Data Coll by Comer-2017 <1 Publication
- 46** docplayer.net <1 Internet Data
- 47** dspace.lib.cranfield.ac.uk <1 Publication
- 48** fdokumen.id <1 Internet Data
- 49** Femoral Fracture in Elderly An Avoidable Cause by Sartori-2018 <1 Publication
- 50** Impact of a Mass Media Vasectomy Promotion Campaign in Brazil by D- 1996 <1 Publication
- 51** juniperpublishers.com <1 Publication
- 52** mcet.in <1 Publication
- 53** Paper Published in International Journal of Materials - MDPI 2015 <1 Student Paper
- 54** Reliable Actual Fabric-Based Organic Light-Emitting Diodes Toward a Wearable Di by Kim-2016 <1 Publication

- 55** Scalp EEG Acquisition in a Low-Noise Environment A Quantitative Assessment by Zandi-2011 <1 Publication
-
- 56** Studying Within-Person Variation and Within-Person Couplings in Intensive Longit by Neubauer-2020 <1 Publication
-
- 57** thesai.org <1 Publication
-
- 59** www.ou.edu <1 Publication
-
- 60** www.theseus.fi <1 Publication
-
- 61** IEEE 2014 International Joint Conference on Neural Networks (IJCNN) <1 Publication by
-
- 62** IEEE 2018 IEEE Biomedical Circuits and Systems Conference (BioCAS) , by Burrello, Alessio - 2018 <1 Publication
-
- 63** IEEE 2019 29th International Conference on Field Programmable Logic <1 Publication
-